



Thèse de Doctorat

Martin d'HALLUIN

Mémoire présenté en vue de l'obtention du grade de Docteur de l'Université de Nantes sous le sceau de l'Université Bretagne Loire

École doctorale : Matière, Molécules, Matériaux en Pays de la Loire

Discipline : Chimie Organique, Minérale, Industrielle (Section32)

Spécialité : Chimie organique

Unité de recherche : Laboratoire CEISAM

Soutenue le 27 octobre 2016

Fonctionnalisation covalente de la cellulose : Préparation de dispositifs à base de papier

JURY

Président du jury Éric FOUQUET, Professeur, Université de Bordeaux

Rapporteurs : Julien BRAS, Maitre de conférences, INP Grenoble

Stéphane GRELIER, Professeur, Université de Bordeaux

Directeur de Thèse : François-Xavier FELPIN, Professeur, Université de Nantes

Co-directeur de Thèse : Erwan LE GROGNEC, Chargé de recherche, CNRS, Université de Nantes

Remerciements

Dans un premier temps, je tiens à remercier Monsieur Bruno Bujoli pour son accueil au sein du laboratoire CEISAM (Chimie et Interdisciplinarité : Synthèse, Analyse et Modélisation).

Je remercie tout particulièrement Monsieur Julien Bras et Monsieur Stéphane Grelier d'avoir accepté de juger ce travail de thèse en tant que rapporteurs. Je remercie également Monsieur Eric Fouquet d'avoir accepté d'être examinateur de ce travail.

Mes plus grands remerciements vont à mes directeurs de thèse, F-X et Erwan qui m'ont accueilli au sein de leur équipe durant ces trois années de thèse. J'ai particulièrement apprécié votre disponibilité, votre encadrement et les conseils que vous avez pu m'apporter tout au long de ce travail. Merci également pour tous les bons moments que l'on a pu passer ensemble, j'ai beaucoup appris grâce à vous et je n'en serai pas là aujourd'hui sans votre aide.

J'en profite également pour remercier Jordi avec qui j'ai passé presque un an et demi à travailler sur ce sujet de recherche. Tu m'as apporté une aide précieuse tout au long de ce projet, sans tes conseils et ton travail ce projet n'aurait certainement pas avancé autant. Je te souhaite bon courage pour ton postdoc à Strasbourg et de la réussite dans la suite de ta carrière.

Je n'oublie pas non plus Thibaud, j'ai vraiment apprécié t'encadrer pendant ton stage de Master 1. J'ai passé un très bon moment avec toi et je te souhaite beaucoup de courage et de réussite pour ta thèse. Et n'oublie surtout pas : « Das ist verboten » !

Bien évidemment, je tiens à remercier toute l'équipe CORAIL où j'ai passé ces 3 superbes années.

Merci Sami pour tous le temps qu'on a pu passer ensemble durant cette thèse, ça va être dur de trouver un collègue de boulot aussi sympa... Je te souhaite bon courage pour ton CAPES et pour la suite.

Muchas gracias Dimitri para todo, es una maravilla de conocerte, te deseo el mejor para los próximos años y buena suerte para el concurso de maître de conf. Hasta la vista chamo.

Tibo, merci pour toutes ces soirées jeux chez toi c'était vraiment super, je ne me fais pas de doutes sur le fait que tu vas tout déchirer au concours!

Nico, mon cher collaborateur pendant les 2 premières années de thèse, merci pour tout, ça a été un vrai plaisir de bosser avec toi, j'espère qu'on aura le plaisir de se voir régulièrement dans le Nord.

Un grand merci à Florian, Medy, Alexandre, Yoann, Guillaume ainsi que tous les stagiaires de l'équipe pour toutes les pauses café que l'on a pu passer ensemble j'ai vraiment apprécié votre compagnie. Merci à tous les permanents de l'équipe : Mireia, Françoise, Isabelle, Karine, Valérie, Vincent, Pierrick, Stéphane, Seb & David, pour toutes les discussions autour d'un verre ou non, et les bons moments.

Un immense merci à tous les thésards avec qui j'ai partagé ces 3 années. Renaud merci pour ces séances pleines de testostérone à la salle de muscu ou ailleurs... J'ai vraiment aimé travailler avec toi et j'espère que tu vas vite trouver un poste! Je n'oublie pas Pauline et Yoann mes 2 autres collègues fraichement docteurs eux aussi, merci pour votre bonne humeur (surtout Pauline:-p) et pour les moments que l'on a pu passer ensemble. Dans le désordre mais j'espère n'oublier personne, merci à Joanna, Manon, Dorine, Cloé, Khaoula, Kasia, Laetitia, Florian, Boris, Titou, Tangi, Valentin, Jérémy, Antoine, David, JC, Didier, Kévin, Mbaye et Maxime.

Je remercie également l'ensemble du personnel du CEISAM avec qui j'ai pu travailler ou simplement discuter, en particulier Nathalie, Virginie, Julie, François-Xavier, Denis, Benoit, Clémence, Yann, Errol, Hamada et Louis.

Un grand merci à tous mes amis du Master de Bordeaux et d'ailleurs, Simon, Lélé, Michou, Hélène, Vincent, Bébert, Guillaume, Caro, Laure, Yoann, Totor, j'espère vous voir tous pour le prochain salon des vignerons à Bordeaux! Vivement qu'on reparte ensemble pour des vacances pétanques/apéros!

Cimer à tous mes amis de l'ENSCBP et de CPI, Lise, Mylène, Mika, Jojo, JBe, Mathieu, Aurélien, Coco, Bébé, Théo, tous les dieux et déesses de la prépa (^^) et ceux que j'oublie certainement! Merci pour tous ces WEI, WED, WEK, WEG, WELM, WEB, j'espère vous voir bientôt pour un WEL;)

Iulian (mon frère de l'Est) et les tous les autres moldaves mulţumesc pentru toate. A bientôt paour se faire un petit barbeuc dans un parc avec une bonne bouteille de коньяк Kvint!

Merci à mes amis du Nord que je vais bientôt revoir plus souvent. Matthieu et Amandine merci pour ces soirées barbecue et ces week-end ch'ti, j'espère qu'on va enfin trouver du temps pour aller manger ce fameux croque boum-boum. Aurélien (Alias Boulicaut) merci pour tous les bons moments passés ensemble à Mouvaux ou en Vendée!

Un immense merci à Didier Astruc, votre présence le jour de ma soutenance m'a vraiment touchée. Si j'en suis là aujourd'hui c'est en partie grâce à vous qui avez toujours cru en moi et m'avez soutenu durant mon passage à Bordeaux et même après. J'en profite pour remercier tous mes collègues du labo NaNo, Chris, Amalia, Dong & Lina, Yanlan, Haibin, Roberto, Virginie et bien sûr Jaime!

Je remercie bien entendu l'ensemble de ma famille pour leur soutien tout au long de mes études. Mon père, ma mère ainsi que leurs conjoints respectifs pour leur aide durant toutes ces années. Romain, mon petit frère, merci pour ton soutien et j'espère qu'on se verra plus souvent dans les années à venir. Estelle, David et les enfants, ma famille de Nantes, merci pour votre aide, soutien et pour tout ce que vous avez pu m'apporter pendant ces 3 années, sans vous cette thèse n'aurait pas été aussi agréable. Abrial, mon cousin belge, j'ai hâte de te retrouver en Belgique pour que l'on passe de bons moments ensemble avec Tiff et Pierre.

Enfin, un grand merci à ma chérie, Clémence, merci de m'avoir supporté pendant toutes ces années, je sais que ça n'a pas toujours été facile notamment à cause de la distance... Mais je sais qu'on va réussir à trouver un moyen de vivre ensemble rapidement. Encore merci pour tout, je t'aime.

Table des matières

INTRO	DUCTION	1
СНАРІТ	TRE 1 LA CELLULOSE	5
I	GENERALITES SUR LA CELLULOSE	
II	HISTOIRE DE LA DETERMINATION DE LA STRUCTURE DE LA CELLULOSE	
1		
2	. La cellulose au niveau moléculaire	8
3	. La cellulose au niveau macromoléculaire	<i>9</i>
4	. La cellulose au niveau supramoléculaire et macroscopique	10
Ш	QUELQUES EXEMPLES DE MATERIAUX A BASE DE CELLULOSE	12
1	. La nitrocellulose et le celluloïd	12
2	. La rayonne	13
3	. Les esters et éthers organiques de cellulose	14
4	. Les nanocelluloses	
IV	FONCTIONNALISATION DE LA CELLULOSE SOUS FORME DE PAPIER	16
1	. Estérification de la cellulose	17
2	. Addition de l'alcool sur une fonction réactive	20
3	. Substitution de la fonction alcool	22
4	. Conclusion sur la fonctionnalisation du papier	23
V	Bibliographie	24
CHAPIT	RE 2 PREPARATION D'UN NOUVEAU MATERIAU POUR LE STOCKAGE D'INFORMATION	2 9
1	Introduction	31
Ш	WRITING AND ERASING HIDDEN OPTICAL INFORMATION ON COVALENTLY MODIFIED CELLULOSE PAPER	33
Ш	Partie expérimentale	48

CHAP	ITRE 3	PREPARATION D'UN OUTIL DE DETECTION DE L'ION HSO ₄ . DANS L'EAU	55
ı	Intro	DDUCTION	57
Ш	PAPE	R-BASED SENSOR FOR ON-SITE DETECTION OF HYDROGEN SULFATE IN WATER	58
Ш	CHEN	IICALLY-MODIFIED CELLULOSE PAPER AS SMART SENSOR DEVICE FOR COLORIMETRIC AND OPTICAL DETECTION OF	
HYE	ROGEN S	ULFATE IN WATER	61
IV	Part	IE EXPERIMENTALE	74
СНАР	ITRE 4	PREPARATION D'UN DISPOSITIF A BASE DE PAPIER CAPABLE DE REDUIRE LE CU(II) EN	
		CU(I): APPLICATION A LA DETECTION ET LA CATALYSE	77
1	INTRO	DDUCTION	79
П	A PAI	PER-BASED BIOMIMETIC DEVICE FOR THE REDUCTION OF CU(II) TO CU(I) — APPLICATION TO THE SENSING OF	
	Cu(II)	81
Ш	PART	IE EXPÉRIMENTALE	94
IV	HARN	IESSING THE DUAL PROPERTIES OF THIOL-GRAFTED CELLULOSE PAPER FOR CLICK REACTIONS: POWERFUL	
RED	UCING A	GENT AND ADSORBENT FOR CU	97
V	Part	IE EXPERIMENTALE	108
СНАР	ITRE 5	PREPARATION D'UN NOUVEAU MATERIAU POUR L'ELIMINATION DE METAUX DANS	
		L'EAU	125
1	Intro	DDUCTION	127
II	CHEN	TICALLY MODIFIED CELLULOSE FILTER PAPER FOR UNIVERSAL HEAVY METAL REMEDIATION	129
CONC	LUSION	GENERALE ET PERSPECTIVES	149
ANNE	XES		153
RESUI	ME ETEI	NDU EN FRANÇAIS	183

Introduction

Avec plus de 160 000 publications contenant le mot-clé « Cellulose » depuis le milieu du XIXème siècle¹ (Figure 1a), ce matériau biosourcé renouvelable et durable fait l'objet de recherche dans de nombreux domaines (Figure 1b).

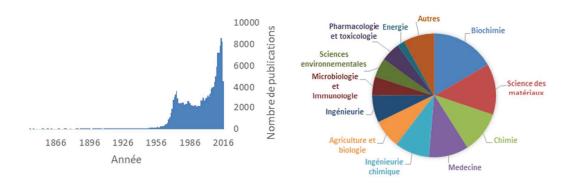


Figure 1 a) Evolution du nombre de publications contenant le mot-clé « cellulose » par an depuis 1850. b) Répartition des publications dans les différents domaines de recherche

Employée depuis des siècles par l'Homme comme matériau de construction, source d'énergie, support pour l'écriture ou encore élément de base pour la fabrication du textile, la cellulose peut également être modifiée chimiquement afin de fournir des matériaux possédant des propriétés nouvelles. Si la modification par des procédés de physisorption a été massivement étudiée et permet d'apporter de nouvelles fonctionnalités à ce matériau, ces procédés présentent l'inconvénient d'être sensibles à la désorption. C'est pourquoi le développement de matériaux cellulosiques plus robustes reste un enjeu considérable. C'est dans ce contexte que ce travail de thèse s'inscrit. Plus précisément, l'objectif de cette thèse était de préparer de nouveaux dispositifs à base de papier via des réactions de fonctionnalisations covalentes de la cellulose. L'ensemble de ces travaux ont été menés en collaboration avec le Dr. Rull-Barrull, post-doctorant au laboratoire pendant quinze mois.

Le premier chapitre de cette thèse présente quelques généralités sur la cellulose ainsi qu'un historique des découvertes majeures à propos de la détermination de la structure de ce matériau, la fin de cette première partie de chapitre est consacrée à la présentation de quelques dérivés de la cellulose notables.

La deuxième partie de ce chapitre présente un aperçu des techniques permettant la modification covalente de la cellulose sous forme de papier.

Le deuxième chapitre porte sur le développement d'une nouvelle méthode d'écriture à la surface du papier grâce au greffage de molécule photosensible permettant ainsi le stockage d'informations complexes à la surface du papier à l'aide de technique de photoimpression résolue spatialement.

Le troisième chapitre concerne la préparation d'une sonde moléculaire greffée de manière covalente à la surface du papier pour la détection de l'ion hydrogénosulfate (HSO₄-) dans l'eau. Le dispositif ainsi obtenu se présente sous la forme de bandelettes de papier, analogue au papier pH, qui peuvent changer de couleur en fonction de la concentration en HSO₄- dans le milieu.

Le quatrième chapitre présente la synthèse d'un outil de détection de l'ion Cu²⁺ dans l'eau. Cet outil à base de papier sur lequel de l'acide thioglycolique a été greffé présente également la capacité de réduire le Cu(II) en Cu(I). Cette propriété a été mise à profit dans la réaction « click » de Huisgen où ce papier modifié a servi de réducteur supporté.

Le dernier chapitre de cette thèse porte sur la préparation d'une membrane à base de papier permettant la décontamination des eaux contenant des métaux lourds. Cet outil, préparé par fonctionnalisation du papier avec une molécule aux propriétés chélatantes, s'est révélé être efficace pour l'élimination de nombreux métaux dont l'étain, le plomb ou encore le cadmium.

Après les conclusions et perspectives de ces travaux, se trouvent en annexes des travaux réalisés au cours de ma première année de thèse qui concernait l'utilisation de sel de diazonium dans des procédés en flux continu.

Chapitre 1 La cellulose

I <u>Généralités sur la cellulose</u>

La cellulose est un biopolymère linéaire constitué d'unité D-glucose liées entre-elles par des liaisons de type β 1 \rightarrow 4 (Schéma 1), ce motif de répétition composé de deux glucoses étant appelé anhydrocellobiose.

Schéma 1 Structure de la cellulose avec comme motif de répétition l'anhydrocellobiose

Les principales sources de cellulose sont le bois, le coton, le chanvre et d'autres plantes, la cellulose s'y trouve en mélange avec d'autres biopolymères, la lignine et l'hémicellulose ainsi que de petites molécules en proportion variables (Tableau 1)¹.

Source	Composition (%)			
Source	Cellulose	Hémicellulose	Lignine	
Bois dur	43-47	25-35	16-24	
Bois tendre	40-44	25-29	25-31	
Bagasse	40	30	20	
Mais (épi)	45	35	15	
Coton	95	2	1	
Lin	71	21	2	
Chanvre	70	22	6	
Jute	71	14	13	
Paille (blé)	30	50	15	

Tableau 1 Composition de quelques plantes lignocellulosiques

La production annuelle de cellulose par les plantes est estimée à $1,5x10^{12}$ tonnes (plus de 50% de la biomasse) faisant de la cellulose une matière première durable et quasi inépuisable.²

II Histoire de la détermination de la structure de la cellulose

1. <u>La cellulose au niveau élémentaire</u>

L'histoire moderne de la cellulose commence en 1838 avec la découverte par Payen (chimiste Français) d'un résidu fibreux solide résultant du traitement du bois par des acides et de l'ammoniaque suivi de plusieurs extractions. Dans cette étude, Payen a déterminé que ce résidu avait une composition élémentaire de 44% de carbone et 56% d'eau, alors que le bois de hêtre de départ avait une composition de 54% de carbone 6,2% d'hydrogène et 39,8% d'oxygène³. Il démontre alors que cette substance fibreuse est un carbohydrate isomère de l'amidon (Schéma 2) dont la composition avait été déterminée par Gay-Lussac et Thénard en 1811^{3,4}.

Schéma 2 Structure de l'amidon

C'est à la suite de ces travaux que l'académie des sciences française dans un rapport de 1839 donne le nom de cellulose à cette substance fibreuse extraite du bois^{3,5}.

2. La cellulose au niveau moléculaire

L'élucidation de la structure moléculaire de la cellulose a débuté avec les travaux pionniers de Braconnot en 1819^{3,6} montrant le lien existant entre les végétaux et le sucre. Par la suite des études sur l'hydrolyse acide de la cellulose menées notamment par Ost et Wilkening en 1910^{3,7} et par Willstatter et Zechmeister en 1913^{3,8} ont prouvé le lien entre direct entre la cellulose et le glucose. En 1921, Monier-William^{3,9} montre que cette relation entre glucose et cellulose est quasi quantitative et suit l'équation suivante (Schéma 3).

$$(C_6H_{10}O_5)_n + nH_2O \xrightarrow{H^+} C_6H_{12}O_6$$

Schéma 3 Equation bilan de la réaction d'hydrolyse acide de la cellulose

Les travaux de Denham et Woodhouse en 1913 sur la méthylation de la cellulose^{3,10} repris en 1923 par Irvine et Hirst^{3,11,12} ont permis de déterminer que les hydroxyles en position 2, 3 et 6 étaient libres et que donc par conséquent les résidus glucoses au sein de la cellulose contiennent un alcool primaire et deux alcools secondaires. En 1912, Pringsheim^{3,13} découvre que sous l'action de bactéries, la cellulose se dégrade et produit du glucose ainsi que de la cellobiose. Des études sur la configuration de la cellobiose ont par la suite été menées par Haworth *et al.*^{3,14,15}, elles ont permis de déterminer que les deux unités glucose constituant la cellobiose sont liées entre elle par une liaison de type β 1 \rightarrow 4 (Schéma 3).

Schéma 4 Structure de la cellobiose

3. <u>La cellulose au niveau macromoléculaire</u>

Dans le même temps, la structure macromoléculaire de la cellulose a fait l'objet de nombreux débats au sein de la communauté scientifique³. Deux théories étaient en compétition, la première dite « théorie de l'association » (également appelée « théorie micellaire ») défendait l'idée que la cellulose était composée de petites molécules qui avaient la capacité de s'associer entre elles sous l'effet de forces de Van der Waals ou selon la théorie de la valence partielle^{3,12}. La deuxième théorie dont les premières briques ont été posées par Tollens en 1914^{3,12,16}, décrit la cellulose comme un enchaînement linéaire de glucose. Plusieurs formules ont été proposées entre le milieu de XIXème et le début du XXème siècle, certaines sont représentées ci-dessous (Schéma 5).

Schéma 5 Différentes structures erronées de la cellulose

Jusqu'au début des années 1920, c'est la première théorie (celle de l'association) qui convient à la majorité de la communauté scientifique. La publication de Staudinger en 1920^{3,12,17} qui introduit le concept de polymère au sens où on l'entend aujourd'hui va relancer le débat et les travaux de Freudenberg en 1921^{3,12,18} sur la cinétique de dégradation de la cellulose en cellobiose viennent appuyer la théorie d'une structure polymérique linéaire de la cellulose. Les travaux de Staudinger en 1925¹⁹ et 1926²⁰ sur la polymérisation du formaldéhyde et d'autres molécules viennent lever les derniers doutes sur la structure macromoléculaire de la cellulose.

4. <u>La cellulose au niveau supramoléculaire et macroscopique</u>

Au niveau supramoléculaire, les chaînes linéaires de cellulose s'assemblent pour former un réseau compact et très dense de liaisons hydrogènes inter- et intramoléculaires (Schéma 5).

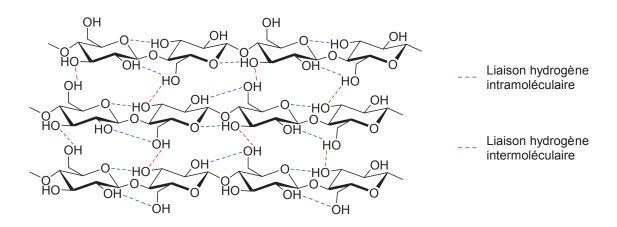


Schéma 6 Liaisons hydrogènes inter et intramoléculaires

Sous l'effet de ce réseau de liaisons hydrogènes, les chaînes de cellulose s'organisent de manière à former des microfibrilles qui elles-mêmes s'assemblent pour former des fibres de plus grandes tailles (Figure 1).

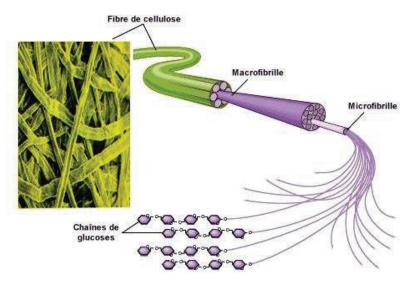


Figure 1 Représentation de la structure fibrillaire de la cellulose²¹

Cet assemblage macroscopique peut conduire à des structures amorphes ou cristallines, conférant des propriétés différentes à ce matériau (Figure 2).

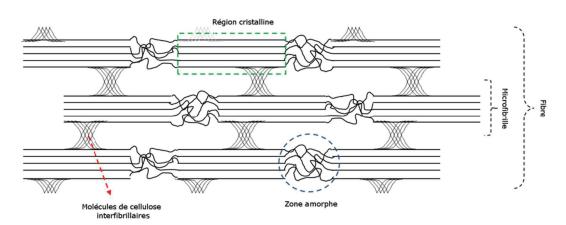


Figure 2 Représentation des domaines cristallins et amorphes dans les microfibrilles de cellulose adaptée de la référence²²

La structure cristalline de la cellulose la plus commune est appelée Cellulose I ou cellulose native (c'est celle que l'on retrouve naturellement dans les plantes)³.

III Quelques exemples de matériaux à base de cellulose

1. La nitrocellulose et le celluloïd

Bien que la structure de la cellulose ne fut bien établie qu'à partir du XXème siècle, cela n'a pas empêché le développement de produits dérivés de la cellulose. Le premier exemple de dérivé de la cellulose, la nitrocellulose (Schéma7), date des années 1830 avec notamment les travaux de Braconnot²³ sur le xyloïdine (produit résultant du mélange d'amidon ou de sciure de bois avec de l'acide nitrique concentré) et les travaux de Pelouze²⁴ sur « le papier nitré ». Dans les deux cas, le produit formé est très inflammable et instable. En 1846 Schönbein²⁵ réalise la nitration du coton dans un mélange d'acide nitrique et d'acide sulfurique, le produit obtenue appelé « fulmicoton » est hautement inflammable et explosif et sera utilisé par la suite comme poudre à canon en remplacement de la poudre noire.

Schéma 7 Structure d'une nitrocellulose partiellement fonctionnalisée

La nitrocellulose ne trouve pas seulement des applications comme agent détonant, mélangée à du camphre on obtient un nouveau matériau flexible et transparent. Le développement industriel de ce matériau commence dans les années 1870 avec les frères Hyatt, ils nomment ce produit celluloïd²⁶ qui est considéré comme le premier plastique artificiel. Dans les années suivantes, le celluloïd est principalement utilisé pour la fabrication de pellicules cinématographiques, cependant à cause de son inflammabilité ce produit fut abandonné aux alentours des années 1950. De nos jours, on utilise encore le celluloïd pour fabriquer par exemple les balles de ping-pong.

2. <u>La rayonne</u>

La rayonne (ou soie artificielle), fait partie de la famille des celluloses dites régénérées. C'est-à-dire que la cellulose est d'abord rendue soluble puis elle subit d'autres traitements afin de la rendre insoluble et ainsi reformer des fibres. La rayonne n'est donc pas un produit dérivé de la cellulose puisque le produit fini est entièrement composé de cellulose pure. Cependant son obtention passe par des étapes de modifications de la cellulose. De nouveau, c'est à un Français que l'on doit les premiers travaux sur ce sujet, en 1884 le comte Hilaire de Chardonnet développe le premier fil de soie artificielle en filant une solution de nitrocellulose au travers d'un fin tube de verre²⁷. En 1892, Beadle, Bevan et Cross²⁵ développent un autre procédé permettant d'obtenir des fibres de cellulose régénérées, ce procédé sera appelé par la suite « procédé viscose », les principales étapes sont résumées ci-dessous (Figure 3).

Figure 3 Schématisation du procédé viscose

Les fibres ainsi obtenues ont été utilisées principalement dans la fabrication de textiles. Il est également possible de préparer des films à partir de ce procédé, le produit le plus notable fabriqué par cette technique est sans conteste le film alimentaire également appelé cellophane. Cependant à cause de la toxicité et de l'inflammabilité du disulfure de carbone (CS₂) utilisé dans le procédé viscose, un autre procédé appelé lyocell fut développé dans les années 1980. Dans ce dernier, la cellulose est solubilisée sans passer par une étape de fonctionnalisation intermédiaire à l'aide d'un solvant capable de

dissoudre directement la cellulose comme par exemple le NMO (*N*-Methylmorpholine-*N*-oxide).

3. Les esters et éthers organiques de cellulose

Deux autres familles de dérivées cellulosiques ont également fait l'objet de nombreuses études et développement industriels. Il s'agit des esters et éthers organiques de cellulose. Le premier exemple d'esters de cellulose date de 1865 avec les travaux de Schützenberger sur l'acétylation de la cellulose^{28,29}. L'acétate de cellulose rencontre par la suite un vif intérêt de la part des industriels, de nombreux brevets sont déposés et l'acétate de cellulose est alors utilisé dans de nombreux domaines, comme vernis, fibre textile, film plastique et pellicule cinématographique (en remplacement de la nitrocellulose) ainsi que pour la fabrication d'objets moulés. De nos jours l'acétate de cellulose est principalement utilisé pour la fabrication de fibres textiles et de membranes de filtration et en particulier comme matière première pour la fabrication de filtres de cigarettes. D'autres esters de cellulose ainsi que des esters mixtes (composés de fonctions ester différentes) existent également.

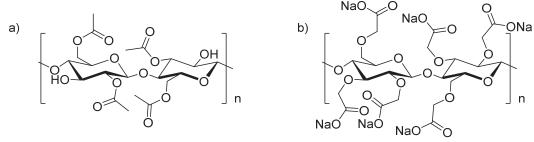


Schéma 8 (a) Structure du triacétate de cellulose ; (b) structure de la carboxyméthylcellulose de sodium

Les éthers de cellulose quant à eux font leur apparition au début du XXème siècle avec les travaux de Suida^{30–32} sur la préparation de la méthylcellulose. Le premier dérivé à avoir eu un réel intérêt industriel et commercial est la carboxyméthylcellulose développée dans les années 1920. Ce dernier est principalement utilisé sous la forme de son sel de sodium pour de nombreuses applications, par exemple comme agent épaississant dans

l'industrie alimentaire (E466) ou dans la formulation de détergents et de cosmétiques. La production mondiale de carboxyméthylcellulose représente environ 230 000 tonnes par an soit plus de la moitié de la production globale des éthers de cellulose³¹.

4. <u>Les nanocelluloses</u>

Le mot nanocellulose est un terme générique qui regroupe plusieurs types de composés dont notamment, la cellulose micro- et nanofibrillée (CMF et CNF) et les micro- et nanocristaux de cellulose (MCC et NCC)^{33–35}. Les CMF et CNF peuvent être obtenues à l'aide d'un traitement mécanique des fibres de cellulose, alors que les MCC et NCC sont eux obtenues par traitement chimique. Les principales différences entre les nanocristaux et les nanofibres de cellulose sont leur taille et leur degré de cristallinité (Tableau 2).

	Taille			
Туре	Longueur (µm)	Largeur (nm)	Hauteur (nm)	Cristallinité (%)
Fibre native	>2000	20 -50 (μm)	20-50 (μm)	43-65
CMF	0,5 – 10	10-100	10-100	51-69
CNF	0,5-2	4-20	4-20	-
MCC	10-50	10-50 (μm)	10-50 (μm)	80-85
NCC	0,05-0,5	3-5	3-5	54-88

Tableau 2 Caractéristiques des « Nanocelluloses » adaptées de la référence³³

Ces différents composés trouvent des applications dans de nombreux domaines comme par exemple, les additifs alimentaires³⁴, les matériaux composites, les emballages^{36,37}, l'électronique³⁸ ou encore la préparation de films³⁵. Depuis quelques années la production de nanocellulose est passée à l'échelle industrielle³⁹, il est certain que ces matériaux trouveront énormément de débouchés dans les années à venir.

IV <u>Fonctionnalisation de la cellulose sous forme de papier</u>

*La modification chimique de la cellulose à fait l'objet de nombreuses recherches et plusieurs revues donnent un bon aperçu des possibilités de fonctionnalisation de ce matériau^{2,40–43}. Comme vu précédemment, la cellulose est composé d'unité anhydroglucose possédant chacune une fonction alcool primaire et deux fonctions alcool secondaire (Schéma 9).

Schéma 9 Représentation des fonctions alcools présentent dans la cellulose

Les réactions les plus couramment utilisées sont, les estérifications, « l'addition » de l'alcool sur un substrat, la substitution de l'hydroxyle, la fonctionnalisation à l'aide de dérivés silylés ou encore des réactions de greffage photoinduites. Ces modifications peuvent être classées en deux catégories, (i) les modifications du squelette du polymère, (ii) la fonctionnalisation des fonctions alcools sans altération du squelette de la cellulose.

Les exemples présentés dans cette partie correspondent à cette deuxième catégorie et sont appliqués à de la cellulose sous forme de papier dans des procédés hétérogènes.

1. Estérification de la cellulose

La réaction la plus régulièrement utilisée est certainement l'estérification. Pour ce faire, l'une des fonctions hydroxyles de la cellulose réagit avec un acide carboxylique ou un dérivé activé (halogénure d'acide, anhydride d'acide) pour former un ester (Schéma 10).

Schéma 10 La réaction d'estérification

La réaction d'estérification a par exemple été utilisée à de nombreuses reprises afin de greffer à la surface de la cellulose le 2-bromoisobutyrylbromide, un amorceur de polymérisation radicalaire par transfert d'atome (ATRP)^{44–52}. Cette technique permet de réaliser la polymérisation de différents monomères (acrylate de méthyle, méthacrylate de méthyle, styrène, vinylpyridine, *N*-isopropylacrylamide) de manière contrôlée (Schéma 11).

Schéma 11 Estérification avec l'amorceur ATRP et polymérisation à la surface de la cellulose

La taille des chaînes de polymère ainsi greffées dépend du taux de greffage de l'amorceur, de la concentration en catalyseur et en monomère introduit lors de la réaction. La polymérisation suit le mécanisme suivant (Schéma 12).

$$R-Br + Cu(I)Br$$
 $R + Cu(II)Br_2$ $M = monomère$

Schéma 12 Schéma général de la polymérisation ATRP

La réaction d'estérification a également permis de greffer à la surface du papier un agent de transfert utilisable en polymérisation radicalaire contrôlée par transfert de chaîne réversible par addition-fragmentation (RAFT)(Schéma 13)^{53,54}.

Schéma 13 Greffage de l'amorceur RAFT par estérification puis polymerisation

Ces techniques de polymérisation dites vivantes et contrôlées permettent ainsi de greffer à la surface de la cellulose de nombreux types de polymères bien définis et permettent même de préparer des copolymères à blocs^{45,47}. D'autres types de molécules ont également été greffées à la surface de la cellulose *via* une réaction d'estérification. L'utilisation d'acide citrique a permis de réaliser la réticulation des fibres de celluloses entre elles à l'aide de chaînes de polyéthylène glycol⁵⁵ ainsi que le greffage de β-cyclodextrine, une molécule permettant l'encapsulation de principes actifs⁵⁶. L'estérification du papier a également été réalisée avec des acides gras afin de préparer des surfaces hydrophobes⁵⁷, de l'anhydride succinique afin de préparer un papier permettant d'adsorber des cations métalliques⁵⁸, des acides gras possédant une insaturation terminale permettant par la suite une fonctionnalisation *via* la réaction click thiol-ène⁵⁹. Le greffage de molécules possédant un noyau tétrazole a permis par la suite de réaliser une réaction de cycloaddition avec un alcène^{60,61} (Schéma 14).

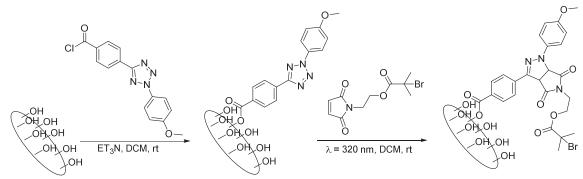


Schéma 14 Greffage d'un tétrazole par estérification puis cycloaddition

La réaction d'estérification à la surface du papier a également été utilisée afin de réaliser des réactions de polymérisation par ouverture de cycle (ROP) avec des monomères de types lactones⁶² ou carbonates⁶³ (Schéma 15).

Schéma 15 Exemples de fonctionnalisations par polymérisation d'ouverture de cycles

D'autres exemples impliquant une réaction d'estérification à la surface du papier ont également été décrits pour réaliser une réaction de polymérisation par métathèse d'ouverture de cycle (ROMP)⁶⁴ et une réaction d'hétéro Diels-Alder⁶⁵ notamment^{66–68}.

La fonctionnalisation de la cellulose *via* la réaction d'estérification permet donc d'obtenir en peu d'étapes des matériaux aux propriétés nouvelles. L'utilisation de réactions de polymérisations vivantes contrôlées permet de moduler les caractéristiques du produit obtenu en modulant le ratio amorceur greffé/monomère et la concentration en catalyseur. De plus, les chlorures d'acides ou les anhydrides d'acides généralement utilisés sont facilement synthétisables et parfois même commerciaux. Enfin les sousproduits de la réaction sont peu nombreux ce qui confère à la réaction une très bonne économie d'atomes.

2. Addition de l'alcool sur une fonction réactive

Une autre stratégie permettant de modifier la cellulose consiste à faire réagir les hydroxyles présents à la surface de la cellulose avec des fonctions chimiques réactives (autres que les acides carboxyliques et ses dérivés). Par exemple, il est possible de réaliser des additions de type Michael sur des alcènes activés comme par exemple la divivinylsulfone^{69,70}, qui permet d'introduire un alcène à la surface de la cellulose suceptible de subir une deuxième réaction d'addition afin d'introduire une autre molécule (Schéma 16).

Schéma 16 Addition de type Michael de la cellulose sur la divinylsulfone

L'utilisation de composés comportant une fonction isocyanate permet également la fonctionnalisation de la cellulose *via* la formation d'un carbamate^{71,72} (Schéma 17).

Schéma 17 Addition d'une fonction alcool de la cellulose sur un isocyanate

Des réactions d'addition ou de substitution nucléophile à la surface du papier ont également été utilisées avec respectivement des époxydes⁷³ et des dérivés halogénés⁷⁴ (Schéma 18).

Schéma 18 Exemple de réaction d'addition et de substitution nucléophile à la surface de la cellulose

Enfin, le greffage de polymère avec des acrylates ou des méthacrylates par voie radicalaire utilisant un sel de diazonium comme amorceur a également été reporté⁷⁵ (Schéma 19).

Schéma 19 Polymérisation de monomère de type acrylate à la surface du papier

L'addition de l'alcool sur une fonction réactive est une technique de fonctionnalisation de la cellulose intéressante, elle permet de greffer divers types de molécules à la surface du papier en générant peu de sous-produits. Ce type de réactions peut même dans certains cas être réalisé en milieux aqueux ce qui est un avantage pour le développement de procédés de fonctionnalisation plus respectueux de l'environnement.

3. <u>Substitution de la fonction alcool</u>

Afin de fonctionnaliser la cellulose, il est également possible de réaliser des réactions de substitution de la fonction alcool présent à la surface de la cellulose. La stratégie la plus communément employée consiste à activer cet alcool pour réaliser par la suite une réaction de substitution nucléophile. L'activation de l'alcool se fait généralement *via* l'introduction d'un groupement tosylate à la surface de la cellulose^{76–79} (Schéma 20).

Schéma 20 Tosylation de la cellulose

Le groupement tosyle ainsi introduit peut par exemple être substitué par un cyclopentadiène qui par la suite permet de réaliser des réactions de cycloadditions [4+2] de type hétéro Diels-Alder^{76,77} (Schéma 21).

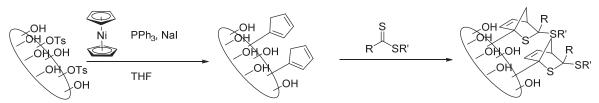


Schéma 21 Introduction de cyclopentadiène à la surface du papier puis réaction de cycloaddition [4+2]

Cette stratégie a également permis de fonctionnaliser la cellulose avec le *p*-hydroxybenzaldéhyde afin de réaliser par la suite une réaction de cycloaddition [2+2] avec un alcène⁷⁹, ou encore la 7-hydroxylméthylcoumarine dans le but de préparer un matériau sur lequel il est possible de réaliser de la photoimpression chimique⁷⁸ (schéma 22).

OH OH OTS OH OH OH OTS OH OH
$$\lambda = 455 \text{ nm}$$

Schéma 22 Greffage et arylation de l'hydroxyméthylcoumarine à la surface du papier

La substitution d'une fonction alcool de la cellulose nécessite une première étape d'activation, en utilisant notamment le chlorure de tosyle, suivi de l'étape de fonctionnalisation avec la molécule d'intérêt. Le fait de réaliser cette fonctionnalisation en deux temps peut entraîner des problèmes dans la détermination du taux de greffage à la surface de la cellulose. En effet si la seconde étape n'est pas totale, la détermination du degré de fonctionnalisation par analyse élémentaire ou par gravimétrie sera faussée.

4. <u>Conclusion sur la fonctionnalisation du papier</u>

Ces différents exemples donnent un aperçu des techniques permettant la fonctionnalisation du papier, il est à noter que d'autres types de réaction comme le greffage de dérivés silylés^{80–85} ou le greffage de polymères par l'intermédiaire de réactions photocatalysées^{86–91} ont également été reportés dans la littérature.

Pour la suite de ce travail, nous avons décidé d'utiliser principalement des réactions d'estérifications pour fonctionnaliser la cellulose sous forme de papier. Ce type de réaction s'est montré efficace et permet d'obtenir un matériau aux propriétés nouvelles en une seule étape ce qui limite les risques d'altérer l'intégrité physique du papier. De plus, la détermination du degré de substitution est facilitée car il n'y a pas d'étapes intermédiaires avant le greffage de la molécule d'intérêt. Enfin, la préparation des réactifs est aisée et dans certains cas bien décrite dans la littérature.

V <u>Bibliographie</u>

- 1 D. Klemm, H.-P. Schmauder and T. Heinze, in *Biopolymers vol 6*, (Eds.: E. Vandamme, S. De Beats, A. Steinbüchel), Wiley-VCH, Weinheim, 2004, pp. 275–312.
- 2 D. Klemm, B. Heublein, H.-P. Fink and A. Bohn, *Angew. Chem. Int. Ed.*, 2005, **44**, 3358–3393.
- 3 D. N.-S. Hon, *Cellulose*, 1994, **1**, 1–25.
- 4 J. Gay-Lussac and J. Thénard, *Rech. Phys.-Chim.*, 1811, **2**, 291–292.
- 5 A. Brongniart, T. J. Pelouze and A. B. Dumas, *C. R. Hebd. Séances Acad. Sci.*, 1839, **8**, 51–53.
- 6 H. Braconnot, Ann. Chim., 1819, 12, 172–195.
- 7 H. Ost and L. Wilkening, *Chem. -Ztg.*, 1910, **34**, 461–462.
- 8 R. Willstätter and L. Zechmeister, Berichte Dtsch. Chem. Ges., 1913, 46, 2401–2412.
- 9 G. W. Monier-Williams, J. Chem. Soc. Trans., 1921, **119**, 803–805.
- 10 W. S. Denham and H. Woodhouse, J. Chem. Soc. Trans., 1913, 103, 1735–1742.
- 11 J. C. Irvine and E. L. Hirst, J. Chem. Soc. Trans., 1923, 123, 518–532.
- 12 H. F. Mark, Chem. Eng. News Arch., 1976, **54**, 176–189.
- 13 H. Pringsheim., *Hoppe-Seyler's Z. Für Physiol. Chem.*, 2009, **78**, 266–291.
- 14 W. N. Haworth and E. L. Hirst, J. Chem. Soc. Trans., 1921, 119, 193–201.
- 15 W. N. Haworth, C. W. Long and J. H. G. Plant, *J. Chem. Soc. Resumed*, 1927, 2809–2814.
- 16 B. Tollens, *Handbuch der kohlenhydrate*, Vol. II, 3rd Edn. Leipzig, J. A. Barth, 1914, vol. 2.
- 17 H. Staudinger, Berichte Dtsch. Chem. Ges. B Ser., 1920, **53**, 1073–1085.
- 18 K. Freudenberg, Berichte Dtsch. Chem. Ges. B Ser., 1921, **54**, 767–772.
- 19 H. Staudinger and M. Lüthy, *Helv. Chim. Acta*, 1925, **8**, 41–64.
- 20 H. Staudinger, Berichte Dtsch. Chem. Ges. B Ser., 1926, **59**, 3019–3043.
- 21 G. Bourbonnais, "Structure de la cellulose", 2009, accessed on 30 June 2016 can be found under http://www2.cegep-ste
 - foy.qc.ca/profs/gbourbonnais/pascal/fya/chimcell/notesmolecules/glucides_3.htm,

- 22 M. Börjesson and G. Westman, in *Cellulose Fundamental Aspects and Current Trends*, eds. M. Poletto and H. L. Ornaghi, InTech, 2015, pp. 159–191.
- 23 H. Braconnot, Ann. Chim. Phys., 1833, 52, 290-294.
- 24 J. Pelouze, C. R. Hebd. Séances Acad. Sci., 1838, 7, 713–715.
- 25 J.-M. Michel, *Contribution à l'histoire industrielle des polymères en France*, Société Chimique de France, 2012, accessed on 30 June 2016 can be found under http://www.societechimiquedefrance.fr/contribution-a-l-histoire-industrielle-despolymeres-en-france-par-jean-marie-michel.
- 26 C. W. Saunders and L. T. Taylor, *J. Energ. Mater.*, 1990, **8**, 149–203.
- 27 G. Bertrand, Les découvertes scientifiques du comte de Chardonnet et l'invention de la soie artificielle discours prononcé ... à l'occasion du cinquantenaire de la soie artificielle, à Besançon, le jeudi 28 mai 1936, Gauthier-Villars, Paris, 1937, vol. Tome l.
- 28 P. Schutzenberger, CR Hébd Seances Acad Sci, 1865, 3, 485–486.
- 29 K. Balser, L. Hoppe, T. Eicher, M. Wandel, H.-J. Astheimer and H. Steinmeier, in *Ullmann's Encyclopedia of Industrial Chemistry*, Wiley-VCH Verlag GmbH & Co. KGaA, 2000.
- 30 W. Suida, *Monatshefte Für Chem. Verwandte Teile Anderer Wiss.*, 1905, **26**, 413–427.
- 31 H. Thielking and M. Schmidt, in *Ullmann's Encyclopedia of Industrial Chemistry*, Wiley-VCH Verlag GmbH & Co. KGaA, 2000.
- 32 D. Klemm, B. Philipp, T. Heinze, U. Heinze and W. Wagenknecht, in *Comprehensive Cellulose Chemistry*, Wiley-VCH Verlag GmbH & Co. KGaA, 1998, pp. 207–210.
- 33 R. J. Moon, A. Martini, J. Nairn, J. Simonsen and J. Youngblood, *Chem. Soc. Rev.*, 2011, **40**, 3941-3994.
- 34 T. Wüstenberg, *Cellulose and cellulose derivatives in the food industry: fundamentals and applications*, John Wiley & Sons, 2014.
- 35 D. Klemm, F. Kramer, S. Moritz, T. Lindström, M. Ankerfors, D. Gray and A. Dorris, *Angew. Chem. Int. Ed.*, 2011, **50**, 5438–5466.
- 36 N. Lavoine, J. Bras and I. Desloges, J. Appl. Polym. Sci., 2014, 131, 40106–40117.
- 37 N. Lavoine, I. Desloges and J. Bras, *Carbohydr. Polym.*, 2014, **103**, 528–537.
- 38 F. Hoeng, A. Denneulin and J. Bras, *Nanoscale*, 2016, **8**, 13131-13154.

- 39 J. Miller, "Nanocellulose state of the industry," can be found under http://www.tappinano.org/media/1114/cellulose-nanomaterials-production-state-of-the-industry-dec-2015.pdf, 2015.
- 40 E. Malmström and A. Carlmark, *Polym. Chem.*, 2012, **3**, 1702–1713.
- 41 A. Carlmark, E. Larsson and E. Malmström, Eur. Polym. J., 2012, 48, 1646–1659.
- 42 D. Roy, M. Semsarilar, J. T. Guthrie and S. Perrier, *Chem. Soc. Rev.*, 2009, **38**, 2046–2064.
- 43 K. Missoum, M. N. Belgacem and J. Bras, *Materials*, 2013, **6**, 1745–1766.
- 44 A. Carlmark and E. Malmström, J. Am. Chem. Soc., 2002, **124**, 900–901.
- 45 A. Carlmark and E. E. Malmström, *Biomacromolecules*, 2003, **4**, 1740–1745.
- 46 J. Lindqvist and E. Malmström, J. Appl. Polym. Sci., 2006, **100**, 4155–4162.
- 47 J. Lindqvist, D. Nyström, E. Östmark, P. Antoni, A. Carlmark, M. Johansson, A. Hult and E. Malmström, *Biomacromolecules*, 2008, **9**, 2139–2145.
- 48 S. Hansson, T. Tischer, A. S. Goldmann, A. Carlmark, C. Barner-Kowollik and E. Malmström, *Polym. Chem.*, 2012, **3**, 307–309.
- 49 E. Larsson, S. A. Pendergraph, T. Kaldéus, E. Malmström and A. Carlmark, *Polym. Chem.*, 2015, **6**, 1865–1874.
- 50 L. Q. Xu, K.-G. Neoh, E.-T. Kang and G. D. Fu, *J. Mater. Chem. A*, 2013, **1**, 2526.
- 51 W. Wu, J. Li, W. Zhu, Y. Jing and H. Dai, *Fibers Polym.*, 2016, **17**, 495–501.
- 52 F. Tang, L. Zhang, Z. Zhang, Z. Cheng and X. Zhu, *J. Macromol. Sci. Part A*, 2009, **46**, 989–996.
- 53 M. Barsbay, O. Güven, T. P. Davis, C. Barner-Kowollik and L. Barner, *Polymer*, 2009, **50**, 973–982.
- 54 D. Roy, J. T. Guthrie and S. Perrier, *Macromolecules*, 2005, **38**, 10363–10372.
- 55 P. de Cuadro, T. Belt, K. S. Kontturi, M. Reza, E. Kontturi, T. Vuorinen and M. Hughes, React. Funct. Polym., 2015, **90**, 21–24.
- 56 O. Cusola, N. Tabary, M. N. Belgacem and J. Bras, J. Appl. Polym. Sci., 2013, 129, 604–613.
- 57 K. Lee, J. Hwang and Y. Ahn, *Bull. Korean Chem. Soc.*, 2014, **35**, 1545–1548.
- 58 L. V. A. Gurgel, O. K. Júnior, R. P. de F. Gil and L. F. Gil, *Bioresour. Technol.*, 2008, **99**, 3077–3083.

- 59 G.-L. Zhao, J. Hafrén, L. Deiana and A. Córdova, *Macromol. Rapid Commun.*, 2010, **31**, 740–744.
- 60 M. Dietrich, G. Delaittre, J. P. Blinco, A. J. Inglis, M. Bruns and C. Barner-Kowollik, *Adv. Funct. Mater.*, 2012, **22**, 304–312.
- 61 T. Tischer, C. Rodriguez-Emmenegger, V. Trouillet, A. Welle, V. Schueler, J. O. Mueller, A. S. Goldmann, E. Brynda and C. Barner-Kowollik, *Adv. Mater.*, 2014, 26, 4087–4092.
- 62 H. Lönnberg, Q. Zhou, H. Brumer, T. T. Teeri, E. Malmström and A. Hult, *Biomacromolecules*, 2006, **7**, 2178–2185.
- 63 S. A. Pendergraph, G. Klein, M. K. G. Johansson and A. Carlmark, *RSC Adv.*, 2014, **4**, 20737–20743.
- 64 L. Carlsson, E. Malmström and A. Carlmark, *Polym. Chem.*, 2012, **3**, 727-733.
- 65 T. Tischer, T. K. Claus, K. K. Oehlenschlaeger, V. Trouillet, M. Bruns, A. Welle, K. Linkert, A. S. Goldmann, H. G. Börner and C. Barner-Kowollik, *Macromol. Rapid Commun.*, 2014, 35, 1121–1127.
- 66 T. Tischer, T. K. Claus, M. Bruns, V. Trouillet, K. Linkert, C. Rodriguez-Emmenegger, A. S. Goldmann, S. Perrier, H. G. Börner and C. Barner-Kowollik, *Biomacromolecules*, 2013, 14, 4340–4350.
- 67 G. Delaittre, M. Dietrich, J. P. Blinco, A. Hirschbiel, M. Bruns, L. Barner and C. Barner-Kowollik, *Biomacromolecules*, 2012, **13**, 1700–1705.
- 68 F. Deiss, W. L. Matochko, N. Govindasamy, E. Y. Lin and R. Derda, *Angew. Chem. Int. Ed.*, 2014, **53**, 6374–6377.
- 69 A. Yu, J. Shang, F. Cheng, B. A. Paik, J. M. Kaplan, R. B. Andrade and D. M. Ratner, *Langmuir*, 2012, **28**, 11265–11273.
- 70 N. Jirakittiwut, N. Panyain, T. Nuanyai, T. Vilaivan and T. Praneenararat, *RSC Adv.*, 2015, **5**, 24110–24114.
- 71 E. hadji B. Ly, J. Bras, P. Sadocco, M. N. Belgacem, A. Dufresne and W. Thielemans, *Mater. Chem. Phys.*, 2010, **120**, 438–445.
- 72 V. R. Botaro and A. Gandini, *Cellulose*, 1998, **5**, 65–78.
- 73 A. J. de Menezes, D. Pasquini, A. A. da S. Curvelo and A. Gandini, *Carbohydr. Polym.*, 2009, **76**, 437–442.
- 74 B. Yang and W. Wu, *React. Funct. Polym.*, 2013, **73**, 1553–1558.

- 75 J. Credou, R. Faddoul and T. Berthelot, RSC Adv., 2014, 4, 60959–60969.
- 76 A. S. Goldmann, T. Tischer, L. Barner, M. Bruns and C. Barner-Kowollik, *Biomacromolecules*, 2011, **12**, 1137–1145.
- 77 T. Tischer, A. S. Goldmann, K. Linkert, V. Trouillet, H. G. Börner and C. Barner-Kowollik, *Adv. Funct. Mater.*, 2012, **22**, 3853–3864.
- 78 P. Schroll, C. Fehl, S. Dankesreiter and B. König, *Org. Biomol. Chem.*, 2013, **11**, 6510–6514.
- 79 M. Conradi, G. Ramakers and T. Junkers, *Macromol. Rapid Commun.*, 2016, **37**, 174–180.
- 80 C. Tyagi, L. K. Tomar and H. Singh, *J. Appl. Polym. Sci.*, 2009, **111**, 1381–1390.
- 81 B. Ly, M. N. Belgacem, J. Bras and M. C. Brochier Salon, *Mater. Sci. Eng. C*, 2010, **30**, 343–347.
- 82 H. Koga, T. Kitaoka and A. Isogai, *J. Mater. Chem.*, 2011, **21**, 9356-9361.
- 83 S. Wang, L. Ge, L. Li, M. Yan, S. Ge and J. Yu, *Biosens. Bioelectron.*, 2013, **50**, 262–268.
- 84 C. Tyagi, L. K. Tomar, P. Kumar, V. Pillay and H. Singh, *Anal. Methods*, 2014, **6**, 7374–7383.
- 85 H. I. A. S. Gomes and M. G. F. Sales, *Biosens. Bioelectron.*, 2015, **65**, 54–61.
- 86 L. Cen, K. G. Neoh and E. T. Kang, *Langmuir*, 2003, **19**, 10295–10303.
- 87 M. Barsbay, O. Güven, M. H. Stenzel, T. P. Davis, C. Barner-Kowollik and L. Barner, *Macromolecules*, 2007, **40**, 7140–7147.
- 88 R. Bongiovanni, E. Zeno, A. Pollicino, P. M. Serafini and C. Tonelli, *Cellulose*, 2010, **18**, 117–126.
- 89 M. Barsbay, Y. Kodama and O. Güven, *Cellulose*, 2014, **21**, 4067–4079.
- 90 R. Bongiovanni, S. Marchi, E. Zeno, A. Pollicino and R. R. Thomas, *Colloids Surf. Physicochem. Eng. Asp.*, 2013, **418**, 52–59.
- 91 A. Böhm, M. Gattermayer, C. Trieb, S. Schabel, D. Fiedler, F. Miletzky and M. Biesalski, *Cellulose*, 2012, **20**, 467–483.

Chapitre 2 Préparation d'un nouveau matériau pour le stockage d'information

I Introduction

Les premiers travaux réalisés au cours de cette thèse traitent du développement d'une nouvelle méthode d'écriture à la surface de la cellulose permettant ainsi le stockage d'informations à la surface de ce matériau.

Inspiré par les travaux de Sallé¹ sur l'utilisation des propriétés de photodimérisation réversible des coumarines pour le stockage d'information (Figure 1b) et les travaux de König² sur le greffage de coumarines à la surface de la cellulose (Figure 1a), nous avons décidé de réaliser la fonctionnalisation covalente du papier avec cette molécule.

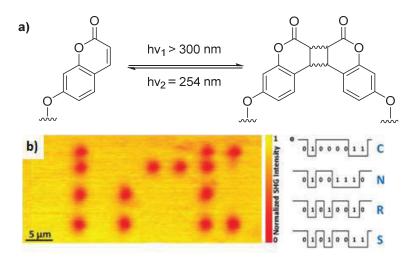


Figure 1 a) Principe de la photodimerisation réversible de la coumarine b) Stockage d'informations binaires à la surface d'un film de PMMA reproduit des travaux de Sallé¹

Dans un premier temps, nous avons réalisé des études de chimie théorique afin de valider la possibilité de réaliser la dimérisation des coumarines à la surface de la cellulose. Après avoir réalisé la fonctionnalisation du papier *via* une réaction d'estérification, les propriétés de photodimérisation du matériau ainsi obtenu ont été étudiées. Le matériau obtenu s'est révélé être très robuste et réversible puisqu'il a été possible de réaliser plusieurs cycles de Dimérisation/Rétrocyclisation.

31

- 1. K. Iliopoulos, O. Krupka, D. Gindre and M. Sallé, *J. Am. Chem. Soc.*, 2010, **132**, 14343-14345.
- 2. P. Schroll, C. Fehl, S. Dankesreiter and B. König, *Org. Biomol. Chem.*, 2013, **11**, 6510-6514.

Enfin, l'utilisation d'un photomasque a permis de réaliser la réaction de dimérisation des coumarines de manière spatialement contrôlée permettant ainsi l'encodage d'informations à la surface du matériau. Dans un premier temps, nous avons réalisé la photoimpression covalente du logo de l'université de Nantes puis nous avons inscrit à la surface de ce matériau un motif plus complexe, un QRCode (Figure 2).

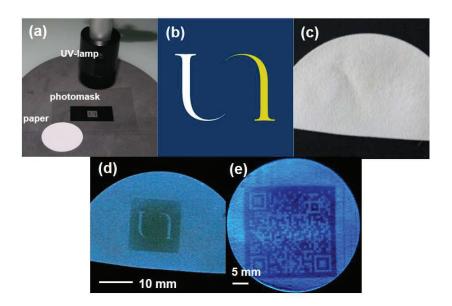


Figure 2 Illustration du système de photoimpression covalente

Ces travaux ont fait l'objet, d'une publication dans le journal *Chemical Communications*³ (ci-après) et du dépôt d'un brevet intitulé «*Méthode d'écriture réversible d'un motif sur un élément cellulosique et produit cellulosique associé*»⁴

³²

^{3.} M. d'Halluin, J. Rull-Barrull, E. Le Grognec, D. Jacquemin, F.-X. Felpin, *Chem. Commun.* **2016**, *52*, 7672–7675.

^{4.} M. d'Halluin, J. Rull-Barrull, E. Le Grognec, D. Jacquemin, F.-X. Felpin. Date of filing 10.02.16, Application FR 16/00227

II Writing and erasing hidden optical information on covalently modified cellulose paper

An unprecedented strategy for preparing a photoresponsive cellulose paper enabling the storage of short-lived optical data by covalent photopatterning is disclosed. An ab initio design hinting that the covalent grafting of coumarins on the paper could yield valuable photoresponsive units was first performed. Second, a light sensitive paper that can be reversibly altered upon irradiation at a specific wavelength was prepared by covalent surface functionalization with coumarins. Third, the validity of this strategy is demonstrated with the photolithography of several gripping patterns such as a dynamic QR Code.

Counterfeiting is a major economic problem since it accounts for ca. 7% of world trade with a worldwide annual cost estimated to reach \$600 billion. Cellulose paper is one of the most prevalent media in manufacturing and has been widely used for labelling, packing and bills. Many of these applications require anticounterfeit technologies, for tracking through both the production and the distribution chain.¹ Since a single technology cannot provide a full protection against counterfeiting, many approaches have been developed for cellulosic materials and the most widely used include holograms, bar codes, intaglio printing, special inks, RFID tags, security threads, microtaggants and watermarks.².³ All these technologies, visible to naked-eyes, negatively affect the paper aspect, and, to the exception of RFID tags and bar codes, do not allow identification and traceability since information cannot be encoded.

Storing hidden (covert) information not affecting the paper aspect is therefore of great importance for security, anticounterfeiting and tracking applications. To date, hidden writing on cellulose paper has been mostly addressed with the use of photoluminescent inks. 4-7 However, irrespective of the complexity of the inks developed, such patterning relies on physical adsorption processes and the ability of cellulose to retain physisorbed inks can significantly vary. In particular, many

adsorbed patterns can be easily erased or degraded by solvents. Moreover, most invisible inks can be easily duplicated because of their relatively low cost.

Developing hidden writing with covalent modifications of cellulose paper is clearly of astonishing interest as it gives access to more robust and tamper-proof materials, still without affecting the physical appearance of the paper. In the context of short-lived data storage, an even more ambitious objective is the development of a material allowing for reversible properties upon external stimuli for erasing and rewriting, still through covalent modifications.

Examples of spatially-resolved functionalizations by a covalent approach on cellulose paper are rare 9-14 and molecularly imprinted information on cellulose paper by covalent means that are reversible for erasing and rewriting has never been reported yet, a gap that the present contribution fills, paving the way to a new anti-counterfeiting technology for cellulose paper. Here, we report an unprecedented strategy, raised as proof of concept, allowing the covalent photopatterning of a smart paper device for hidden and reversible optical data storage.

Modulating the properties of cellulose paper on demand for writing-erasing-rewriting sequences, requires a reversible stimulus-responsive material. We considered that designing a reversible photoresponsive cellulose paper would be particularly well suited for data storage since light allows on demand time- and spatially-resolved irradiation. Several reversible photoresponsive reactions are known, including [2+2] cycloadditions of coumarins, or cinnamates, [4+4] cycloadditions of anthracenyl derivatives and the ring opening-ring closing of photochromic compounds such as diarylethenes and spiropyrans.

We have selected coumarins as the photoresponsive molecules as their ability to photodimerize to cyclobutane dimers through a [2+2]-cycloaddition upon irradiation at $\lambda > 300$ nm and to cycloreverse upon exposure at shorter wavelength (< 280 nm) is well-known and already led to several applications

including self-healing polymers, 20 3D data storage, 21,22 and controlled drug delivery. 23,24 While the use of coumarins has already been envisaged for the preparation of photoresponsive nanocrystalline cellulose, 25,26 the grafting of cellulose paper with photoresponsive coumarin for short-lived optical data storage has not been reported to date.

In solution, coumarins efficiently photodimerize, producing a blend of four possible cyclobutane isomers.²⁷ While the optical changes in solution are well known, once grafted on a solid support, the situation might become more complex. On the one hand, the conformational constraints become more important, so that the spatial proximity of the two monomers, required for [2+2]-photoaddition, is not granted. On the other hand, the inhomogeneity of the medium could yield broader absorption bands, making the distinction between the monomers and dimers more challenging.

The design of a photoresponsive cellulose paper allowing reversible processes requires a subtle combination of factors allowing the facile dimerization, a good stability over successive processes and a significant contrast between the spectral signatures of the two forms. The nature of the linker used for the grafting is an important factor. We reasoned that a short linker of 3-4 atoms would confer flexibility to the grafted groups, allowing spatial arrangement for the [2+2]-cycloaddition. To avoid a lengthy experimental campaign, we first adopted a computational approach (see the ESI for details).

We found that significant p-p* interactions between two dyes are possible when two coumarin monomers are attached to two consecutive glucose units or with a one-on-two pattern (Fig. 1), the latter allowing a better organization for dimerization. The modelling predicts that while the 7-OMe-coumarin presents a vertical transition at ca. 292 nm a significant broadening appears after grafting due to the coumarin-coumarin and coumarin-cellulose interactions: the top structure of Fig. 1 presents a main peak at 294 nm and smaller absorptions at larger wavelengths (314 and 304 nm), whereas the bottom structure presents strong vertical absorptions at 306 and 294 nm.

For the one-on-two pattern, we could find several possible thermodynamically stable dimers, the most stable being displayed in Fig. 2. Interestingly this [2+2] product is only 6.6 kcal.mol⁻¹ less stable than the parent non-dimerized derivative (bottom of Fig. 1). In gas-phase, the difference attains ca. 7.0 kcal.mol⁻¹, indicating that grafting does not induce large variations of the relative energies of the two forms. For the structure showed in Figure 2, theory predicts several dipole-allowed absorptions in the 260-230 nm range. In short, the theoretical investigation predicted that the dimerization of coumarin units was thermodynamically feasible using an acetate linker, and that the hallmark spectral signatures of the coumarins and their dimers are preserved despite band broadening.

As stated in the introduction, covalent surface modifications of cellulose paper 28 - 32 have been much less studied than functionalisation by adsorption means mainly because the low reactivity of the surface hydroxyl groups makes the covalent approach particularly challenging. In order to breaks hydrogen bonds, making hydroxyl groups more reactive to chemical functionalization, the cellulose paper was treated with an aqueous NaOH solution (10 wt.-%) for 24 hours at 25 $^{\circ}$ C. 33,34

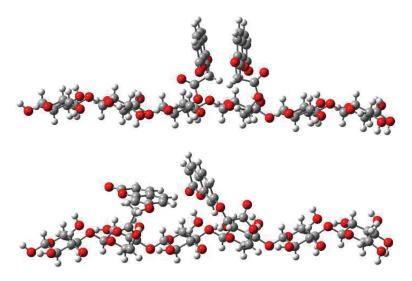


Fig. 1 Selected typical DFT geometries for two coumarins attached to cellulose with a consecutive (top) or one-on-two (bottom) patterns (see the ESI for details).

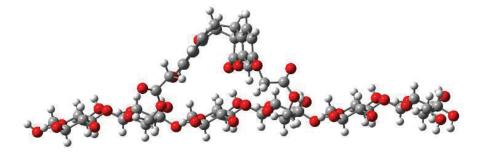


Fig. 2 A possible geometry for a one-on-two dimer.

Our strategy leans on the grafting of spatially close coumarin units through an esterification process. To achieve this goal, 7-hydroxycoumarin **1**, functionalized with a linker bearing an acid chloride function, was prepared in 3 steps from inexpensive commercially available starting materials (Scheme 1).²⁴ The grafting of paper with acid chloride **4** provided the expected coumarin-functionalized cellulose paper.

Paper-grafted coumarins

Scheme 1. Preparation of the photoresponsive paper.

A high degree of substitution in the range of 0.45-0.5 was estimated by X-ray photoelectron spectroscopy (XPS), indicating that 5 hydroxyl groups were functionalized with coumarin units every ten glucose units. The successful grafting was confirmed by UV-visible spectroscopy with the apparition of the characteristic absorbance band of 7-alkoxycoumarins with a maximum at 324 nm (Fig. 3). The broad bandwidth is attributed to the presence of several conformations as explained above.

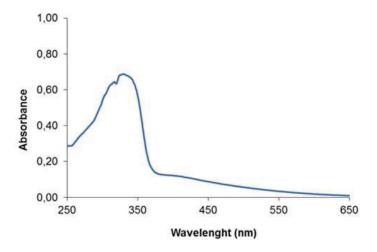


Fig. 3 UV-Visible spectrum of paper-grafted coumarins

To cross-evidence the successful grafting, we recorded the FT-IR spectra of both pristine and functionalized papers (Fig. 4). Two significant bands appeared on the IR spectrum of the functionalized paper (Fig. 4b). The sharp signal in the region of carbonyl groups presents two maxima at 1711 an 1727 cm⁻¹ accounting for the C=O stretching of the ester linkage and lactone ring respectively, while the band at 1612 cm⁻¹ is assigned to the C=C stretching frequency. We repeated the functionalization step on a control sample using carboxylic acid **3** that is expected to be unable to covalently link to cellulose, instead of acid chloride **4**. Analysis of the cellulose surface after washing revealed no band in the 1600-1700 cm⁻¹ region, ruling out adsorption of coumarin chromophores in the cellulose fibre networks (Fig. 4).

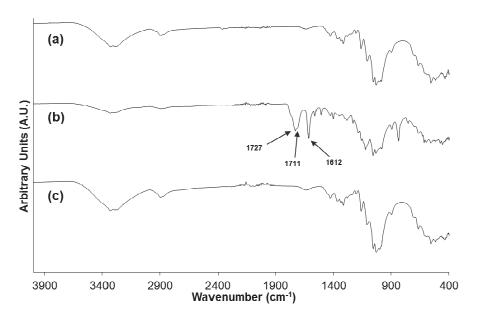


Fig. 4 FT-IR spectra of (a) pristine paper, (b) functionalized paper with (4), (c) paper stirred with coumarin (3)

Preserving the physical integrity of the material is one of the main requirements to obtain smart packing or label. With our approach, requiring only one chemical step, the paper was not wrinkled and the whiteness was not altered. The morphology of the fibres was also unaffected, as evidenced by scanning electron microscopy (SEM) images (Fig. 5).

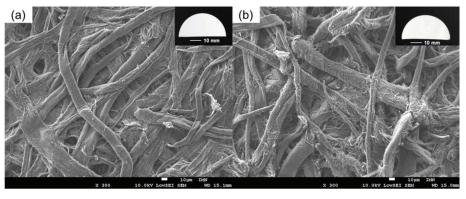


Fig. 5 SEM images of (a) pristine paper, (b) paper-grafted coumarins with the corresponding photograph as inset.

The structural evolution and the surface composition were both investigated by XPS, (Fig. 6). Full scan spectra of both pristine and grafted cellulose papers

showed carbon and oxygen elements only, attesting that washing steps were successful in removing unreacted chemicals and solvents. Important changes can be seen on the C1s spectrum of the grafted paper with a significant increase of the peak accounting for C-C bonds at 285.1 eV and the apparition of a signal at 289.1 eV attributed to carbonyl functions. These results confirm the successful grafting of cellulose paper with coumarin 4.

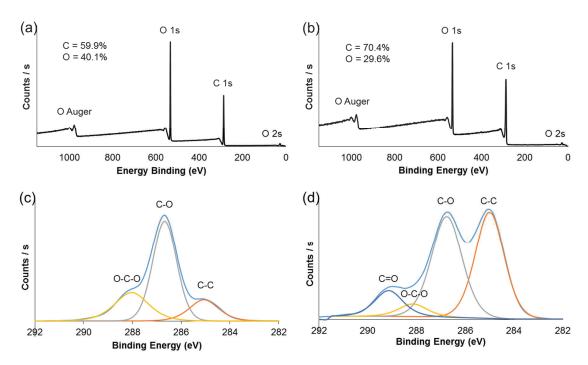


Fig. 6 Survey scan spectra of (a) pristine paper, (b) paper-grafted coumarins.

High resolution C1s spectra of (c) pristine paper and (d) paper-grafted coumarins

The UV diffuse reflectance spectrum of paper-grafted coumarins were recorded as a function of time upon irradiation at λ = 340 nm (Fig. 7). The sharp decrease of the absorption band at ca. 330 nm indicated the successful photodimerization of coumarins.

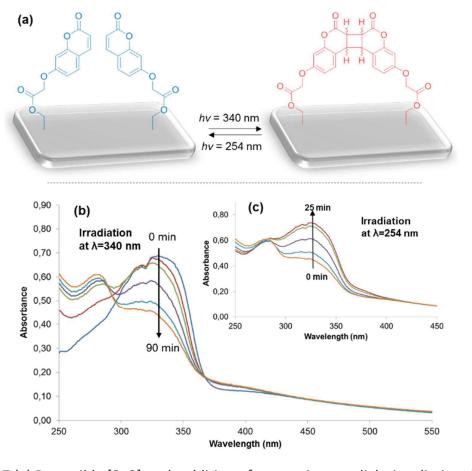


Fig. 7 (a) Reversible [2+2]-cycloaddition of coumarin upon light irradiation. (b) Decrease of the absorbance of the paper-grafted coumarins as a function of time upon irradiation at 340 nm and (c) the corresponding reversible process upon irradiation at 254 nm.

The degree of dimerization was estimated to attain ca. 35%. Two factors can limit the degree of dimerization: (a) the uncomplete conversion of the reaction at room temperature without any solvent or catalyst and, (b) the spatial distance between some coumarin units preventing their dimerization. Upon extended irradiation times no further significant evolutions were noticed. As expected, there is not a proper isobestic point in Fig. 7a though the curves crosses at ca. 290 nm, which indicates that several species are in equilibrium. Importantly, irradiation of the photopatterned cellulose paper at 254 nm resulted in the reversibility of this process through the photocleavage of the coumarin dimers, regenerating the absorption band of the coumarins within 25 minutes (Fig. 7c).

We observed that the photocleavage at 254 nm proceeded faster than the photodimerization at 340 nm. A fatigue resistance test of the photoresponsive material was conducted over 3 cycles of writing-erasing at 340 and 254 nm respectively (Fig. 8).

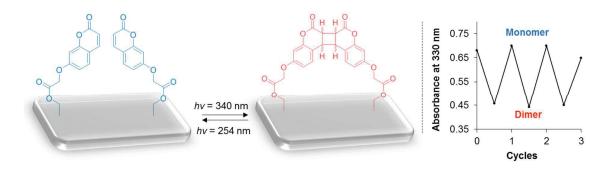


Fig. 8 Fatigue test resistance of the patterned paper upon alternate irradiation at 340 (decrease in absorbance) and 254 nm (increase in absorbance)

Impressively, the material showed a good resistance to successive irradiations since the absorbance was almost fully restored after the third cycle. This result implies that both the writing and the erasing steps can be successfully performed at least three times.

Photopatterning of the cellulose paper was achieved by covering the photoresponsive surface with a photomask resulting in the irradiation of predetermined areas (Fig. 9a). The storage of optical data was performed using a mercury-xenon lamp equipped with a filter at 340 nm. Experimentally, the irradiation of a piece of cellulose paper was carried out in the dry state, without any solvent nor catalyst.

We patterned the paper with the logo of our University (Fig. 9b). While the pattern cannot be discerned under visible light (Fig. 9c), the spatially-resolved fluorescent logo is visible upon interrogation using a UV lamp at 365 nm (Fig. 9d). We further pushed our photopatterning for the storage of more complex

informations under the form of an elaborated Quick Response Code (QR Code) as depicted in Fig. 9e.

QR codes are used in a plethora of applications including product tracking, identification and marketing due to their high storage capacities and fast readabilities. Interestingly, we were able to pattern our photoresponsive cellulose paper with a dynamic QR Code readable with a smart phone (see video in ESI). The precision lithography allows QR Code patterns with square dots of ca. 500 μm .

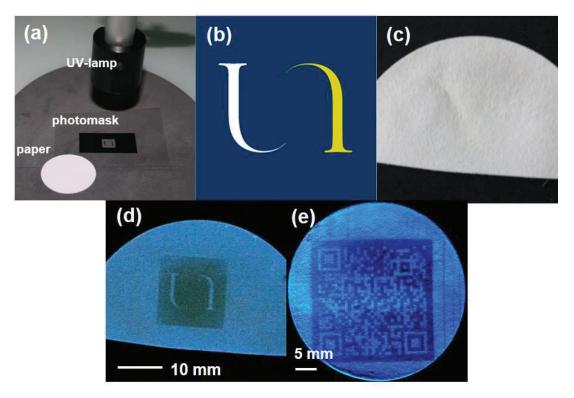


Fig. 9 Illustration of the photopatterning process with (a) Photograph of the custom-built photopatterning equipment, (b) Original logo of the University of Nantes, (c) Photograph of the patterned paper, (d) Logo of the University of Nantes recorded on the cellulose paper and revealed with a UV lamp at 365 nm and (d) Photograph of the QR Code pattern revealed with a UV lamp.

In summary, we designed the first photoresponsive cellulose paper allowing the writing and erasing of hidden optical data. Our strategy, based on the reversible

light-mediated dimerization of coumarin units covalently grafted to the paper surface, allows writing complex patterns such as a QR Code. This work is an important breakthrough in paper patterning since we unveiled the first approach allowing hidden and reversible optical data storage through covalent means, while patterning by adsorption processes were the standard from literature precedents. We believe that this unprecedented photoresponsive biomaterial would find huge applications in smart devices for hidden optical data storage especially for tracking and anti-counterfeiting applications.

MdH thanks the "Région des Pays de la Loire" and the CNRS for the grant. Denis Loquet and François-Xavier Lefèvre (University of Nantes) were gratefully acknowledged for Elemental and SEM analyses. D.J. acknowledges the European Research Council (ERC) and the Région des Pays de la Loire for financial support in the framework of a Starting Grant (Marches-278845) and the LUMOMAT project, respectively. DJ and FXF are members of the Institut Universitaire de France (IUF).

Notes and references

- 1 R. Y. Shah, P. N. Prajapati and Y. K. Agrawal, *J. Adv. Pharm. Technol. Res.*, 2010, **1**, 368-373.
- 2 R. L. V. Renesse, ECOS 97, European Conference on Security and Detection, 1997.
- 3 A. K. Deisingh, *Analyst*, 2005, **130**, 271-279.
- 4 M. You, J. Zhong, Y. Hong, Z. Duan, M. Lin and F. Xu, *Nanoscale*, 2015, **7**, 4423-4431.
- 5 P. Kumar, J. Dwivedi and B. K. Gupta, *J. Mat. Chem. C*, 2014, **2**, 10468-10475.
- 6 L. L. da Luz, R. Milani, J. F. Felix, I. R. B. Ribeiro, M. Talhavini, B. A. D. Neto, J. Chojnacki, M. O. Rodrigues and S. A. Júnior, ACS Appl. Mater. Interfaces, 2015, 7, 27115-27123.
- J. Andres, R. D. Hersch, J.-E. Moser and A.-S. Chauvin, *Adv. Funct. Mat.*, 2014, 24, 5029-5036.
- 8 J. Finnell, *Library & Archival Security*, 2011, **24**, 19-24.
- 9 M. Dietrich, G. Delaittre, J. P. Blinco, A. J. Inglis, M. Bruns and C. Barner-Kowollik, *Adv. Funct. Mater.*, 2012, **22**, 304-312.
- 10 A. Yu, J. Shang, F. Cheng, B. A. Paik, J. M. Kaplan, R. B. Andrade and D. M. Ratner, *Langmuir*, 2012, **28**, 11265-11273.
- P. Schroll, C. Fehl, S. Dankesreiter and B. Konig, *Org. Biomol. Chem.*, 2013, **11**, 6510-6514.
- T. Tischer, T. K. Claus, M. Bruns, V. Trouillet, K. Linkert, C. Rodriguez-Emmenegger, A. S. Goldmann, S. Perrier, H. G. Börner and C. Barner-Kowollik, *Biomacromolecules*, 2013, **14**, 4340-4350.
- T. Tischer, T. K. Claus, K. K. Oehlenschlaeger, V. Trouillet, M. Bruns, A. Welle, K. Linkert, A. S. Goldmann, H. G. Börner and C. Barner-Kowollik, *Macromol. Rapid Commun.*, 2014, **35**, 1121-1127.
- T. Tischer, C. Rodriguez-Emmenegger, V. Trouillet, A. Welle, V. Schueler, J. O. Mueller, A. S. Goldmann, E. Brynda and C. Barner-Kowollik, *Adv. Mater.*, 2014, 26, 4087-4092.
- S. R. Trenor, A. R. Shultz, B. J. Love and T. E. Long, *Chem. Rev.*, 2004, **104**, 3059-3078.

- D. Bassani, in *CRC Handbook of Organic Photochemistry and Photobiology*, eds.
 W. M. Horspool and F. Lenci, CRC Press, 2nd edn., 2003, vol. 1 & 2, pp. 20/21-20/20.
- J.-F. Xu, Y.-Z. Chen, L.-Z. Wu, C.-H. Tung and Q.-Z. Yang, *Org. Lett.*, 2013, **15**, 6148-6151.
- 18 M. Irie, T. Fukaminato, K. Matsuda and S. Kobatake, *Chem. Rev.*, 2014, **114**, 12174-12277.
- 19 R. Klajn, Chem. Soc. Rev., 2014, 43, 148-184.
- 20 B. Kiskan and Y. Yagci, *J. Polym. Sci. Pol. Chem.*, 2014, **52**, 2911-2918.
- 21 K. Iliopoulos, O. Krupka, D. Gindre and M. Sallé, *J. Am. Chem. Soc.*, 2010, **132**, 14343-14345.
- 22 M. V. S. N. Maddipatla, D. Wehrung, C. Tang, W. Fan, M. O. Oyewumi, T. Miyoshi and A. Joy, *Macromolecules*, 2013, **46**, 5133-5140.
- 23 N. K. Mal, M. Fujiwara and Y. Tanaka, *Nature*, 2003, **421**, 350-353.
- 24 J. W. Chung, K. Lee, C. Neikirk, C. M. Nelson and R. D. Priestley, *Small*, 2012, 8, 1693-1700.
- 25 M. V. Biyani, C. Weder and E. J. Foster, *Polym. Chem.*, 2014, **5**, 5501-5508.
- O. Grigoray, H. Wondraczek, S. Daus, K. Kühnöl, S. K. Latifi, P. Saketi, P. Fardim, P. Kallio and T. Heinze, *Macromol. Mater. Eng.*, 2015, **300**, 277-282.
- X. Yu, D. Scheller, O. Rademacher and T. Wolff, *J. Org. Chem.*, 2003, **68**, 7386-7399.
- 28 M. Barsbay, O. Güven, T. P. Davis, C. Barner-Kowollik and L. Barner, *Polymer*, 2009, **50**, 973-982.
- A. S. Goldmann, T. Tischer, L. Barner, M. Bruns and C. Barner-Kowollik, *Biomacromolecules*, 2011, **12**, 1137-1145.
- 30 G. Delaittre, M. Dietrich, J. P. Blinco, A. Hirschbiel, M. Bruns, L. Barner and C. Barner-Kowollik, *Biomacromolecules*, 2012, **13**, 1700-1705.
- 31 S. Hansson, T. Tischer, A. S. Goldmann, A. Carlmark, C. Barner-Kowollik and E. Malmstrom, *Polym. Chem.*, 2012, **3**, 307-309.
- J. Rull-Barrull, M. d'Halluin, E. Le Grognec and F.-X. Felpin, Chem. Commun., 2016, 52, 2525-2528.

- 33 M. Barsbay, O. Güven, M. H. Stenzel, T. P. Davis, C. Barner-Kowollik and L. Barner, *Macromolecules*, 2007, **40**, 7140-7147.
- J. Rull-Barrull, M. d'Halluin, E. Le Grognec and F.-X. Felpin, *Chem. Commun.*, 2016,52, 6569-6572.

III Partie expérimentale

Material and methods

All commercial solvents and reagents were used as received from Sigma-Aldrich, Fischer Scientific Ltd, Alfa Aesar. Whatman® grade 6 filter paper (42.5 mm \emptyset) was used as cellulose source. ¹H and ¹³C, recorded at 400 MHz, 100 MHz, respectively, were performed on a Bruker Advance 400. Proton chemical shifts were internally referenced to the residual proton resonance in DMSO (2.50 ppm). Carbon chemical shifts were internally referenced to the deuterated solvent signals in DMSO (39.52 ppm). Melting points were recorded on a Stuart Scientific 7SMP3 apparatus. FT-IR spectra were recorded on a Bruker Tensor 27 spectrometer with ATR technic. HRMS in ESI mode were recorded on a LTQ-Orbitrap (ThermoFisher Scientific) at the ENV of Nantes. Scanning electron microscopy (SEM) images were recorded with a JEOL 7600 F at the "Centre de microcaractérisation de l'IMN, Université de Nantes". X-Ray diffraction (XRD) patterns were recorded on a Bruker D8 Advance X-Ray Diffractometer. X-ray photoelectron spectroscopy was performed on a ThermoFisher Scientific K-ALPHA spectrometer was used for disk surface analysis with a monochromatized AlK α source (hv = 1486.6 eV) and a 200 micron spot size. A pressure of 10^{-7} Pa was maintained in the chamber during analysis. The full spectra (0-1150eV) were obtained at a constant pass energy of 200eV and high resolution spectra at a constant pass energy of 40 eV. Charge neutralization was required for all insulating samples. High resolution spectra were fitted and quantified using the AVANTAGE software provided by ThermoFisher Scientific. Thermogravimetric analysis (TGA) profiles were obtained between 25 and 600°C using a Netzsch STA-449 F3 TGA/DSC at a heating rate of 5°C min⁻¹. UV-visible absorption spectra were recorded using a Varian Model Cary 5E spectrophotometer, using an integrating sphere DRA 2500. Photodimerization reaction was performed using a white light source Hg-Xe lamp (Hamamatsu-LC8) equipped with a narrow bandpass filter at 340 nm (12 nm fwmh) and a 6W UV lamp working at 254 nm. QR Code was read with a Samsung Galaxy S5 using QR Code Reader application from Scan,Inc. available for free on Google Play.

Preparation of coumarin derivatives

Preparation of ethyl 2-((2-oxo-2H-chromen-7-yl)oxy)acetate (2)¹

7-Hydroxycoumarin (5 g, 27.8 mmol) and potassium carbonate (3.8 g, 27,8 mmol) were placed in a 100 ml round bottom flask containing 25 ml of Acetone. Then ethyl-2-bromoacetate (3.4 ml, 30.5 mmol) was added dropwise. The reaction mixture was refluxed for 16 h under N₂. The reaction mixture was then cooled to room temperature. After salt filtration, acetone was evaporated and the product was recrystallized from ethanol giving pale yellow needles (5.6 g, 81%). mp. 114-116 °C [lit.¹ 113-115 °C]. 1 H NMR (400 MHz, DMSO,) δ 7.99 (d, 1H, J = 9.5 Hz), 7.64 (d, 1H, J = 8.4 Hz), 7.0-6.96 (m, 2H), 6.31 (d, 1H, J = 9.5 Hz), 4.92 (s, 1H), 4.19 (q, 2H, J = 7.1 Hz), 1.22 (t, 3H, J = 7.1 Hz); 1 3C NMR (100 MHz, DMSO) δ 168.1, 160.6, 160.1, 155.1, 144.1, 129.5, 112.9 (2C), 112.6, 101.5, 65.0, 60.8, 14.0; IR (ATR) v 3077, 2991, 1708, 1611, 1561, 1509, 1454, 1400, 1376, 1350, 1285, 1264, 1221, 1192, 1157, 1124, 1069, 1017, 981, 897, 861, 840, 811, 755, 725, 689, 630, 617, 588, 477, 460 cm⁻¹; HRMS (ESI) calcd for C₁₃H₁₃O₅ [M+H⁺]: 249.0757, found: 249.0757.

Preparation of 2-((2-oxo-2H-chromen-7-yl)oxy)acetic acid (3)¹

Compound **2** (5 g, 20 mmol) and sodium hydroxide (11.2 g, 280 mmol) were dissolved in 500 mL of water/dioxane (4/6 v/v). The solution was stirred overnight at room temperature, then the solvent was evaporated under reduced pressure. The yellow residue was dissolved in 50 mL of water and acidified with concentrated hydrochloric acid under ice cooling. The white precipitate was collected by filtration, washed with water, recrystallized from ethanol and dried in vacuum at room temperature giving a white solid (3.4 g, 77%). mp. 213-217 °C [lit. 209-213 °C].

¹H NMR (400 MHz, DMSO,) δ 13.09 (bs, 1H), 7.98 (d, 1H, J = 9.5 Hz), 7.64 (m, 1H), 6.97-6.94 (m, 2H), 6.30 (d, 1H, J = 9.5 Hz), 4.82 (s, 1H); ¹³C NMR (100 MHz, DMSO) δ 169.5, 160.8, 160.1, 155.1, 144.2, 129.4, 112.8, 112.7, 112.5, 101.5, 64.8; IR (ATR) ν 3079, 2908, 2791, 2591, 1708, 1608, 1561, 1511, 1491, 1459, 1430, 1418, 1403, 1350, 1275, 1250, 1208, 1156, 1123, 1072, 99, 895, 832, 767, 751, 728, 671, 627, 617, 552, 518, 478, 463, 453, 399, 395 cm⁻¹; HRMS (ESI) calcd for C₁₁H₈O₅Na [M+Na⁺]: 243.0269, found: 243.0272.

Preparation of 2-((2-oxo-2H-chromen-7-yl)oxy)acetyl chloride (4)²

Carboxylic acid 3 (880 mg, 4 mmol) and a catalytic amount of DMF were suspended in chloroform (30 ml). Then, thionyl chloride (2.8 ml, 38 mmol) was added dropwise. The reaction mixture was refluxed for 2 h under N_2 . Then the solution was evaporated under reduce pressure and dry toluene was added to remove remaining thionyl chloride. Acyl chloride 4 was obtained as a white solid and was used directly without further purification.

Preparation of cellulosic material

General procedure for the pre-treatment of cellulose paper³

Five piece of cellulose filter paper (approx. 750 mg) were dispersed in 250 ml of 10% NaOH. This mixture is then shacked for 24 h on a shacking device. The cellulose samples were then washed 6 times with 50 ml of EtOH and stored in EtOH.

General procedure for the preparation of paper-grafted coumarins⁴

After being washed 2 times with 10 ml pyridine, a piece of pretreated cellulose paper (approx. 145 mg, 0.9 mmol) was immersed in 25 ml of dry pyridine. A catalytic amount of DMAP was added to the reaction media and stirred for 5 minutes. Acyl chloride **4** (476 mg, 2 mmol) dissolved in 5 ml of dry DMF was then added dropwise to the solution. The mixture is then stirred for 20 h at 60 °C under N_2 . The piece of paper was then sonicated in DMF, EtOH, Acetone and DCM before being dried under vacuum. The sample was kept in dark with an aluminum foil during all the preparation and storage.

General procedure for the photodimerization of coumarin modified cellulose paper

A piece of coumarin modified cellulose paper was fixed on a glass microscope slide. This piece of paper was then irradiated with both 340 and 254 nm light sources.

Computational details

We have carried out our theoretical simulations using Density Functional Theory (for ground-state) and Time-Dependent Density Functional Theory (for the excited-states). More precisely, we have selected the PBEO hybrid functional⁵ to perform our calculations, as this functional was previously reported to be adequate to determine the spectral properties of coumarin derivatives,⁶ and the 6-31G(d) atomic basis set. In addition, we have added dispersion correction that are potentially necessary to accurately describe the interactions between coumarins as well as the interactions between cellulose and the dyes. The dispersion corrections were added using the D3-BJ empirical scheme.⁷ To perform our calculations, we have extracted a segment of 6 D-

glucose units from an experimentally available X-Ray structure, 8 and added the coumarins and their grafting moiety. In other words, primary hydroxyl groups of glucose units were functionalized with 7-hydroxycoumarin through an acetate linker. Several relative positions of the coumarins have been tested (attached to the third and fourth or to the third and fifth glucose - more distant arrangements making dimerization clearly very unlikely) and for each case, several starting conformations have been considered. We nevertheless underline that our goal was not to provide a complete investigation of all possible isomers and conformers of coumarin grafted on cellulose, but rather to confirm the viability of the proposed strategy. Optimization, considering a frozen structure for the cellulose (and unconstrained structures for coumarins and their arms) were then carried out via a standard force minimization process until the rms force was smaller than 10⁻⁵ a.u., corresponding to the so-called *tight* threshold. Several structures were obtained, but only the lowest energy ones are discussed in the main text. The excited-state calculations have been performed at the TD-PBEO/6-31G(d) level, considering the vertical approximation and the most stable systems obtained at the optimization step, so to provide indications of the influence of the dimerization on the optical spectra of grafted coumarins. Calculations (same level of theory) have also been performed on the 7-OMe-coumarin and the corresponding dimer for comparison purposes. All calculations were performed with the Gaussian09.D01 program.⁹

References

- 1 Y. Chujo, K. Sada and T. Saegusa, *Macromolecules*, 1990, **23**, 2693-2697.
- 2 S. Chimichi, M. Boccalini and B. Cosimelli, *Tetrahedron*, 2002, **58**, 4851-4858.
- 3 M. Barsbay, O. Güven, M. H. Stenzel, T. P. Davis, C. Barner-Kowollik and L. Barner, *Macromolecules*, 2007, **40**, 7140-7147.
- 4 G. Chen, L. Tao, G. Mantovani, V. Ladmiral, D. P. Burt, J. V. Macpherson and D. M. Haddleton, *Soft Matter*, 2007, **3**, 732-739.
- 5 C. Adamo and V. Barone, *J. Chem. Phys.*, 1999, **110**, 6158-6170.
- D. Laurent, C. Adamo and D. Jacquemin, *Phys. Chem. Chem. Phys.*, 2014, 16, 14334-14356.
- 7 S. Grimme, S. Ehrlich and L. Goerigk, J. Comput. Chem., 2011, **32**, 1456-1465.

- 8 Y. Nishiyama, J. Sugiyama, H. Chanzy and P. Langan, *J. Am. Chem. Soc.*, 2003, **125**, 14300-14306.
- M. J. Frisch, G. W. Trucks, H. B. Schlegel, G. E. Scuseria, M. A. Robb, J. R. Cheeseman, G. Scalmani, V. Barone, B. Mennucci, G. A. Petersson, H. Nakatsuji, M. Caricato, X. Li, H. P. Hratchian, A. F. Izmaylov, J. Bloino, G. Zheng, J. L. Sonnenberg, M. Hada, M. Ehara, K. Toyota, R. Fukuda, J. Hasegawa, M. Ishida, T. Nakajima, Y. Honda, O. Kitao, H. Nakai, T. Vreven, J. A. Montgomery, Jr., J. E. Peralta, F. Ogliaro, M. Bearpark, J. J. Heyd, E. Brothers, K. N. Kudin, V. N. Staroverov, R. Kobayashi, J. Normand, K. Raghavachari, A. Rendell, J. C. Burant, S. S. Iyengar, J. Tomasi, M. R. Cossi, N., J. M. Millam, M. Klene, J. E. Knox, J. B. Cross, V. Bakken, C. Adamo, J. Jaramillo, R. Gomperts, R. E. Stratmann, O. Yazyev, A. J. Austin, R. Cammi, C. Pomelli, J. W. Ochterski, R. L. Martin, K. Morokuma, V. G. Zakrzewski, G. A. Voth, P. Salvador, J. J. Dannenberg, S. Dapprich, A. D. Daniels, Ö. Farkas, J. B. Foresman, J. V. Ortiz, J. Cioslowski and D. J. Fox, Gaussian, Inc., Wallingford CT, 2009.

Chapitre 3 Préparation d'un outil de détection de l'ion HSO₄- dans l'eau

I Introduction

Ce chapitre présente la préparation et le greffage à la surface du papier d'une sonde organique sélective de l'ion HSO₄- fournissant ainsi un outil de détection sous la forme de bandelette de papier (analogue au papier pH).

Le développement de sonde organique pour la détection d'ions dans l'eau est un domaine de recherche très étudié, notamment pour la détection de polluant. Pour réaliser ce travail, nous avons décidé de travailler avec des dérivés de la rhodamine B, une famille de molécules déjà décrite pour la détection d'ions en solution¹. La détection est due à la formation de liaison hydrogène entre la sonde et l'analyte, ce qui induit une délocalisation des électrons au sein de la rhodamine passant alors de sa forme spirolactame incolore à une forme ouverte fortement colorée (Schéma 1).

Schéma 1 Représentation du principe de détection d'un ion par une Rhodamine

Ici, la fonctionnalisation du papier est réalisée en deux étapes, une première réaction d'estérification permet de greffer à la surface de la cellulose un aldéhyde qui subit par la suite une réaction d'amination réductrice avec le dérivé de la rhodamine B portant un bras éthylène diamine. Le matériau ainsi obtenu a ensuite été immergé dans des solutions aqueuses contenant différents anions. Cette sonde hétérogène s'est révélée être sélective de l'anion HSO_4^- (même en présence d'un tampon de pH = 7.4); de manière intéressante cette sonde permet une détection colorimétrique à l'œil nu, des analyses par spectroscopie UV-Visible permettent quant à elles une détection optique avec une concentration limite détectable estimée à 120 µmol/L soit 11,6 ppm.

Ces travaux ont fait l'objet d'une publication dans le journal *Chemical Communications*² et d'un abstract de vulgarisation sur le site www.atlasofsciences.org.

57

- 1. Kim, H. N.; Lee, M. H.; Kim, H. J.; Kim, J. S.; Yoon, J. *Chem. Soc. Rev.* 2008, **37**, 1465-1472.
- 2. J. Rull-Barrull, M. d'Halluin, E. Le Grognec, F.-X. Felpin, *Chem. Commun.* 2016, **52**, 2525–2528.

II <u>Paper-based sensor for on-site detection of hydrogen sulfate in</u> water

In 2013 UNICEF reported that ca. 2200 children below 5 years old die every day of diarrheal diseases. This report also indicates that around 90% of these deaths are the consequence of unsafe drinking water. The detection of pollutants in water is of primal importance as it is the first step in water decontamination process. In occupational settings, the detection of pollutants is usually achieved with inductively coupled plasma mass spectrometry or gas chromatography coupled to mass spectrometry. While excellent limits of detection can be reached, these techniques suffer from the use of expensive instruments and require highly trained operators. Therefore, traditional detection methods are not well suited for developing countries.

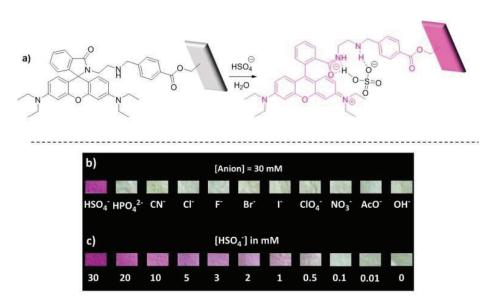


Fig. 1. (a) Representation of the general strategy. (b) Colorimetric detection of various anions in water at 30 mM through simple naked-eye analysis of the dipped paper strip. (c) Effect of the concentration of HSO₄⁻ anions on the color change of the paper strip.

We recently set forth a simple and low-cost paper based sensor, used as a paper strip, for the detection of hydrogen sulfate, a pollutant found in many fertilizers. This simple technology allows portability for direct use on-site and operational simplicity for lowskilled operators. Our device features a rhodamine-based sensor anchored by covalent bonds on hydrophilic cellulose paper for water compatibility and biodegradability (Fig. 1a). The covalent immobilization, by contrast with physisorption, prevents the sensor from being washed off upon contact of the paper strip with an aqueous liquid. Rhodamine was finely tuned to specifically interact with sulfate anions. Rhodamine exists as a colorless closed form and a deep purple opened one. Upon contact with sulfate anions, the originally closed colorless sensor opens and become strongly colored allowing an immediate naked-eye detection (Fig. 1b). The high specificity for sulfate anions vs other anions is attributed to amphiphilic properties of HSO₄⁻ that interacts with the sensor by hydrogen bonding (Fig. 1a). A color gradient from deep purple to pale rosy was observed upon decreasing the concentration of hydrogen sulfate allowing a visual limit of detection in the range 10-50 mg/L (Fig. 1c). For more accurate results, the paper strip can be analyzed with specific equipment (i.e. UV-Visible spectrometer) giving a limit of detection as low as 12 mg/L (12 ppm).

This practical technology should find broad applications in environmental and analytical sciences and could be adapted for the detection of other toxic pollutants including mercury, lead and cyanide.

III <u>Chemically-modified cellulose paper as smart sensor device for</u> colorimetric and optical detection of hydrogen sulfate in water

A portable, recyclable and highly selective paper-based sensor device for the colorimetric and optical detection of hydrogen sulfate anions in water was developed. The detection system features a rhodamine-based sensor covalently grafted onto the highly hydrophilic surface of cellulose paper.

The selective sensing of inorganic anions and metallic cations is an area of growing interest, mainly because it has considerable applications for environmental and biological purposes. 1-7 In occupational settings, the detection of anions and cations is usually achieved with inductively coupled plasma mass spectrometry (ICP-MS) or inductively coupled plasma atomic emission spectroscopy (ICP-AES). While excellent limits of detection can be reached, these techniques suffer from the use of expensive instruments, hazardous sample preparation and require highly trained operators.

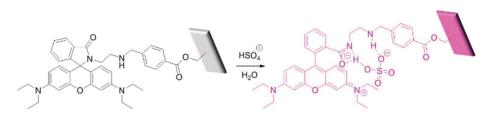
Chemosensors allowing colorimetric and/or optical detection are particularly appealing technologies since they feature operational simplicity and low detection limits. Many anion-selective chemosensors have been designed and synthesized, especially for the recognition of fluoride and cyanide anions because their high nucleophilic properties are often exploited in the detection systems. ^{5, 6, 8} By contrast, the sensing of hydrogen sulfate anions has been much less studied likely because its amphiphilic properties make the design of a selective chemosensor more complex. The detection of hydrogen sulfate anions is of primary importance in environmental science since they lead to unit outage in coal-fired power plants, ⁹ affect adversely the vitrification process in radioactive waste remediation ¹⁰ and are found in many fertilizers, contaminating cultivated grounds.

Chromogenic sensors specific to HSO_4^- anions have been designed following two different strategies through metal-ligand coordinative interaction and hydrogen bonding, leading to fluorescent enhancement (turn-on receptor) or fluorescence quenching (turn-off receptor). None of these chemosensors works in water, without any

organic co-solvent, due to the large energy of hydration of HSO₄⁻ anions and the low solubility of the organic sensor. Since chemosensors-based technologies specific to hydrogen sulfate anions allow solution-phase sensing only and require the use of organic solvents, they are still far from real applications.

Therefore, for real on-site sensing of hydrogen sulfate-containing aqueous samples, the design and the fabrication of solid supported sensors, offering both colorimetric and optical detection, high selectivity, portability and operational simplicity for use by low-skilled operators, are of great interest.

We reasoned that taking advantage of the amphiphilic properties of HSO₄⁻ anions for the design of a specific chemosensors covalently anchored onto a solid support would set up for a groundbreaking approach, unexplored so far. In this contribution, we disclose the design and the fabrication of a smart paper-based analytical device, enabling real on-site sensing of HSO₄⁻ anions in aqueous samples. The system features a rhodamine-based sensor, covalently anchored onto the highly hydrophilic surface of cellulose paper. Upon opening into its deep colored form in the presence of amphiphilic HSO₄⁻ anions, our specifically designed chemosensor exhibits both hydrogen bond receptor and donor sites as depicted in Scheme 1. We selected cellulose paper as platform for the sensor since it features low cost, water compatibility, portability, and disposability.



Scheme 1 Representation of the general strategy.

The surface functionalization of paper requires the chemical modification of hydroxyl groups from glucose units, but the dense hydrogen bond network and the bulk nature of paper strongly decrease their reactivity compared to soluble or highly dispersed polysaccharides. Therefore, prior to the surface functionalization,

Whatman® #6 filter papers, exhibiting a high content of α -cellulose and a medium density (~100 g/m²), were soaked for 24 hours in 10% NaOH aqueous solution to break hydrogen bonds, increasing both the surface area of cellulose fibers and the reactivity of hydroxyl groups. $\frac{22}{\alpha}$

The activated paper was functionalized with benzaldehyde groups by esterification of hydroxyl functions with 4-formylbenzoyl chloride (Scheme 2). We assume that the esterification mainly took place on primary alcohols, certainly more reactive than the remaining secondary alcohols of glucose units. The paper-grafted benzaldehyde was subsequently treated with rhodamine-ethylenediamine 2, easily obtained by refluxing rhodamine B with ethylenediamine, ²³ under reductive amination conditions, affording the expected analytical device. The degree of substitution was determined by elemental analysis to be ca. 4%, meaning that one hydroxyl group is functionalized with a rhodamine sensor every 25 glucose units. This value could be estimated to be somewhat low, but it ensures conserving both the physical integrity and the whiteness of paper.

Scheme 2 Preparation of the paper-based analytical device

The successive chemical modifications of the cellulose paper was followed and ascertained by FT-IR as depicted in Fig. 1. The spectrum of pristine paper exhibits characteristic absorption bands of cellulosic material in the region of 3400, 2900 and 1100 cm⁻¹ accounting for the stretching vibrations of O-H, C-H and C-O-C bonds respectively. The grafting of the cellulose paper with benzaldehyde groups through an ester ligation was clearly evidenced by the apparition of new bands at 1723 and 1700 cm⁻¹ in the region of carbonyls, attributed to the C=O stretching frequency of ester and aldehyde groups respectively. The band at 1204 cm⁻¹ was assigned to the C-O stretching of the ester group. The grafting of rhodamine was confirmed by the apparition of three characteristic bands of rhodamine at 1654, 1634 and 1613 cm⁻¹ accounting for the stretching vibrations of the C=O bonds of the lactam group and aromatic C=C bonds.

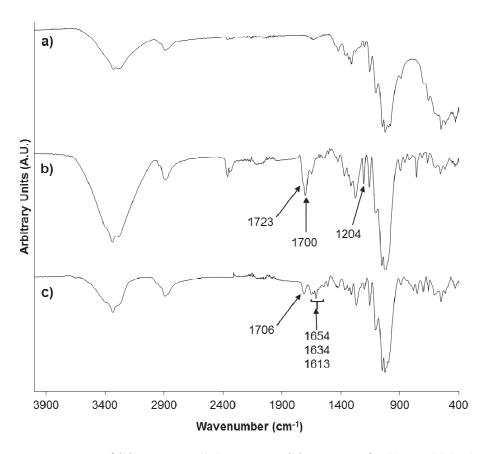


Fig. 1 FT-IR spectra of (a) pristine cellulose paper, (b) paper-grafted benzaldehyde and (c) paper-grafted rhodamine.

The integrity of the cellulose fibers was essentially not affected by the three successive chemical steps required for the preparation of the sensor device, as evidenced by the representative scanning electron microscopy (SEM) images presented in Fig. 2. The diameter of fibers in pristine and grafted-papers are in the range of 8-14 μ M (Fig. 2a-c). The direct consequences for preserving the structure of fibers are important since the grafted-paper is not wrinkled and the whiteness is preserved, allowing a high contrast for the colorimetric detection (vide infra).

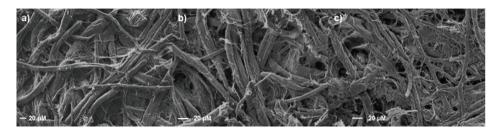


Fig. 2 SEM images of (a) pristine paper, (b) paper-grafted benzaldehyde and (c) paper-grafted rhodamine.

Analysis of the surface composition of the material by X-ray photoelectron spectroscopy (XPS) after each chemical step, confirms the successful grafting of the rhodamine sensor. Full scan spectra of pristine paper and paper-grafted benzaldehyde only display carbon and oxygen elements, suggesting that adsorbed salts, reactants and solvents were efficiently removed during the washing steps. The full scan spectrum of the paper-grafted rhodamine showed the presence of N 1s peak, confirming the grafting of the sensor. High resolution spectra of C 1s region proved the successful surface modification with the significant increase of the peak accounting for C-C bonds at 283.9 eV and the apparition of a peak at 288.5 eV attributed to carbonyl functions (Fig. 3d and f vs. Fig. 3b).

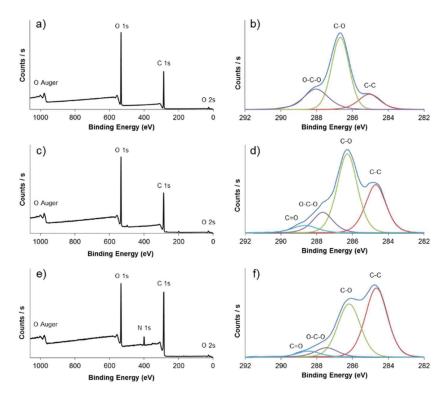


Fig. 3 Survey scan spectra of (a) pristine paper, (c) paper-grafted benzaldehydes and (e) paper-grafted rhodamine. High resolution C 1s spectra of (b) pristine paper, (d) paper-grafted benzadehyde and (f) paper-grafted rhodamine.

With this new analytical device in hand, we investigated the colorimetric detection of anions. Colorimetric assay is the simplest technology in the quest of low-cost, portable and disposable analytical devices dedicated to on-site naked-eye detection. As expected, an intense pink color appeared on the paper strip dipped in a solution of hydrogen sulfate at 30 mM while the coloration response was not affected in the presence of other anions (HPO₄²⁻, CN⁻, Cl⁻, F⁻, Br⁻, I⁻, ClO₄⁻, NO₃⁻, AcO⁻ and OH⁻) in solution in water at 30 mM (Fig. 4a).

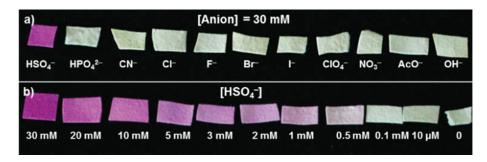


Fig. 4 (a) Colorimetric detection of tetrabutylammonium salts in water at 30 mM through simple naked-eye analysis of the dipped paper strip. b) Effect of the concentration of HSO₄ anions on the color change of the paper strip.

A color gradient from deep pink to pale rosy was clearly observed upon decreasing the concentration of HSO_4^- , allowing a semi-quantitative estimation of the sample concentration in water by simple visual analysis (Fig. 4b). The limit of detection by naked eye is in the range of 0.1-0.5 mM. We stress, that the determination of the HSV or HSL color coordinates from the RGB color model could be used for quantification.^{24, 25}

In a second time, we assessed the UV-vis spectroscopic properties of the paper strip. Upon immersion in distilled water, in the absence of anions, a very weak absorption band at ca. 560 nm was observed (Fig. 5a). By contrast, in the presence of 30 mM of hydrogen sulfate anions the sensor device showed a broad absorption band with a maximum at 564 nm, attributed to the open form of rhodamine as a monomer. Moreover, the shoulder at ca. 533 nm also suggests the presence of several aggregated forms on the cellulosic material.²⁶

Since the development of an analytical device, expected to be used in real conditions, requires a high selectivity, we further studied the cross-response of the paper strip to a large selection of anions such as OH⁻, NO₃⁻, I⁻, Br⁻, Cl⁻, F⁻, CN⁻, ClO₄⁻, HPO₄²⁻ and AcO⁻ in water at 30 mM. The sensor selectively recognized HSO₄⁻, since the absorptions of the paper strips, dipped into the solutions containing the anions, were essentially not affected compared to the paper immersed in the anion-free water solution (Fig. 5a and b). Remarkably, even at a high concentration of anions (30 mM), the sensor device was not sensitive to HPO₄²⁻. The good recognition of sulfate *vs.* phosphate deserves emphasis, since the ability of both anions to interact with sensors through hydrogen

bonding often led to poor discrimination. $^{\underline{10}, \ \underline{11}, \ \underline{14}, \ \underline{27}}$ The high discrimination of our device for HSO_4^- with respect to HPO_4^{2-} is attributed to the poor ability of HPO_4^{2-} to interact with the sensor due to its lower hydrogen donor properties.

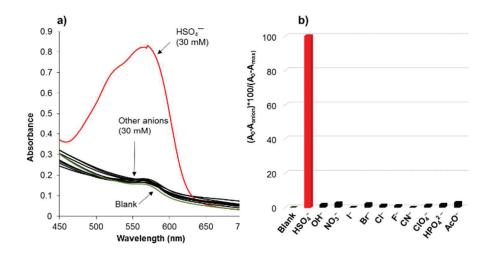


Fig. 5 (a) UV-vis absorption spectra of the paper strip dipped into aqueous solutions of HSO₄-, OH-, NO₃-, I-, Br-, Cl-, F-, CN-, ClO₄-, HPO₄²⁻ and AcO- at 30 mM. b) Normalized absorbance response of the paper strip.

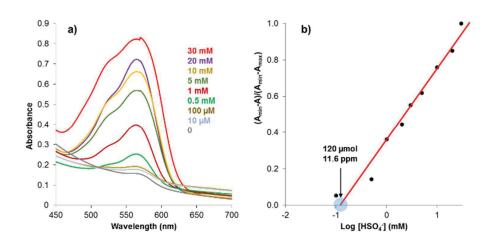


Fig. 6 (a) UV-vis absorption spectra of the paper strip various concentration of HSO₄⁻. (b) Calibration curve of HSO₄⁻concentration for the determination of the detection limit.

The spectrophotometric titration experiments were carried out on the paper strip at different concentration of HSO_4^- anions (Fig. 6). The absorption band centered at 564 nm becomes more intense upon increasing concentration. Although an increase of the absorption band, with respect to the blank, can be detected at concentration of HSO_4^- anions as low as 10 μ M, the limit of detection in reproducible conditions was calculated with the set of data collected from the titration experiments (Fig. 6b).²⁸

The absorption data collected at 564 nm at various concentrations were normalized between the minimum intensity recorded on the sensor device dipped in HSO_4 -free water and the maximum intensity observed at 30 mM. A linear regression curve was fitted to the concentration values 0.5-30 mM of Fig. 6 and a detection limit as low as 120 μ mol (corresponding to 11.6 ppm) was determined by extrapolation of the straight line on the abscissa axis.

With the objective of limiting the cost of this technology, we assessed the reusability of the paper strip. To this end, we developed a simple methodology allowing several coloration-discoloration cycles for the sensing of different aqueous samples containing HSO₄⁻ anions with the same paper strip. As shown in Fig. 7a, the deep pink paper, obtained from the sensing of an aqueous sample containing 5 mM HSO₄⁻, quickly discolored when dipped in a 1 M NaOH aqueous solution under sonication for 5 minutes. The discolored strip paper turned back to deep pink when exposed again to HSO₄⁻ anions. This procedure was successfully repeated on four cycles, but the fragility of the paper strip might limit the number of successive reuses to get reliable results.

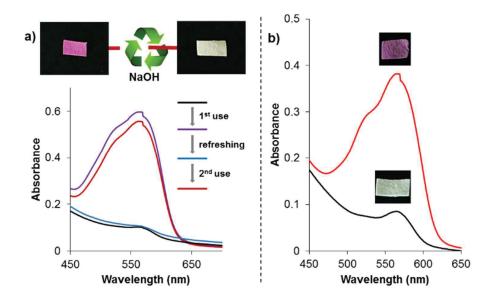


Fig. 7 (a) UV-vis absorption spectra of the paper strip upon two successive reuses. As inset, pictures of the paper strip dipped in a solution of HSO₄⁻ anions (left) and refreshed in a solution of 1 M NaOH (right). (b) UV-vis absorption spectrum of the paper strip dipped into an aqueous solution containing NO₃⁻, I⁻, Br⁻, Cl⁻, ClO₄⁻ anions at 5 mM, with (red line) and without HSO₄⁻ (black line) with a photograph of the paper as inset.

With the objective of developing an analytical device working in real situation, we analyzed two aqueous samples containing a cocktail of anions. In the first sample, NO_3^- , I^- , Br^- , Cl^- , and ClO_4^- anions were mixed at 5 mM in water, while the same cocktail was used for the second sample but with the additional presence of HSO_4^- anions. As it can be seen on the UV-vis absorption spectra of the paper strip dipped in these solutions, the analytical device was not sensitive to a cocktail of anions in the absence of HSO_4^- (Fig. 7b). Conversely, both the coloration and the UV-vis responses of HSO_4^- were not affected by the presence of other anions, demonstrating the absence of interference and the high selectivity of the device.

In summary, we developed the first hydrogen sulfate-sensitive solid-state sensor working in water through colorimetric and optical detection. The smart device fabricated by grafting a rhodamine-modified sensor onto the highly hydrophilic surface of paper, allows on-site analysis of aqueous samples and does not require skilled operator for the colorimetric detection. The high selectivity of the device for HSO₄- anions, even in the presence of other amphiphilic anions, is the result of the unique combination of hydrogen bond receptor and donor sites in the opened form of rhodamine. This practical technology should find broad applications in environmental and analytical sciences. We are currently working on the diversification of this technology to the sensing of other liquid and gas analytes.

MdH thanks the "Région des Pays de la Loire" and the CNRS for the grant. FXF is member of the "Institut Universitaire de France, IUF." Dr. Christine Labrugère (PLACAMAT, Bordeaux) is gratefully acknowledged for XPS analyses.

Notes and references

- 1 H. Li, J. Fan and X. Peng, *Chem. Soc. Rev.*, 2013, **42**, 7943-7962.
- 2 K. P. Carter, A. M. Young and A. E. Palmer, *Chem. Rev.*, 2014, **114**, 4564-4601.
- 3 X. H. Li, X. H. Gao, W. Shi and H. M. Ma, *Chem. Rev.*, 2014, **114**, 590-659.
- 4 P. Mahato, S. Saha, P. Das, H. Agarwalla and A. Das, RSC Adv., 2014, 4, 36140-36174.
- 5 R. Saini, N. Kaur and S. Kumar, *Tetrahedron*, 2014, **70**, 4285-4307.
- 6 P. A. Gale and C. Caltagirone, *Chem. Soc. Rev.*, 2015, **44**, 4212-4227.
- S. Lee, K. K. Y. Yuen, K. A. Jolliffe and J. Yoon, *Chem. Soc. Rev.*, 2015, 44, 1749-1762.
- F. Wang, L. Wang, X. Q. Chen and J. Y. Yoon, *Chem. Soc. Rev.*, 2014, 43, 4312-4324.
- 9 F. Si, C. E. Romero, Z. Yao, Z. Xu, R. L. Morey and B. N. Liebowitz, *Fuel Process. Technol.*, 2009, **90**, 56-66.
- J. L. Sessler, E. Katayev, G. D. Pantos and Y. A. Ustynyuk, *Chem. Commun.*, 2004, 1276-1277.
- 11 R. Shen, X. Pan, H. Wang, J. Wu and N. Tang, *Inorg. Chem. Commun.*, 2008, **11**, 318-322.
- 12 R. Shen, X. Pan, H. Wang, L. Yao, J. Wu and N. Tang, *Dalton Trans.*, 2008, 3574-3581.
- S. Samanta, P. K. Samanta, S. Dutta and P. Biswas, *Spectrochim. Acta, Part A*, 2015, **147**, 262-269.
- 14 L.-L. Zhou, H. Sun, H.-P. Li, H. Wang, X.-H. Zhang, S.-K. Wu and S.-T. Lee, *Org. Lett.*, 2004, **6**, 1071-1074.
- 15 X. He, S. Hu, K. Liu, Y. Guo, J. Xu and S. Shao, *Org. Lett.*, 2006, **8**, 333-336.
- 16 H. J. Kim, S. Bhuniya, R. K. Mahajan, R. Puri, H. Liu, K. C. Ko, J. Y. Lee and J. S. Kim, *Chem. Commun.*, 2009, 7128-7130.
- 17 M. Alfonso, A. Tárraga and P. Molina, *Org. Lett.*, 2011, **13**, 6432-6435.
- A. Mallick, T. Katayama, Y. Ishibasi, M. Yasuda and H. Miyasaka, *Analyst*, 2011, **136**, 275-277.

- 19 W. Xue, L. Li, Q. Li and A. Wu, *Talanta*, 2012, **88**, 734-738.
- 20 S.-T. Yang, D.-J. Liao, S.-J. Chen, C.-H. Hu and A.-T. Wu, *Analyst*, 2012, **137**, 1553-1555.
- 21 P. Kaur, H. Kaur and K. Singh, *Analyst*, 2013, **138**, 425-428.
- A. S. Goldmann, T. Tischer, L. Barner, M. Bruns and C. Barner-Kowollik, *Biomacromolecules*, 2011, **12**, 1137-1145.
- 23 C. Kaewtong, B. Wanno, Y. Uppa, N. Morakot, B. Pulpoka and T. Tuntulani, *Dalton Trans.*, 2011, **40**, 12578-12583.
- 24 A. Hakonen, J. E. Beves and N. Stromberg, *Analyst*, 2014, **139**, 3524-3527.
- 25 H. I. A. S. Gomes and M. G. F. Sales, *Biosens. Bioelectron.*, 2015, **65**, 54-61.
- A. Reisch, P. Didier, L. Richert, S. Oncul, Y. Arntz, Y. Mély and A. S. Klymchenko, *Nat. Commun.*, 2014, **5**, 4089.
- 27 C. Tan and Q. Wang, *Inorg. Chem.*, 2011, **50**, 2953-2956.
- 28 M. Shortreed, R. Kopelman, M. Kuhn and B. Hoyland, *Anal. Chem.*, 1996, **68**, 1414-1418.

IV Partie expérimentale

Materials

All commercial solvents and reagents were used as received without further purification from Sigma-Aldrich, Fischer Scientific Ltd, Alfa Aesar. Whatman® grade 6 filter paper $(42.5 \text{ mm } \emptyset)$ was used as cellulose source.

Analytical methods

¹H and ¹³C NMR spectra, recorded at 400 MHz and 100 MHz respectively, were performed on a Bruker Advance 400. Proton chemical shifts were internally referenced to the residual proton resonance in CDCl₃ (7.26 ppm). Carbon chemical shifts were internally referenced to the deuterated solvent signals in CDCl₃ (77.0 ppm). FT-IR spectra were recorded on a Bruker Tensor 27 spectrometer with ATR technique. Scanning Electron Microscopy (SEM) was performed on a JEOL JSH7600F (field emission gun, accelerating voltage: 5 kV, in lens detector of secondary electrons). X-ray photoelectron spectroscopy (XPS) was performed on a ThermoFisher Scientific K-ALPHA spectrometer for disk surface analysis with a monochromatized AlK α source (hv = 1486.6 eV) and a 200 micron spot size. A pressure of 10⁻⁷ Pa was maintained in the chamber during analysis. The full spectra (0-1150 eV) were obtained at a constant pass energy of 200 eV and high resolution spectra at a constant pass energy of 40 eV. Charge neutralization was required for all insulating samples. High resolution spectra were fitted and quantified using the AVANTAGE software provided by ThermoFisher Scientific. UV-visible absorption spectra were recorded using a Varian Model Cary 5E spectrophotometer, using an integrating sphere DRA 2500.

Synthetic procedures

Compound 2^{S1} .

$$\operatorname{\mathsf{Et}}_2\mathsf{N}$$
 $\operatorname{\mathsf{N}}$ $\operatorname{\mathsf{N}}\mathsf{Et}_2$ $\operatorname{\mathsf{N}}$ $\operatorname{\mathsf{N}}\mathsf{H}_2$

To a solution of Rhodamine B (1) (2.0 g, 4.2 mmol) in ethanol (50 mL) was added dropwise an excess of ethylenediamine (2.20 mL, 33 mmol). The resulting pink mixture was refluxed for 24 hours and became orange. The solvent was removed under reduced pressure, water (35 mL) was added to the residue and the solution was extracted with CH_2Cl_2 (3 x 35 mL). The combined organic phases were washed with water, brine and dried over anhydrous MgSO₄. The solvent was removed under reduced pressure, and the product was dried under vacuum, affording a pale-orange solid **2** (2.0 g, yield 90%). ¹H NMR (400 MHz, CDCl₃) δ 7.90-7.88 (m, 1H), 7.42-7.41 (m, 2H), 7.09-7.06 (m, 1H), 6.43 (s, 1H), 6.41 (s, 1H), 6.37 (s, 2H), 6.28-6.25 (m, 2H), 3.32 (q, J= 7.2 Hz, 8H), 3.18 (t, 2H, J = 6.8 Hz), 2.40 (t, 2H, J = 6.8 Hz), 1.15 (t, 12H, J = 7.2 Hz); ¹³C NMR (100 MHz, CDCl₃) δ 168.5, 153.4, 153.3, 148.8, 132.3, 131.2, 128.6, 128.0, 123.8, 122.7, 108.1, 105.7, 97.7, 64.9, 44.3, 43.9, 40.8, 12.5; FT-IR (ATR) ν 2970, 2926, 2903, 2871, 1686, 1631, 1613, 1545, 1510, 1467, 1447, 1423, 1376, 1352, 1328, 1306, 1261, 1215, 1152, 1115, 1090, 1067, 1017, 816, 784, 756, 700, 535 cm⁻¹; MS (EI) : m/z = 484 (M⁺), 454 (M-CH₂NH₂⁺).

General procedure for the pre-treatment of cellulose paper. Ten pieces of cellulose filter papers (approx. 1.50 g) were immersed in a freshly prepared aqueous solution of 10% NaOH (300 mL). This mixture was shacked overnight on an orbital agitator. The cellulose samples were washed 3 times with 50 mL of EtOH and stored in EtOH.

General procedure for the preparation of paper-grafted benzaldehyde. A pre-treated cellulose filter paper (approx. 145 mg, 0.90 mmol glucose units) washed 2 times with 5 mL of pyridine, was immersed in dry pyridine (25 mL). A catalytically amount of 4-DMAP was added to the reaction media and stirred for 5 minutes. Then, 4-formylbenzoyl chloride (455 mg, 2.7 mmol) dissolved in dry DMF (5 mL) was then added dropwise to

the solution. The mixture was stirred for 16 h at 70 °C under N_2 atmosphere. The piece of paper was sequentially washed with EtOH, MeOH, acetone and CH_2Cl_2 under sonication. The sample was dried under vacuum and stored under nitrogen.

General procedure for the paper-grafted rhodamine. Rhodamine 2 (1.53 g, 3.16 mmol), AcOH (two drops) and MgSO₄ (100 mg) were added to the paper-grafted benzaldehyde (approx. 170 mg, 1.05 mmol) immersed in dry toluene (30 mL). This heterogeneous mixture was refluxed for 16 hours. After cooling the mixture to room temperature, the cellulose paper was washed with EtOH, acetone and CH_2Cl_2 under sonication and dried under vacuum. To the resulting material immersed in dry MeOH (30 mL), NaBH₃CN (333 mg, 16 mmol) was added portionwise over 3 hours and the resulting mixture was further stirred for 3 h at room temperature. Finally, the piece of paper was sequentially washed with MeOH, acetone and CH_2Cl_2 under sonication, dried under vacuum and stored under nitrogen.

Reference

S1 D. Y. Q. Wong, J. Y. Lau and W. H. Ang, *Dalton Trans.*, 2012, **41**, 6104-6111.

Chapitre 4 Préparation d'un dispositif à base de papier capable de réduire le Cu(II) en Cu(I): Application à la détection et la catalyse

I Introduction

Ce chapitre décrit la préparation d'un matériau bioinspiré à base de papier capable de détecter le Cu²⁺ dans l'eau et son l'utilisation comme réducteur supporté pour la réaction click de cycloaddition 1,3-dipolaire de Huisgen.

De nouveau, la fonctionnalisation du papier a été réalisée *via* une réaction d'estérification permettant d'introduire une fonction thiol à la surface de la cellulose. Le matériau ainsi obtenu a ensuite été mis en contact avec différents ions métalliques et a montré une grande sélectivité envers Cu(II). Dans le cas présent, la détection a lieu grâce à la formation d'un complexe thiol-cuivre induisant un transfert de charge S->Cu entrainant une coloration du papier.

De manière similaire à l'étude précédente, cette sonde peut être utilisée pour la détermination colorimétrique à l'œil nu de la présence du cuivre et également par l'utilisation de la spectroscopie UV-Visible permettant une détection jusqu'à 33 μmol/L soit 2 ppm de Cu(II). De plus, grâce à l'utilisation d'une technique d'analyse d'images, il a été possible de réaliser l'analyse d'un échantillon inconnu en étudiant la coloration du papier (coordonnées de couleurs) et en comparant ces résultats avec une courbe de calibration préalablement établie. Des analyses par spectrométrie photoélectronique X (XPS) ont révélé que le cuivre présent à la surface de ce matériau se trouve au degré d'oxydation +1 sous la forme de nanoparticules d'oxyde de cuivre Cu₂O.

Ce résultat nous a donné l'idée d'utiliser ce dispositif comme réducteur supporté pour la réaction click de formation de triazoles. Cette stratégie inédite de réducteur immobilisé sur un support a été appliquée pour la préparation de plus de 19 produits différents avec de bons rendements. De manière intéressante, ce dispositif possède également la capacité de retenir le cuivre à la surface de la cellulose permettant ainsi de récupérer après une simple filtration un brut réactionnel quasiment exempt de cuivre.

79

^{1.} J. Rull-Barrull, M. d'Halluin, E. Le Grognec, F.-X. Felpin, *Chem. Commun.*, 2016, **52**, 6569–6572.

^{2.} J. Rull-Barrull, M. d'Halluin, E. Le Grognec, F.-X. Felpin, *Angew. Chem. Int. Ed.,* 2016, **55**, 13549-13552

Ces travaux ont fait l'objet d'une publication dans le journal *Chemical Communications*¹ (détection) et une publication dans le journal *Angewandte Chemie International Edition*² (application à la catalyse).

- 1. J. Rull-Barrull, M. d'Halluin, E. Le Grognec, F.-X. Felpin, *Chem. Commun.*, 2016, **52**, 6569–6572.
- 2. J. Rull-Barrull, M. d'Halluin, E. Le Grognec, F.-X. Felpin, *Angew. Chem. Int. Ed.,* 2016, **55**, 13549-13552

II A paper-based biomimetic device for the reduction of Cu(II) to Cu(I) – application to the sensing of Cu(II)

A biomimetic device for the reduction of Cu(II) to Cu(I) consisting of thioglycolic acid covalently grafted to cellulose paper was developed. The device displays exceptionally fast reducing properties allowing the reduction of Cu(II) in seconds and the formation of deeply colored Cu(I)-SCH₂R complexes onto the cellulose paper. This biomimetic and biomaterial-based concept was exploited for the detection of copper in water samples with a limit of detection as low as 2 ppm.

Nature has been a permanent source of inspiration for chemists and this interest has been recognized as a field of research known as the biomimetic chemistry. Biomimetic chemistry takes inspiration from the chemical transformations occurring in biological systems. Copper is an important mineral nutrient for mammalian cells, acting as a cofactor for many enzymes. The cellular copper homeostasis is mainly assured by glutathione (GSH) through the formation of a GSH-Cu(I) complex transferring copper into the active sites of enzymes. Copper uptake occurring mainly as Cu(II) species, cysteine residues in proteins are suspected to reduce Cu(II) to Cu(I) with the simultaneous oxidation of thiol functions to disulfides. The ability of thiols to reduce Cu(II) to Cu(I) and form stable complexes in living systems associated to their highly colored properties due to S→Cu charge transfers prompted us to develop a biomimetic approach for the colorimetric detection of copper in aqueous samples.

Being at the end of the food chain, humans are highly exposed to bio-accumulating contaminants such as pollutants and metals. Excessive copper uptake from contaminated food and drink and/or alteration of cellular homeostasis leading to high cellular copper concentration can severely affect human health, especially through liver damages. The World Health Organization (WHO) recommends that intake of copper from diet (food and drink) do not exceed 10 mg/day. Therefore, detecting copper in the environment is essential to

control food and water supply. In occupational settings, copper-containing samples are usually analyzed by inductively coupled plasma mass spectrometry atomic emission spectroscopy (ICP-AES) or inductively coupled plasma mass spectrometry (ICP-MS). These remarkably accurate techniques allow very low detection limits, in the ppb level, but require expensive instruments, highly trained operators and tedious sample pretreatment.

To prevent the use of expensive and complex instruments , colorimetric and/or optical copper chemosensors involving solution-phase sensing through metalligand coordinative interactions has been envisaged as an appealing technology featuring operational simplicity, high selectivity and good sensitivity; 5-14 the coordination behavior being, however, possibly significantly affected by the nature of the solvent analyzed. For real on-site detection of copper, paper-based sensors offering portability and operational simplicity have been proposed by physisorption of molecular sensors 15-18 but this technology may suffer from detection inaccuracy and reproducibility issues since weakly bound molecules can be washed off when dipping the solid sensor in the solvent to be analyzed.

We considered that an innovative approach addressing the drawbacks discussed above was highly desired. To this end, we designed a simple and robust paper-based analytical technology for Cu(II) in water. The main features of our sensor include: (1) a covalent anchoring of a chemosensor onto cellulose paper, (2) an optical and colorimetric detection of Cu(II), (3) a biomimetic detection based on the chemical reduction of Cu(II) to Cu(I) by thiol functions.

Paper-based sensor have been introduced as low-cost, user-friendly, portable and disposable analytical devices encompassing many applications such as biodiagnosis, water and seafood control as well as environmental markers. ^{19,20} Cellulose paper can be viewed as an ideal platform for the immobilization of chemosensors since cellulose is the cheapest and the most abundant biopolymer on Earth and the high hydrophilicity of paper is ideally suited for the analysis of aqueous samples. However, analytical devices based on the covalent

immobilization of a chemosensor onto cellulose paper are still scarce despite outstanding properties. This could be explained by the low reactivity of hydroxyl groups from glucose units due to the dense intra- and intermolecular hydrogen bond network, resulting in a low degree of surface functionalization.

Therefore, prior to surface modification, pristine cellulose paper was soaked for 24 hours in 10% NaOH aqueous solution at 25 °C to break hydrogen bonds and enhance the reactivity of hydroxyl groups. Then, the activated paper was esterified with thioglycolic acid using catalytic amount of *p*-toluene sulfonic acid (PTSA). We assume that the functionalization mainly occurred on primary hydroxyl functions of the glucose units, but we cannot ruled out that remaining less reactive secondary alcohols were marginally esterified (Scheme 1). A high degree of substitution of c.a. 0.7 was estimated by elemental analysis, indicating that seven hydroxyl groups were functionalized with thioglycolic acid every ten glucose units.

Scheme 1 Preparation of the paper-based biomimetic device.

The covalent grafting of thiogycolic acid on the cellulose paper was followed by FT-IR (Fig. S1 in ESI). The spectrum of pristine paper exhibits characteristic stretching vibrations for O-H, C-H and C-O-C bonds at 3400, 2900 and 1100 cm⁻¹ respectively. The successful grafting of thioglycolic acid to cellulose is ascertained by the apparition of an intense band at 1721 cm⁻¹ accounting for the carbonyl group of the ester function along with a small band at 662 cm⁻¹ attributed to the C-S stretching vibration. The S-H stretching vibration can be barely discerned at 2550 cm⁻¹, but the dense hydrogen bond network excessively broadened the expected band. The volatility of thioglycolic acid prevented the presence of

adsorbed residues after a thermal treatment of the biomaterial at 120 °C for 12 hours under vacuum.

The surface composition of the grafted paper was analysed by X-ray photoelectron spectroscopy (XPS) and compared to the pristine paper (Fig. 1). The determination of the valence state of the carbon element on the high resolution XPS spectra of the C1s region reveals the increase of the peak accounting for C–C bonds at 284.7 eV and the apparition of a peak at 288.9 eV attributed to ester function. S2p peak at 164.1 eV indicates the presence of thiol functions. A high resolution spectrum of the S2p region shows closely spaced spin-orbit components (S2p $_{1/2}$ at 165.3 eV and S2p $_{3/2}$ at 164.1 eV) of S2p orbitals; the spin-orbit splitting being measured at 1.2 eV.

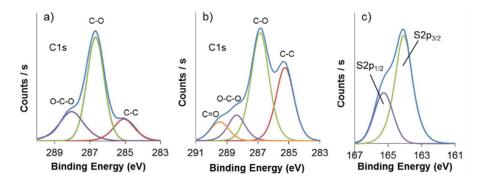


Fig. 1 High resolution C1s XPS spectra of (a) pristine paper, (b) paper-grafted thioglycolic acid. (c) High resolution S2p XPS spectrum of paper-grafted thioglycolic acid.

Scanning electron microscopy (SEM) images, depicted in Fig. 2, reveal that the morphology of the cellulose fibers is not affected by the grafting step, the diameter of fibers being in the range of $10\text{-}20~\mu m$ for both materials, while the whiteness of the cellulose paper is also preserved (photograph as inset), allowing a high contrast for the colorimetric detection (vide infra). These results suggest that the grafting of thioglycolic acid do not alter the physical properties of the paper.

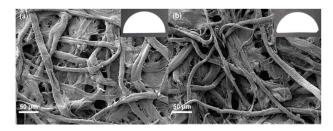


Fig. 2 SEM images of (a) pristine cellulose paper, (b) functionalized paper with photograph as inset.

As expected, our paper-based sensor exhibits intense colorimetric changes easily detected by naked eyes upon contact with a solution of Cu(II), (Fig. 3). A gradient color from black to pale brownish is observed on the paper strips upon decreasing the concentration of Cu(II). The estimated limit of detection by naked eyes is about 0.1 mM corresponding to ca. 6 ppm Cu. Colorimetric detection is the simplest technology for on-site naked-eye pollutant detection carried out by low skilled workers and even non-scientific individuals.

By contrast, optical detection requires dedicated instruments but it can be complementary to the colorimetric analysis and may furnish more accurate results in the region of the detection limit. The UV diffuse reflectance spectrum of the paper strips dipped in aqueous solutions of Cu(II) of various concentration were recorded. When the paper strip is immersed in a copper-free water sample, a single absorption band is observed at ca. 257 nm and attributed to the carbonyl groups of the ester function. Upon increasing the concentration of copper, two bands corresponding to S→Cu charge transfers appear at ca. 506 and 665 nm.⁴ The band broadening observed is attributed to the inhomogeneity of the medium leading to several complexes in equilibrium.

The limit of detection by optical means was calculated on the absorption band centered at 506 nm with the set of data collected from the recording of absorbance at various concentration of Cu(II). The value of the absorbance at 506 nm of 9 solutions containing different concentration of Cu(II) was normalized between the blank and the solution titrating at 10 mM. A linear regression curve was fitted to the concentration values 0.1–10 mM extracted from Fig. 3b and a detection limit of 33 μ M (corresponding to 2 ppm) was determined by extrapolation of the straight line on the abscissa axis.

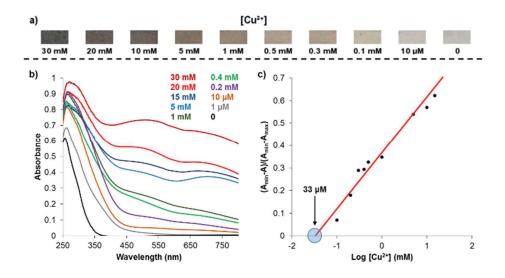


Fig. 3 (a) Colorimetric detection of Cu(II) in water at different concentrations. (b) UV spectra of the paper strips at various concentration of Cu(II). (c) Calibration curve for the determination of the detection limit.

With the objective of developing a universal analytical device for the detection of copper in real water samples, we examined the selectivity of the sensor on a selection of cations frequently detected in contaminated tap water.

Both optical and colorimetric detections confirmed the high selectivity of the sensor for Cu(II). The absorbance values measured at 506 nm for Hg(II), Zn(II), Sn(II), Ni(II) Li(I), Pb(II), Fe(III), Ag(I), Cr(I), Cr(II), Cr(III), Ca(II) and Cd(II) is not significantly discernible from the blank even at concentrations as high as 30 mM (Fig. 4a).

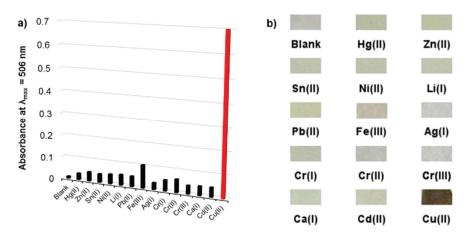


Fig. 4 (a) Absorbance response of the paper strip at 506 nm for various metal chloride salts. (b) Colorimetric detection of cations in water at 30 mM through simple naked-eye analysis of the dipped paper strip.

Similarly, for the naked-eye detection, a marked colour change was exclusively observed when the paper strip was immersed in a sample of water containing Cu(II) (Fig. 4b). We investigated the influence of the pH of copper-containing aqueous solutions on the sensitivity of our sensor. It was observed that the device

displays a comparable sensing sensitivity in solutions with pH ranging from 4 to 12, while a quench of the detection was observed for pH values below 4.

This results reveals that in standard conditions, our detection device is reliable for a wide range of pH values. The colorimetric detection allows a semi-quantitative estimation of the concentration of copper in the analyte by visual comparison with a colour chart. The quantitative determination of copper concentration of unknown water samples can be assessed from the colour coordinates extracted from the paper strip.

The RGB (Red, Green, Blue) colour model is a universal model for electronic devices. The RGB system use a Cartesian coordinate system and can be more intuitively and perceptually represented by the cylindrical-coordinate HSL (for Hue, Saturation, Lightness) or HSV (for Hue, Saturation, Value) representations.

The quantification of copper in unknown water samples requires the preparation of a calibration curve from a set of standards in order to establish a relationship between the colour coordinates and the concentration of copper. The RGB colour coordinates were extracted with the open-source GIMP raster graphics editor on a square region of approximately 900 pixels from the paper strips immersed in standards. The RGB coordinates were converted into the HSL representation and a linear calibration curve was fitted to the concentration range of 0.1-20 mM (Fig. 5a).

An application of our sensor was carried out on a sample contaminated by copper at a level of 2.5 mM as determined by ICP-MS (Fig. 5b). Analysis of the RGB colour coordinates of the paper strip immersed in this sample and conversion to the HSL values allowed the assessment of the copper concentration with the linear regression curve represented in Fig. 5a. A concentration of 2.46 mM was determined, corresponding to a low relative error of -1.6%.

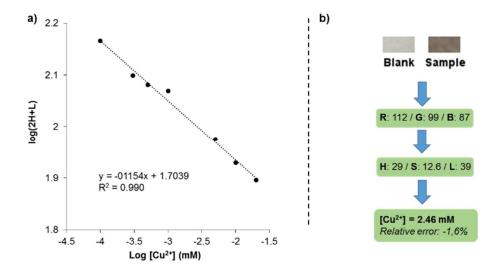


Fig. 5 (a) Calibration curve representing the color coordinates of the paper strips as a function of the Cu(II) concentration. (b) Application for the quantitative determination of Cu(II) concentration in a water sample.

The mechanism responsible of the colorimetric and optical detection was initially assumed to proceed through a thiol-mediated reduction of Cu(II) to Cu(I) resulting of the formation of deeply coloured Cu(I)-SCH₂R complexes due to S \rightarrow Cu charge transfers.

In order to confirm this mechanism we characterised the strip paper immersed in a 20 mM aqueous CuCl₂ solution. The paper strip dipped in the copper solution turns black in a couple of seconds and the SEM images reveal the presence of copper nanoparticles (Fig. 6a-b).

XPS analyses confirm the formation of copper-thiol complexes since two S2p doublets with 9:1 area ratios and splittings of 1.2 eV are observed. The doublet at 163.6 eV is assigned to free-thiols while the new doublet at 161.9 is characteristic of bound thiolate species (Fig. 6d). Analysis of the high resolution XPS spectra of the Cu2p region is even more informative since the two split spin-orbit components of $Cu2p_{1/2}$ and $Cu2p_{3/2}$ at respectively 952.1 and 932.4 eV, associated to the absence of the satellite shake-up near 938-945 eV are characteristic of Cu(I), certainly as Cu_2O nanoparticles (Fig. 6c).

The absence of Cu(II) species suggest that the paper strip acts as a very efficient and exceptionally fast reducing agent; these results validated the initial hypothesis. Quantification of the surface composition by XPS provides direct atomic level spectroscopic evidences of the formation of 1:1 stoichiometric complexes of sulfides with Cu(I) species since the atomic ratio of the total surface copper (0.47 % at.) to the total surface bound sulfur (0.40% at.) is 1.17.

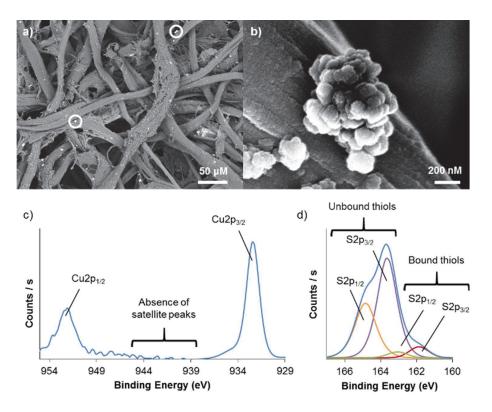


Fig. 6 (a) SEM image of paper-grafted thioglycolic acid with copper nanoparticles (some are showed in a white circle). (b) SEM image of Cu NPs at a high magnification. (c) High resolution Cu2p XPS spectrum showing the absence of satellite peaks characteristic of Cu(II). (d) High resolution S2p XPS spectrum of paper-grafted thioglycolic acid containing Cu NPs.

In summary, we developed the first biomimetic solid-state device for the reduction of Cu(II) to Cu(I) in aqueous conditions. The biomimetic sensor,

consisting of thioglycolic acid covalently immobilized on cellulose paper, showed exceptional sensing properties for the colorimetric and optical detection of Cu(II) in water with a limit of detection as low as 2 ppm. A method for the quantitative determination of copper concentration in water by colorimetric means was developed by extraction of the HSL colour coordinates from the coloured paper strips.

The reduction of Cu(II) to Cu(I) was followed by XPS and the formation Cu_2O NPs was observed by SEM analysis. The formation of 1:1 stoichiometric complexes of sulfides with Cu(I) species was determined by quantification of the surface composition. Studies in the design of biomaterials for the fabrication of biomimetic devices for sensing open exciting new avenues in many areas of chemistry. We believe that this work is a leading contribution to this exciting field of research.

MdH thanks the "Région des Pays de la Loire" and the CNRS for the grant. FXF is member of the "Institut Universitaire de France, IUF." Denis Loquet (University of Nantes), François-Xavier Lefèvre (University of Nantes) and Dr. Christine Labrugère (PLACAMAT, Bordeaux) were gratefully acknowledged for Elemental, SEM and XPS analyses respectively.

Notes and references

- 1 R. Breslow, J. Biol. Chem., 2009, **284**, 1337-1342.
- E. B. Maryon, S. A. Molloy and J. H. Kaplan, *Am. J. Physiol. Cell Physiol.*, 2013, **304**, C768-C779.
- 3 M. Prudent and H. H. Girault, *Metallomics*, 2009, **1**, 157-165.
- 4 A. A. Gewirth and E. I. Solomon, *J. Am. Chem. Soc.*, 1988, **110**, 3811-3819.
- 5 X. Cao, W. Lin and W. Wan, *Chem. Commun.*, 2012, **48**, 6247-6249.
- J. Jo, H. Y. Lee, W. Liu, A. Olasz, C.-H. Chen and D. Lee, J. Am. Chem. Soc., 2012, 134, 16000-16007.
- J. Y. Jung, M. Kang, J. Chun, J. Lee, J. Kim, J. Kim, Y. Kim, S.-J. Kim, C. Lee and J. Yoon, *Chem. Commun.*, 2013, 49, 176-178.
- 8 S. Goswami, S. Maity, A. C. Maity, A. K. Maity, A. K. Das and P. Saha, *RSC Adv.*, 2014, **4**, 6300-6305.
- 9 Y. H. Lee, N. Park, Y. B. Park, Y. J. Hwang, C. Kang and J. S. Kim, *Chem. Commun.*, 2014, **50**, 3197-3200.
- Y. Liu, Q. Fei, H. Shan, M. Cui, Q. Liu, G. Feng and Y. Huan, *Analyst*, 2014, 139, 1868-1875.
- J. J. A. Cotruvo, A. T. Aron, K. M. Ramos-Torres and C. J. Chang, *Chem. Soc. Rev.*,
 2015, 44, 4400-4414.
- 12 Y. Zhang, Q. Li, J. Guo, Y. Li, Q. Yang and J. Du, RSC Adv., 2015, 5, 66674-66680.
- J. Li, S. Chen, P. Zhang, Z. Wang, G. Long, R. Ganguly, Y. Li and Q. Zhang, *Chem. Asia. J.*, 2016, **11**, 136-140.
- 14 P. R. Sahoo and S. Kumar, *RSC Adv.*, 2016, **6**, 20145-20154.
- R. Sheng, P. Wang, Y. Gao, Y. Wu, W. Liu, J. Ma, H. Li and S. Wu, *Org. Lett.*, 2008,
 10, 5015-5018.
- 16 X. Yang, W. Zeng, L. Wang, X. Lu, Y. Yan, J. Qu and R. Liu, RSC Adv., 2014, 4, 22613-22616.
- 17 G. Li, F. Tao, H. Wang, L. Wang, J. Zhang, P. Ge, L. Liu, Y. Tong and S. Sun, RSC Adv., 2015, 5, 18983-18989.

- 18 Y. Qian, L. Cao, C. Jia, P. O. Boamah, Q. Yang, C. Liu, Y. Huang and Q. Zhang, *RSC Adv.*, 2015, **5**, 77965-77972.
- 19 A. W. Martinez, S. T. Phillips, M. J. Butte and G. M. Whitesides, *Angew. Chem. Int. Ed.*, 2007, **46**, 1318-1320.
- A. W. Martinez, S. T. Phillips, G. M. Whitesides and E. Carrilho, *Anal. Chem.*, 2010, **82**, 3-10.
- 21 X. Zhang and J. Huang, *Chem. Commun.*, 2010, **46**, 6042-6044.
- 22 J. Isaad and A. El Achari, *Tetrahedron*, 2011, **67**, 4939-4947.
- 23 L. Q. Xu, K.-G. Neoh, E.-T. Kang and G. D. Fu, J. Mat. Chem. A, 2013, 1, 2526-2532.
- 24 B. Yang and W. H. Wu, *React. Funct. Polym.*, 2013, **73**, 1553-1558.
- Y. Li, Y. Wen, L. Wang, J. He, S. S. Al-Deyab, M. El-Newehy, J. Yu and B. Ding, J. Mat. Chem. A, 2015, 3, 18180-18189.
- J. Rull-Barrull, M. d'Halluin, E. Le Grognec and F.-X. Felpin, *Chem. Commun.*, 2016,52, 2525-2528.
- 27 M. Barsbay, O. Güven, M. H. Stenzel, T. P. Davis, C. Barner-Kowollik and L. Barner, *Macromolecules*, 2007, **40**, 7140-7147.

III <u>Partie expérimentale</u>

Materials

All commercial solvents and reagents were used as received without further purification from Sigma-Aldrich, Fischer Scientific Ltd, Alfa Aesar. Whatman® grade 6 filter paper (42.5 mm Ø) was used as cellulose source.

Analytical methods

FT-IR spectra were recorded on a Bruker Tensor 27 spectrometer with ATR technique. Scanning Electron Microscopy (SEM) was performed on a JEOL JSH7600F (field emission gun, accelerating voltage: 5 kV, in lens detector of secondary electrons). X-ray photoelectron spectroscopy (XPS) was performed on a Thermo Fisher Scientific K-ALPHA spectrometer for disk surface analysis with a monochromatized AIKα source (hv = 1486.6 eV) and a 200 micron spot size. A pressure of 10⁻⁷ Pa was maintained in the chamber during analysis. The full spectra (0–1150 eV) were obtained at a constant pass energy of 200 eV and high resolution spectra at a constant pass energy of 40 eV. Charge neutralization was required for all insulating samples. High resolution spectra were fitted and quantified using the AVANTAGE software provided by Thermo Fisher Scientific. UV-visible absorption spectra were recorded using a Varian Model Cary 5E spectrophotometer, using an integrating sphere DRA 2500. Elemental analysis were performed on a Thermo Fisher Scientific Flash 2000 CHNS organic elemental analyzer.

Procedure

General procedure for the pre-treatment of cellulose paper. Ten pieces of cellulose filter papers (approx. 1.50 g) were immersed in a freshly prepared aqueous solution of 10% NaOH (300 mL). This mixture was shacked overnight on an orbital agitator. The cellulose samples were washed 3 times with 50 mL of EtOH and stored in EtOH.

Procedure for the functionalization of cellulose paper with thioglycolic acid. Thioglycolic acid (257 mg, 194 $\ \Box$ L, 2.79 mmol) and catalytic *p*-TsOH (20 mg) were added to the pretreated filter paper (150 mg, 0.93 mmol) immersed in dry toluene (20 mL).

This mixture was refluxed overnight under nitrogen. After cooling the mixture to room temperature, the cellulose paper was washed successively with MeOH, EtOH, acetone and CH₂Cl₂ under sonication bath, 5 min each, dried under vacuum and stored under nitrogen. Elemental analysis: C: 40.06%, H: 5.12%, S: 10.79%.

General procedure for the colorimetric detection of Cu(II) at different concentration.

Solutions of CuCl₂ at different concentrations were prepared in distilled water. Paper strips were immersed in the corresponding solutions for one hour, dried at 80 °C for one hour and characterized by UV-Vis.

General procedure for the colorimetric detection of cations.

Aqueous solutions of different cations as the corresponding chloride salt at 30 mM (Hg²⁺, Zn²⁺, Sn²⁺, Ni²⁺, Li¹⁺, Pb²⁺, Fe³⁺, Ag¹⁺, Cr¹⁺, Cr²⁺, Cr³⁺, Ca²⁺ and Cd²⁺) were dissolved in distilled water. Paper strips were immersed in the corresponding solutions for one hour, dried at 80 °C for one hour and characterized by UV-Vis.

General procedure for the calibration curve representing the color coordinates of the paper strips as a function of Cu(II) concentration.

The samples were placed on a white background to maintain the same environmental light and photographic conditions. Detail camera set up is shown in Table 1. Digital images were transferred to a computer without any specific software. Colors were obtained from a representative square region of approximately 900 pixels located in each sample images. The average RGB values were measured with GIMP tool color picker. The RGB data codes were converted to HSL data code by an online software (see following link http://www.rapidtables.com/convert/color/rgb-to-hsl.htm).

Digital camera	Canon EOS 400D DIGITAL
Camera maximum resolution	10.1 megapixels
Camera sensor	CMOS 22.2 x 14.8 mm
Exposition time	1/100 s
Focal length	34 mm
White balance	Automatic
Image format	JPEG 3888 X 2592 pixels
Color representation	sRGB (standard RGB)
RGB color measurement	Gimp

Table S1. Digital camera characteristics for Cu(II) determinations. S1

	С	ode RO	ŝВ	Code HSL					
[c] / mM	R	G	В	Н	S	L	2H+L	log (2H+L)	log [Cu ²⁺]
20	106	96.0	91.0	20.0	7.6	38.6	78.6	1.98	-1.70
10	114	102	95.0	22.0	9.1	41.0	85.0	2.01	-2.00
5	132	116	105	24.0	11.4	46.5	94.5	2.06	-2.30
1	153	137	121	30.0	13.6	57.3	117	2.14	-3
0,5	165	150	134	31.0	14.7	58.6	121	2.18	-3.30
0,3	173	158	141	32.0	16.3	61.6	126	2.20	-3.52
0,1	193	183	166	38.0	17.9	70.4	146	2.26	-4.00

Table S2. Average RGB and HSL color values for various concentrations of Cu(II).

Reference

M. L. Firdaus, W. Alwi, F. Trinoveldi, I. Rahayu, L. Rahmidar and K. Warsito, Procedia Environ. Sci., 2014, 20, 298-304. IV Harnessing the dual properties of thiol-grafted cellulose paper for click reactions: powerful reducing agent and adsorbent for Cu

An unprecedented concept exploiting the dual properties of thiol-grafted cellulose paper for promoting copper-catalyzed [3+2]-cycloadditions of organic azides with alkynes and adsorbing residual copper species in solution has been discovered. The thiol-grafted cellulose paper, used as a paper strip, allows the reduction of Cu(II) to catalytically active Cu(I) and acts as a powerful adsorbent for copper, facilitating the work-up process and leaving the crude mixture almost free of copper residues after a single filtration.

The copper-catalyzed [3+2] cycloaddition of an organic azide with a terminal alkyne leading to the corresponding 1,4-disubstituted triazole is one of the most powerful and thoroughly studied ligation tools falling in the family of click reactions.^[1] While the thermal-promoted [3+2] cycloaddition, initially discovered by Huisgen,^[2] suffers from generating both 1,4- and 1,5-disubstituted triazoles with a poor regiocontrol, the copper-catalyzed version independently pioneered by Meldal^[3] and Sharpless^[4] has become an indispensable tool in chemical-biology^[5] and material science^[6] due to its compatibility to aqueous conditions, good tolerance to steric hindrance and functional groups, and excellent regioselectivity for 1,4-triazoles.

Two main experimental protocols emerged from the hundreds of publications reporting the use of this click reaction catalyzed by Cu(I)-species. The first one involves the direct use of Cu(I) salts with a strict exclusion of oxygen due to the high susceptibility of Cu(I) toward oxidation. This approach usually lacks of robustness due to complicating side reactions and copper instability. The use of nitrogen-type ligands greatly enhances both reaction yields and rates since they prevent the degradation of Cu(I) by oxidation or disproportionation.^[7] The second procedure involves the in-situ reduction of Cu(II) salts such as CuSO₄.5H₂O, to Cu(I) with a 3- to 10-fold excess of a reducing agent. Sodium ascorbate is indisputably the most frequently used reducing agent, but hydrazine^[8] and

tris(2-carboxyethyl)phosphine^[9] have been occasionally used as well. This second strategy is by far the preferred procedure since it does not require inert atmosphere, can be carried out in water, gives more reliable results and is accessible to non-experts such as biologists. However, using sodium ascorbate as a reducing agent can be complicated by both the over reduction of Cu(II) to Cu(0) and formation of radical oxygen species.^[10] Moreover, strongly electrophilic by-products of dehydroascorbate have been reported to react with protein chains, altering the chemical structure of DNA.^[11] It must be noted that alternative procedures involving the photo-induced reduction of Cu(II) to Cu(I) showed interesting performances.^[12]

Environmental concerns as well as toxicity issues from copper species in compounds of biological interest, have led to the development of immobilized catalytic systems, allowing an efficient copper removal by a simple filtration. Copper catalysts have been immobilized as molecular complexes and nanoparticles on a variety of supports^[13] including polymers,^[14] silica,^[15] zeolite,^[16] and carbon-based material.^[17] By contrast, the use of immobilized reducing agents is unprecedented, though it could simplify the removal of reducing agent byproducts, especially for biological materials, and increase the selectivity for Cu(I) with regard to Cu(0).

We recently developed a biomimetic reducing agent immobilized on cellulose paper for the highly selective reduction of Cu(II) to Cu(I) with the simultaneous detection of copper by colorimetric and optical tools. Our heterogeneous reducing system consists in a cellulose filter paper covalently grafted with thioglycolic acid (Cell-SH). Upon contact with aqueous CuSO4.5H2O solutions, a piece of paper reduces Cu(II) to Cu(I) nanoparticles in a couple of seconds with the simultaneous oxidation of thiols to disulfide compounds. The effectiveness of the reduction can be easily followed by naked eyes since the white paper strip rapidly turns black due to high S \rightarrow Cu charge transfer.

Herein, we report how this unprecedented reducing agent can be used for the coppercatalyzed Huisgen 1,3-dipolar cycloaddition of organic azides with terminal alkynes. Particularly, we demonstrate how a simple piece of paper functionalized with thiol functions can act as an unprecedented dual tool, promoting the Cu-catalyzed Huisgen synthesis of 1,4-disubstituted triazoles through the reduction of CuSO₄.5H₂O to Cu(I) species and allowing an efficient copper remediation. This bifunctional material leaves the crude product almost free of copper residues and reducing agent by-products after a single filtration.

Pursuing this groundbreaking strategy, we initially focused on a model reaction involving the cycloaddition of benzyl azide 1 with propargyl alcohol 2 in the presence of $CuSO_4.5H_2O$ as catalyst in a mixture of t-BuOH/H₂O (Table 1). The cellulose filter paper covalently grafted with thioglycolic acid used in this work was prepared by esterification of Whatman® paper #6 with thioglycolic acid using PTSA as catalyst following our recently described procedure (Scheme 1). [18-20]

Scheme 1. Preparation of Cell-SH.

At room temperature, we observed a sluggish cycloaddition, requiring a high copper loading, up to 10 mol% Cu, to reach a modest yield of 3 (entries 1-3), using a piece of paper equivalent to 16 mol% of SH functions. Fortunately, working at 70 °C significantly increased the reaction rates without affecting the Cell-SH efficiency since an excellent yield (87%, entry 5) was attained with only 2 mol% Cu. Decreasing the loading of thiol functions to 8 mol% significantly eroded the reaction yield (43%, entry 6), while the reaction background revealed that the use of a piece of paper as reducing agent was essential for promoting the reaction since less than 5% of 3 was obtained in the absence of paper (entry 7).

Table 1. Optimization studies.

N _{3 +} \\\		CuSO ₄ .5H ₂ O Cell-SH		N-N,		
1	OH 2	t-BuOH/H ₂ O 14 hours	3	ОН		
Entry ^a	Cu loading	SH loading	Temp.	Yield		
	(mol%)	(mol%)	(°C)	(%) ^b		
1	1	16	25	34		
2	5	16	25	36		
3	10	16	25	61		
4	1	16	70	85		
5	2	16	70	87		
6	2	8	70	43		
7	2	0	70	<5		

[a] Reaction conditions: benzyl azide 1 (1 mmol), propargyl alcohol 2 (1.5 mmol), $CuSO_4.5H_2O$ and Cell-SH were stirred in 5 mL of t-BuOH/H₂O (1/1) for 14 hours at the specified temperature. [b] Isolated yield.

The optimized conditions of the benchmark reaction were translated to the formation of diversely decorated triazoles (Table 2). In a first set of examples we studied the use of simple ligation partners. We learned from these studies that aromatic and aliphatic alkynes reacted with a similar efficiency and the increase of the steric hindrance of the carbon atom bearing the azide function resulted in diminished reactivities, requiring an increase of copper loading (4 mol%) when switching ethyl azidoacetate for more sterically hindered ethyl 2-azidopropanoate (compounds 8, 10, 12, vs 7, 9, 11). The usefulness of Cell-SH as a powerful reducing agent for CuSO₄.5H₂O was highlighted on two examples showing that almost no conversion occurred when Cell-SH was omitted from reaction mixture (compounds 3, 5, yields in bracket).

Having validated our concept on a set of simple triazoles, we pushed further our studies with the use of densely decorated coupling partners in order to evaluate the robustness and make a balanced analysis of the usefulness of the methodology. As we reasoned that our practical Cell-SH device could be useful for biologists and analytical chemists, we used azides and alkynes bearing sugar, rhodamine, coumarin and cholesterol moieties that are often used in cell recognition, sensing or labelling. The scope of the reaction proved to be quite broad with no obvious limitations since the cycloaddition proceeded with both highly complex alkynes and azides. Impressively, free-carbohydrates also reacted smoothly either as azide or alkyne derivatives (18-19), showing the high tolerance of this process.

Actually, the main limitation of this process is related to solubility issues of highly lipophilic substrates, significantly altering the reaction rate. In order to increase the dispersion of structurally complex and poorly soluble partners such as alkynes bearing cholesterol and rhodamine moieties and attain reasonable rates, the cycloaddition was performed with 4 mol% Cu and in ternary mixtures of solvents using either THF, MeOH or CH₂Cl₂ as additional solvents (compounds 15-16, 21-23). As expected, the cycloaddition occurs regioselectively in favor of the 1,4-disubtituted triazoles, though the 1,5-disubstituted regioisomer was detected in a small amount on two occasions for compounds 10 and 16. In summary, we mention that our catalytic system allows working with highly complex partners having either lipophilic or chelating properties, even those bearing a pyridine group (compound 20), provided that experimental conditions, e.g., solvent and/or time, are adapted.

Table 2. Scope of the reaction.

[a] Reaction conditions: azide (1 mmol), alkyne (1.5 mmol), CuSO4.5H2O (2 mol%) and Cell-SH (16 mol%) were stirred in 5 mL of t-BuOH/H2O (1/1) at 70 °C for 14 h. [b] Yield without Cell-SH in bracket. [c] CuSO4.5H2O (4 mol%). [d] Reaction time: 72 hours. [e] t-BuOH/H2O/THF (1/1/2) as solvent mixture, CuSO4.5H2O (4 mol%) and 14 hours of stirring. [f] CuSO4.5H2O (4 mol%) and 48 hours of stirring [g] MeOH/H2O/CH2Cl2 (1/1/3) as solvent mixture, CuSO4.5H2O (4 mol%) and 48 hours of stirring.

Having demonstrated the powerful reducing properties of Cell-SH for copper sulfate, promoting the [3+2]-cycloaddition of organic azides with alkynes, we explored the adsorption properties of this unusual material (Table 3). In order to accurately determine the level of copper removal, we analyzed the crude solution by inductively coupled plasma mass spectrometry (ICP-MS) after the paper strip has been removed by filtration. We calculated the percentage of copper removal with respect to the initial amount introduced for the reaction (2 mol% Cu). The use of a slight excess of Cell-SH was inefficient in promoting the cycloaddition and removing copper species in solution since only a marginal amount of copper species was adsorbed on the material while the reaction yield was disappointingly low (entry 2). Using a four-fold molar excess of Cell-SH with respect to copper greatly increased the copper remediation to ca. 60%, but unfortunately the reaction yield remained unchanged (entry 3). By contrast, 94% of copper species in solution were removed when a piece of paper corresponding to 16 mol% SH was used, while the reaction yield for obtaining triazole 3 reached 87% (entry 4). Upon increasing the loading of thiol functions to 24 and 32 mol%, the copper removal marginally increased to ca. 97% while the reaction yield reached a plateau at ca. 90% (entries 5-6). These results reveals that the use of an eight-fold molar excess of SH functions with respect to copper constitutes the best compromise regarding the copper removal efficiency and the atom economy.

Table 3. Adsorption properties of Cell-SH.

Entry ^[a]	SH loading	Cu adsorbed	Yield
	(mol%)	(%)	(%) ^[b]
1	0	0	<5
2	3.2	4	41
3	8	58	43
4	16	94	87
5	24	97	88
6	32	97.5	91

[a] Reaction conditions: azide (1 mmol), alkyne (1.5 mmol), CuSO4.5H2O (2 mol%) and Cell-SH (see table) were stirred in 5 mL of tBuOH/H2O (1/1) at 70 °C for 14 h. [b] Isolated yield.

While we demonstrated that Cell-SH enabled the adsorption of ca. 95% of Cu initially introduced, we wondered if the paper strip removed after completion of the reaction could be reused in a second run without requiring additional Cu. The reuse of Cell-SH was explored for the cycloaddition of benzyl azide 1 with propargyl alcohol 2. An identical yield was observed for the 2^{nd} run (88%) while a sharp decrease occurred on the third reuse (ca. 50%) due to the fragility of paper upon successive reuses, leading to the loss of its physical integrity.

We also analyzed the nature of copper species adsorbed onto Cell-SH after one cycle. Scanning electron microscopy showed the formation of spherical copper nanoparticles (Cu NPs) with an average diameter of ca. 36 nm (Figure 1).

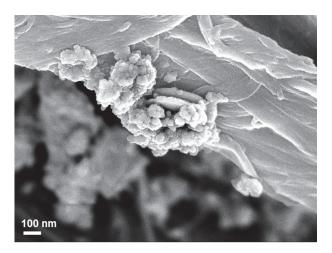


Figure 1. SEM image of copper nanoparticles deposited onto cellulose fibers after one cycle.

X-ray photoelectron spectroscopy of Cu NPs in the Cu2p region shows the absence of satellite peaks near 938-945 eV while the peaks at 932.5 and 952.3 eV accounting for Cu2p_{3/2} and Cu2p_{1/2} spin-orbit components suggest the formation of Cu₂O NPs (Figure 2).

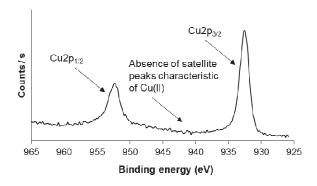


Figure 2. High resolution Cu2p XPS spectrum characteristic of Cu2O.

Since a similar behavior was observed for Cu in the absence of coupling partners, $^{[18]}$ we deduce from these results that Cell-SH rapidly adsorbs and reduces CuSO₄.5H₂O to Cu₂O NPs that act as catalyst for the transformation.

In summary, we unveiled a new concept for the [3+2]-cycloaddition of organic azides with alkynes using a heterogeneous reducing agent also acting has a powerful adsorbent for copper species in solution, leaving the crude product almost free of both copper residues and reducing agent. This technology consists in the use of cellulose paper as a heterogeneous biopolymer for supporting covalently thiol functions and was inspired from living systems that reduce Cu(II) to Cu(I) with cysteine residues from proteins. The robustness of our catalytic system was highlighted through the preparation of highly complex substrates. Inspiration from nature to uncover more sustainable methodologies is a field of research deserving huge attention and we believe that this work is a leading contribution that will be of great interest for synthetic chemists and biologists.

Acknowledgements

MdH thanks the "Région des Pays de la Loire" and the CNRS for the grant. FXF is member of the "Institut Universitaire de France, IUF." Denis Loquet (University of Nantes) and Julie Hémez (University of Nantes) are gratefully acknowledged for elemental and HRMS analyses respectively. We profoundly thank Sami Brument and Dimitri Alvarez-Dorta (University of Nantes) for providing us with cabohydrate-based starting materials.

References

- [1] (a) Bock, V. D.; Hiemstra, H.; van Maarseveen, J. H. Eur. J. Org. Chem. 2006, 51. (b) Gil,
 M. V.; Arévalo, M. J.; López, Ó. Synthesis 2007, 1589. (c) Meldal, M.; Tornøe, C. W. Chem.
 Rev. 2008, 108, 2952. (d) Hassan, S.; Müller, T. J. J. Adv. Synth. Catal. 2015, 357, 617. (e)
 Hein, J. E.; Fokin, V. V. Chem. Soc. Rev. 2010, 39, 1302.
- [2] (a) Huisgen, R. *Angew. Chem. Int. Ed. Engl.* **1963**, *2*, 565. (b) Huisgen, R. *Angew. Chem. Int. Ed. Engl.* **1963**, *2*, 633.
- [3] Tornøe, C. W.; Christensen, C.; Meldal, M. J. Org. Chem. 2002, 67, 3057.
- [4] Rostovtsev, V. V.; Green, L. G.; Fokin, V. V.; Sharpless, K. B. *Angew. Chem. Int. Ed.* **2002**, *41*, 2596.
- [5] (a) Thirumurugan, P.; Matosiuk, D.; Jozwiak, K. *Chem. Rev.* 2013, 113, 4905. (b) Hein,
 C. D.; Liu, X.-M.; Wang, D. *Pharm. Res.* 2008, 25, 2216. (c) Tiwari, V. K.; Mishra, B. B.;
 Mishra, K. B.; Mishra, N.; Singh, A. S.; Chen, X. *Chem. Rev.* 2016, 116, 3086.
- [6] Lutz, J.-F. Angew. Chem. Int. Ed. 2007, 46, 1018.
- [7] (a) Chan, T. R.; Hilgraf, R.; Sharpless, K. B.; Fokin, V. V. *Org. Lett.* **2004**, *6*, 2853. (b) Candelon, N.; Lastecoueres, D.; Diallo, A. K.; Ruiz Aranzaes, J.; Astruc, D.; Vincent, J.-M. *Chem. Commun.* **2008**, 741. (c) Angell, Y.; Burgess, K. *J. Org. Chem.* **2005**, *70*, 9595.
- [8] Pathigoolla, A.; Pola, R. P.; Sureshan, K. M. Appl. Catal. A: Gen. 2013, 453, 151.
- [9] Wang, Q.; Chan, T. R.; Hilgraf, R.; Fokin, V. V.; Sharpless, K. B.; Finn, M. G. *J. Am. Chem. Soc.* **2003**, *125*, 3192.
- [10] Hong, V.; Steinmetz, N. F.; Manchester, M.; Finn, M. G. *Bioconjugate Chem.* **2010**, *21*, 1912.

- [11] Liu, P.-Y.; Jiang, N.; Zhang, J.; Wei, X.; Lin, H.-H.; Yu, X.-Q. *Chem. Biodiversity* **2006**, *3*, 958.
- [12] (a) Harmand, L.; Cadet, S.; Kauffmann, B.; Scarpantonio, L.; Batat, P.; Jonusauskas, G.; McClenaghan, N. D.; Lastecoueres, D.; Vincent, J. M. *Angew. Chem. Int. Ed.* **2012**, *51*, 7137. (b) Harmand, L.; Lambert, R.; Scarpantonio, L.; McClenaghan, N. D.; Lastecoueres, D.; Vincent, J. M. *Chem. Eur. J.* **2013**, *19*, 16231. (c) Beniazza, R.; Lambert, R.; Harmand, L.; Molton, F.; Duboc, C.; Denisov, S.; Jonusauskas, G.; McClenaghan, N. D.; Lastecoueres, D.; Vincent, J. M. *Chem. Eur. J.* **2014**, *20*, 13181.
- [13] (a) Alonso, F.; Moglie, Y.; Radivoy, G. *Acc. Chem. Res.* **2015**, *48*, 2516. (b) Chassaing, S.; Beneteau, V.; Pale, P. *Catal. Sci. Technol.* **2016**, *6*, 923. (c) Gawande, M. B.; Goswami, A.; Felpin, F.-X.; Asefa, T.; Huang, X.; Silva, R.; Zou, X.; Zboril, R.; Varma, R. S. *Chem. Rev.* **2016**, *116*, 3722.
- [14] Yamada, Y. M. A.; Sarkar, S. M.; Uozumi, Y. J. Am. Chem. Soc. **2012**, 134, 9285.
- [15] Miao, T.; Wang, L. Synthesis 2008, 363.
- [16] (a) Boningari, T.; Olmos, A.; Reddy, B. M.; Sommer, J.; Pale, P. Eur. J. Org. Chem. 2010,
 2010, 6338. (b) Chassaing, S.; Sani Souna Sido, A.; Alix, A.; Kumarraja, M.; Pale, P.;
 Sommer, J. Chem. Eur. J. 2008, 14, 6713.
- [17] (a) Sharghi, H.; Khalifeh, R.; Doroodmand, M. M. Adv. Synth. Catal. 2009, 351, 207.
 (b) Lipshutz, B. H.; Taft, B. R. Angew. Chem. Int. Ed. 2006, 45, 8235. (c) Alonso, F.; Moglie, Y.; Radivoy, G.; Yus, M. Adv. Synth. Catal. 2010, 352, 3208. (d) Alonso, F.; Moglie, Y.; Radivoy, G.; Yus, M. Org. Biomol. Chem. 2011, 9, 6385. (e) Alonso, F.; Moglie, Y.; Radivoy, G.; Yus, M. J. Org. Chem. 2011, 76, 8394. (f) d'Halluin, M.; Mabit, T.; Fairley, N.; Fernandez, V.; Gawande, M. B.; Le Grognec, E.; Felpin, F.-X. Carbon 2015, 93, 974.
- [18] Rull-Barrull, J.; d'Halluin, M.; Le Grognec, E.; Felpin, F.-X. *Chem. Commun.* **2016**, *52*, 6569.
- [19] D. Klemm, B. Heublein, H.-P. Fink, A. Bohn, *Angew. Chem. Int. Ed.* **2005**, *44*, 3358-3393.
- [20] M. N. Belgacem, A. Gandini, *Monomers, polymers and composites from renewable resources*, Elsevier, **2011**.
- [21] (a) Carter, K. P.; Young, A. M.; Palmer, A. E. Chem. Rev. 2014, 114, 4564. (b) Cotruvo,
 J. J. A.; Aron, A. T.; Ramos-Torres, K. M.; Chang, C. J. Chem. Soc. Rev. 2015, 44, 4400. (c)

Roopa; Kumar, N.; Bhalla, V.; Kumar, M. *Chem. Commun.* **2015**, *51*, 15614. (d) J. Rull-Barrull, M. d'Halluin, E. Le Grognec, F.-X. Felpin, *Chem. Commun.* **2016**, *52*, 2525.

V Partie expérimentale

Materials

All commercial solvents and reagents were used as received without further purification from Sigma-Aldrich, Fischer Scientific Ltd, Alfa Aesar. Whatman® grade 6 filter paper (42.5 mm Ø) was used as cellulose source.

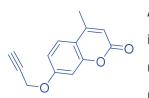
Analytical methods

All reactions were carried out under an atmosphere of nitrogen in dry glassware with magnetic stirring. Extra pure solvents were used without further purification. Purification of products was carried out by column chromatography using silica gel (40-30 $\mbox{2m}$). Analytical thin layer chromatography (TLC) was performed on 0.25 mm silica gel 60-F254 plates. Visualization was accomplished with UV lamp (254 nm) or using a**mmonium phosphomolybdate**. 1 H and 13 C NMR spectra were recorded at 400 MHz and 100 MHz, respectively, and they are reported as δ values (ppm) relative to residual CDCl₃ δ 1 H (7.26 ppm) and CD₃OD (3.31 ppm), CDCl₃ δ 13 C (77.16 ppm) and CD₃OD (49.00 ppm) as internal standards.

Experimental procedures

<u>Procedures for the preparation of starting materials</u>

4-Methyl-7-(propargyloxy)coumarin

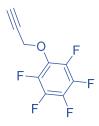


Anhydrous potassium carbonate (4.71 g, 34.1 mmol) was added in a solution of 7-hydroxy-4-methylcoumarin (400 mg, 2.28 mmol) in CH_3CN (25 mL) under inert atmosphere. Then, propargyl bromide (80% in toluene, 305 mL, 2.72 mmol) was

added to the solution and stirred for 12 h at 60 °C. After the completion of the reaction

the solution was filtered and washed twice with CH₃CN (2 x 10 mL). The solvent was evaporated under reduced pressure, diluted in CH₂Cl₂ (50 mL) and sequentially washed with an NH₄Cl saturated aqueous solution (10 mL) and brine (10 mL). The organic layer was dried over anhydrous MgSO₄, filtered and the solvent evaporated under reduced pressure, obtaining a pale yellow solid (463 mg, 97% yield) used in the next step without further purification. mp 130-131 °C, [Lit.^[1] 130-134 °C]. ¹H NMR (400 MHz, CDCl₃, ppm): $\delta_{\rm H}$ 7.49 (d, 1H, J = 8.9 Hz,), 6.89-6.91 (m, 2H), 6.11 (d, 1H, J = 1.1 Hz,), 4.73 (d, 2H, J = 2.4 Hz), 2.56 (t, 1H, J = 2.4 Hz), 2.36 (d, J = 1.2 Hz, 3H). ¹³C NMR (100 MHz, CDCl₃, ppm): $\delta_{\rm C}$ 161.1, 160.4, 155.1, 152.5, 125.7, 114.3, 112.7, 112.4, 102.3, 77.5, 76.6, 56.3, 18.7. HRMS (ESI) calcd for C₁₃H₁₀O₃Na [M+Na]⁺ 237.0528; found: 237.0531.

1,2,3,4,5-Pentafluorophenyl propargyl ether^[2]



A mixture of pentafluorophenol (1.27 g, 6.90 mmol), propargyl bromide (80% in toluene, 769 mL, 6.90 mmol), and anhydrous potassium carbonate (1.20 g, 6.90 mmol) in dry acetone (30 ml) was heated under reflux for 6 h, filtered and the solvent was removed under vacuum at room temperature. The residue was diluted with diethyl ether (30 mL),

washed with aqueous 4 N NaOH (10 mL). The organic phase was dried over MgSO₄ and evaporated under reduced pressure to give the titled compound as a pale yellow oil (1.46 g, 95% yield). 1 H NMR (400 MHz, CDCl₃, ppm): 4.80 (app t, 2H, J = 2.4 Hz), 2.53-2.55 (m, 1H). 13 C NMR (100 MHz, CDCl₃, ppm): $\delta_{\rm C}$ 162.6, 142.5 (m, 2C, 1 $_{\rm J}$ = 249.5 Hz), 138.1 (m, 2C, 1 $_{\rm J}$ = 250.5 Hz), 131.9 (m, 1C), 77.4, 76.8, 62.0.

3-(Prop-2-yn-1-yloxy)cholester[3]

A solution of cholesterol (1.98 g, 4.90 mmol) in THF (27 mL) under nitrogen was treated with NaH (60% in mineral oil, 294 mg, 7.35 mmol) at room temperature. After the suspension was stirred for 30 min, propargyl bromide (80% in toluene, 727 mL, 6.13 mmol) was added and the reaction mixture was stirred at 50 °C for 24 h. Then, the solution was quenched by methanol (10 mL) and the solvent was removed by evaporation under reduced pressure. The residual solid was dissolved in CH_2Cl_2 (50 mL) and washed with water (2 x 20 mL) and brine (20 mL). The organic phase was dried over

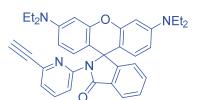
MgSO₄, filtrated and concentrated under reduced pressure. The crude product was further purified by flash chromatography on silica gel (100% petroleum ether) to give a white solid (1.98 g, 95% yield). mp 104-106 °C. 1 H NMR (400 MHz, CDCl₃, ppm): $\delta_{\rm H}$

5.36-5.37 (m, 1H), 4.19 (d, 2H, J = 2.4 Hz), 3.35-3.43 (m, 1H), 2.68-2.76 (m, 1H), 2.36-2.41 (ddd, 1H, J = 2.3 Hz, 4.8 Hz, 13.1 Hz), 2.40 (t, 1H, J = 2.4 Hz), 2.20-2.26 (m, 1H), 1.79–2.05 (m, 5H), 1.44-1.61 (m, 7H), 1.26-1.40 (m, 4H), 1.00-1.21 (m, 9H), 1.01 (s, 3H), 0.93 (d, 3H, J = 6.5 Hz), 0.88 (dd, 6H, J = 1.7 Hz, 6.6 Hz), 0.69 (s, 3H). ¹³C NMR (100 MHz, CDCl₃, ppm): $\delta_{\rm C}$ 140.7, 122.0, 80.6, 78.3, 73.9, 56.9, 56.3, 55.2, 50.3, 42.5, 39.9, 39.7, 38.9, 37.3, 36.9, 36.3, 35.9, 32.1, 32.0, 28.4, 28.2, 28.1, 24.4, 24.0, 22.9, 22.7, 21.2, 19.5, 18.9, 12.0.

a-Propargyl fucose (27)

A suspension of SiO₂ (2.00 g) in dry diethyl ether (10 mL) was treated with concentrated H₂SO₄ (0.60 mL) and shaken with an orbital stirrer during 10 min. The solvent was evaporated under reduced pressure and the resulting H₂SO₄—silica was dried at 110 °C for 3 h. a-p-fucose triacetate (2.70 g, 15 mmol) was suspended in a solution of propargyl alcohol (4.35 mL, 75 mmol) in CH₃CN (15 mL). Then, H₂SO₄—silica (100 mg) was added and the resulting mixture was stirred at 65 °C for 6 h. After cooling at room temperature, the solvent was evaporated under reduced pressure and the crude product was purified by flash chromatography on silica gel (100% CH₂Cl₂ to 5% MeOH-CH₂Cl₂) affording a viscous oil (3.35 g, 65% yield). ¹H NMR (400 MHz, CDCl₃, ppm): $\delta_{\rm H}$ 5.37 (dd, 1H, J = 3.3 Hz, 10.9 Hz), 5.26-5.27 (m, 1H), 5.22 (d, 1H, J = 3.8 Hz), 5.12 (dd, 1H, J = 3.3 Hz, 10.9 Hz), 4.23 (d, 1H, J = 2.4 Hz), 4.17 (q, 1H, J = 6.6 Hz), 2.41 (t, 1H, J = 2.4 Hz), 2.13 (s, 3H), 2.05(s, 3H), 1.95 (s, 3H), 1.11 (d, 3H, J = 6.6 Hz). ¹³C NMR (100 MHz, CDCl₃, ppm): $\delta_{\rm C}$ 170.6, 170.5, 170.0, 95.2, 78.7, 74.9, 71.2, 67.9, 67.9, 65.1, 55.3, 20.8, 20.7, 20.7, 15.8. MS (EI) m/z = 346 (M+NH₄)⁺.

Ethynyl pyridine rhodamine^[4]



2-Amino-6-bromopyridine (500 mg, 2.90 mmol), Pd(PPh₃)₂Cl₂ (60.0 mg, 0.09 mmol) and CuI (5 mg, 0.028

mmol, 5 mol %) were added to dry THF (40 mL) and the mixture was purged by argon for 30 min. The reaction mixture was cooled at 0 °C and triethylamine (10 mL) was added and stirred for 5 min. Then, ethynyltrimethylsilane (500 μL, 3.45 mmol) was subsequently added and stirred at room temperature. After 12 h, the reaction mixture was filtered through a short pad of alumina and washed with THF (50 mL). The solvent was removed under reduced pressure, and the obtained crude product was purified by flash chromatography on silica gel (10% THF-CH₂Cl₂) giving 2-amino-6-[(trimethylsilyl)ethynyl]pyridine as a white solid (450 mg, 82% yield). Subsequently, 2-amino-6-[(trimethylsilyl)-ethynyl]pyridine (450 mg, 2.35 mmol) was stirred in MeOH (30 mL) containing 20% KOH (6.00 g). After 1 h, water (40 mL) was added to dilute the mixture, which was extracted with EtAcO (3 × 50 mL). The combined organic phases were dried over anhydrous MgSO₄ and the solvent was removed under reduced pressure to afford 2-amino-6-ethynylpyridine as a pale brown solid (253 mg, 91% yield). The last step consisted in the reaction of Rhodamine B (844 mg, 1.77 mmol) with 2-amino-6ethynylpyridine (253 mg, 2.13 mmol) at reflux with a catalytic amount of POCl₃ (2 drops) in CH₃CN (40 mL). After 1 h of stirring, the reaction mixture was cooled to room temperature and volatiles were removed under reduced pressure. The crude product was purified by flash chromatography on basic Al₂O₃ (100% CH₂Cl₂), furnishing the titled compound as an orange solid (676 mg, 71% yield). mp 115-118 °C. ¹H NMR (400 MHz, CDCl₃, ppm): $\delta_{\rm H}$ 8.39 (d, 1H, J = 8.5 Hz), 8.01 (dd, 1H, J = 1.2 Hz, 6.2 Hz), 7.42-7.54 (m, 4H), 7.17 (d, 1H, J = 6.7 Hz), 6.96 (d, 1H, J = 7.4 Hz), 6.38-6.42 (m, 4H), 6.14 (dd, 2H, J =2.5 Hz, 8.8 Hz), 3.24-3.36 (m, 8H), 3.00 (s, 1H), 1.13 (t, 12H, J = 7.0 Hz); 13 C NMR (100) MHz, CDCl₃, ppm): δ_C 168.3, 154.3, 153.3, 150.5, 148.6, 139.5, 137.1, 133.8, 130.8, 128.3, 127.9, 124.7, 123.3, 122.9, 115.6, 108.4, 107.1, 98.1, 82.7, 75.4, 66.8, 44.5, 12.8.

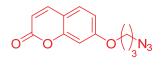
Rhodamine propargyl ether [5]

Rhodamine B (1.87 g, 4.2 mmol) was dissolved in 30 mL of ethanol and ethanolamine (3.50 mL, 56.6 mmol) was added dropwise with vigorous stirring at room temperature and refluxed overnight. Then, the solution was cooled to room temperature and the solvent was removed under reduced pressure. The residue was dissolved in $CHCl_3$ (50 mL) and washed with water (10 mL). The organic extract was dried with $MgSO_4$ and the crude product was purified on a short flash column chromatography (30% EtOAc-

petroleum ether), to give N-(hydroxyethyl)rhodamine as a colorless solid (1.15 g, 68% yield). To a suspension of NaH (60% in mineral oil, 1.70 g, 42.5 mmol) in THF (15 mL) at 0 °C was added a solution of N-(hydroxyethyl)rhodamine (1.15 g, 2.38 mmol) in THF (30 mL). After 10 min of

stirring, propargyl bromide (80% in toluene, 1.15 mL, 11.3 mmol,) was added and the resulting mixture was stirred at room temperature for 12 h. Then, the reaction was quenched with water (30 mL) and extracted with CH_2Cl_2 (2 x 50 mL). The collected organic extracts were washed with water (20 mL) and brine (20 mL) and dried over MgSO₄. Volatiles were removed under reduced pressure and the crude product was purified by flash chromatography on silica gel (30% EtAcO-petroleum ether) to give the titled compound as a rosy solid (1.07 g, yield 86%). mp 154-157 °C. ¹H NMR (400 MHz, CDCl₃, ppm): δ_H 7.87-7.89 (m, 1H), 7.38-7.40 (m, 2H), 7.03-7.06 (m, 1H), 6.43 (d, 2H, J = 8.9 Hz), 6.37 (d, 2H, J = 2.6 Hz), 6.26 (dd, 1H, J = 2.6 Hz, 8.9 Hz), 3.87 (d, 2H, J = 4.8 Hz), 3.35 (t, 2H, J = 7.4 Hz), 3.31 (q, 8H, J = 7.1 Hz), 3.21 (t, 2H, J = 6.6 Hz), 2.26 (t, 1H, J = 2.4 Hz), 3.20 (t, 2H, J = 6.8 Hz), 2.41 (t, 2H, J = 7.0 Hz), 1.14 (t, 12H, J = 7.0 Hz). ¹³C NMR (100 MHz, CDCl₃, ppm): δ_C 168.2, 153.7, 153.3, 148.8, 132.4, 131.0, 128.9, 127.9, 123.8, 122.8, 108.2, 105.6, 97.9, 79.7, 74.2, 66.7, 64.8, 57.7, 44.4, 39.1, 12.6. HRMS (ESI) calcd for $C_{33}H_{38}N_3O_3$ [M+H] $^+$ 524.2913; found: 524.2919.

7-(3-Azidopropyloxy)coumarin^[6]



A mixture of potassium carbonate (30.8 g, 222 mmol) and 1,3-dibromopropane (30.8 g, 154 mmol) was mixed in acetone (50 mL) and stirred under reflux during 10 min. To this resulting

mixture was slowly added 7-hydroxycoumarin (2.50 g, 15.4 mmol) and the reaction was stirred for 2 h under reflux. Acetone was removed under reduced pressure and the crude was diluted in CH_2Cl_2 (50 mL) and water (50 mL). The organic layer was separated, the water phase was extracted twice with CH_2Cl_2 (100 mL) and the combined organic layers were dried over MgSO₄. The crude product was purified by flash chromatography on silica gel (100% petroleum ether, then 100% CH_2Cl_2) to give 7-(3-bromopropyloxy)coumarin as a white solid (3.21 g, 78% yield). A solution of 7-(3-bromopropyloxy)coumarin (2.10 g, 7.35 mmol) and sodium azide (1.75 g, 26.3 mmol) in

DMF (30 mL) was stirred at 60 °C for 1 h. The mixture was cooled to room temperature and diluted with diethyl ether (50 mL). The organic phase was washed with 5% aqueous LiCl (3 x 20 mL), the organic extract was dried over MgSO₄ and evaporated to give the pure titled compound as yellow solid (1.69 g, 100%). mp = 82 °C. ¹H NMR (400 MHz, CDCl₃, ppm): $\delta_{\rm H}$ 7.59 (dd, 1H, J = 2.6 Hz, 9.4 Hz), 7.33 (dd, 1H, J = 3.0 Hz, 8.5 Hz), 6.80 (dt, 1H, J = 2.6 Hz, 8.5 Hz), 6.75-6.76 (m, 1H), 6.19 (dd, 1H, J = 4.6 Hz, 9.4 Hz), 4.05-4.08 (m, 2H), 3.47-3.51 (m, 2H), 3.35-3.39 (m, 2H), 2.03-2.06 (m, 2H), 1.77-1.81 (m, 1H). ¹³C NMR (100 MHz, CDCl₃, ppm): $\delta_{\rm C}$ 161.8, 161.0, 155.8, 143.3, 128.8, 113.1, 112.7, 112.7, 101.5, 65.2, 48.4, 48.0, 28.5, 28.3. HRMS (ESI) calcd for $C_{12}H_{11}N_3O_3Na$ [M+Na]⁺ 268.0698; found: 268.0709.

General procedure for the 1,3-dipolar cycloaddition

In a 25 mL pressure tube equipped with a magnetic stirring bar were sequentially added the azide (1 mmol) and the terminal alkyne (1.5 mmol) in a solution of t-BuOH (2.5 mL). To this mixture, was added an aqueous solution of $CuSO_4.5H_2O$ (2 mol%, 2.5 mL) followed by the addition of fresh thioglycolic-grafted paper (16 mol% SH). The reaction mixture was heated at 70 °C and kept under stirring for 14 hours. After completion, the solution was diluted with water (5 mL) and extracted with CH_2Cl_2 (3 x 10 mL). The organic layers were dried over MgSO₄, filtered and evaporated under reduced pressure. The crude product was purified by flash chromatography or isolated as pure compound after removal of volatiles.

1-(benzyl-1H-1,2,3-triazol-4-yl)methanol (3)

Triazole **3** was isolated as a white solid (164 mg, 87%) after removal of propargyl alcohol in excess under reduced pressure. mp 75-78 °C [Lit.^[7] 76-78 °C]. ¹H NMR (400 MHz, CDCl₃, ppm): $\delta_{\rm H}$ 7.45 (s, 1H), 7.30-7.33 (m, 3H), 7.21-7.24 (m, 2H), 5.45 (s, 2H), 4.70 (s, 2H), 3.88 (br s, 1H). ¹³C NMR (100 MHz, CDCl₃, ppm): $\delta_{\rm C}$ 148.4, 134.6, 129.2, 128.8, 128.2, 121.9, 56.2, 54.2. IR (ATR): 3246, 3138, 3086, 3033, 2936, 2883, 1495, 1455, 1220, 1130, 1062, 1036,

1011, 839, 789, 763, 717, 688, 648 cm⁻¹. HRMS (ESI) calculated for $C_{10}H_{12}N_3O$ [M+H]⁺ 190.0975; found: 190.0971.

4-Pentyl-1-(phenylmethyl)-1*H*-1,2,3-triazole (4)

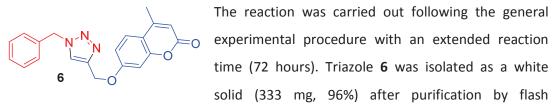
Triazole **4** was isolated as a white solid (224 mg, 98%) after removal of 1-heptyne in excess under reduced pressure. mp 70 °C. ¹H NMR (400 MHz, CDCl₃, ppm): $\delta_{\rm H}$ 7.34-7.36 (m, 3H), 7.23-7.26 (m, 2H), 7.18 (s, 1H), 5.48 (s, 2H), 2.67 (t, 2H, J = 7.6 Hz), 1.62-1.66 (m, 2H), 1.30-1.33 (m, 4H), 0.87 (t, 3H, J = 6.9 Hz). ¹³C NMR (100 MHz, CDCl₃, ppm): $\delta_{\rm C}$ 149.2, 135.2, 129.2, 128.7, 128.1, 120.6, 54.1, 31.6, 29.2, 25.8, 22.5, 14.1. IR (ATR): 3.113, 3064, 3039, 2957, 2926, 2856, 1605, 1551, 1493, 1456, 1435, 1336, 1213, 1182, 1132, 1051, 1029, 861, 822, 797, 698, 653, 578 cm⁻¹. HRMS (ESI) calculated for C₁₄H₂₀N₃ [M+H]⁺ 230.1652; found: 230.1645.

1-benzyl-5-((perfluorophenoxy)methyl)-1*H*-1,2,3-triazole (5)

Triazole **5** was isolated as a white solid (288 mg, 81%) after removal of 1,2,3,4,5-pentafluoro-6-(prop-2-yn-1-yloxy)benzene in excess under reduced pressure (75 °C, 10 mm Hg). mp 77 °C. 1 H NMR (400 MHz, CDCl₃, ppm): $\delta_{\rm H}$ 7.58 (s, 1H), 7.37-7.38 (m, 3H), 7.22-7.24 (m, 2H), 5.54 (s, 2H),

5.28 (s, 2H). ¹³C NMR (100 MHz, CDCl₃, ppm): $\delta_{\rm C}$ 143.1, 142.3 (m, 2C, ¹J = 248.9 Hz), 138.0 (m, 2C, ¹J = 250.9 Hz), 134.5, 132.5 (m, 1C), 129.3, 129.0, 128.1, 123.6, 67.9, 54.4. IR (ATR, cm⁻¹): 3088, 2961, 1518, 1463, 1384, 1338, 1305, 1228, 1157, 1125, 1032, 992, 940, 863, 811, 718, 694. HRMS (ESI) calcd for $C_{16}H_{11}F_{5}N_{3}O$ [M+H]⁺ 356.0817; found: 356.0813.

4-methyl-7-[[1-(phenylmethyl)-1*H*-1,2,3-triazol-4-yl]methoxy]-2*H*-1-Benzopyran-2-one (6)



chromatography on silica gel (5% MeOH-CH₂Cl₂). mp 134-137 °C. ¹H NMR (400 MHz,

CDCl₃, ppm): δ_H 7.52 (s, 1H), 7.40 (d, 1H, J = 8.8 Hz), 7.27-7.29 (m, 3H), 7.19-7.21 (m, 2H), 6.82 (dd, 1H, J = 2.5, 8.8 Hz), 6.78 (d, 1H, J = 2.5 Hz), 6.03 (d, 1H, J = 1.2 Hz), 5.46 (s, 2H), 5.13 (s, 2H), 2.29 (d, 3H, J = 1.2 Hz). ¹³C NMR (100 MHz, CDCl₃, ppm): δ_C 161.2, 161.1, 155.2, 152.5, 143.5, 134.5, 129.2, 128.9, 128.2, 125.8, 123.0, 114.1, 112.5, 112.3, 102.2, 62.4, 54.4, 18.7. IR (KBr pellet, cm⁻¹): 3136, 3071, 2948, 2931, 1718, 1609, 1505, 1457, 1390, 1368, 1341, 1274, 1200, 1157, 1070, 1000, 984, 858, 827, 726, 709. HRMS (ESI) calculated for $C_{20}H_{18}N_3O_3$ [M+H]* 348.1343; found: 348.1338.

1-ethoxycarbonylmethyl-4-hydroxymethyl-1,2,3-triazole (7)

Triazole **7** was isolated as a white solid (148 mg, 80% yield) after removal of propargyl alcohol in excess under reduced pressure. mp 70-75 °C. ¹H NMR (400 MHz, CDCl₃, ppm): $\delta_{\rm H}$ 7.65 (s, 1H), 5.12 (s, 2H), 4.74 (s, 2H), 4.23 (q, 2H, J = 7.2 Hz), 3.56 (br s, 1H), 1.27 (t, 3H, J = 7.2 Hz). ¹³C NMR (100 MHz, CDCl₃, ppm): $\delta_{\rm C}$ 166.5, 148.3, 123.5, 62.5, 56.3, 51.0, 14.1. IR (KBr pellet, cm⁻¹): 3261, 2992, 2867, 1745, 1459, 1422, 1380, 1345, 1237, 1173, 1021, 877, 836, 707, 681. HRMS (ESI) calcd for C₇H₁₂N₃O₃ [M+H]⁺ 186.0872; found: 186.0873.

Ethyl 2-(4-(hydroxymethyl)-1H-1,2,3-triazol-1-yl)propanoate (8)

The reaction was carried out following the general experimental procedure with a higher loading of CuSO₄·5H₂O (4 mol%). Triazole **8** was isolated as a white solid (145 mg, 73%) after removal of propargyl alcohol in excess under reduced pressure. mp 79-80 °C. ¹H NMR (400 MHz, CDCl₃, ppm): $\delta_{\rm H}$ 7.71 (s, 1H), 5.39 (dq, 1H, J = 1.5 Hz, 7.4 Hz), 4.73 (d, 2H, J = 2.1 Hz), 4.18 (dq, 2H, J = 1.5 Hz, 7.4 Hz), 3.62 (br s, 1H), 1.78 (dd, 3H, J = 1.5 Hz, 7.4 Hz), 1.22 (dt, 3H, J = 1.5 Hz, 7.4 Hz). ¹³C NMR (100 MHz, CDCl₃, ppm): $\delta_{\rm C}$ 169.3, 148.1, 121.3, 62.4, 58.3, 56.2, 18.1, 14.0. IR (ATR, cm⁻¹): 3337, 2986, 2944, 1740, 1450, 1382, 1302, 1192, 1159, 1097, 1042, 1014, 860, 821, 767, 689, 613. HRMS (ESI) calcd for C₈H₁₄N₃O₃ [M+H]⁺ 200.1030; found: 200.1024.

ethyl 2-(4-pentyl-1H-1,2,3-triazol-1-yl)acetate (9)

Triazole **9** was isolated as a pale yellow oil (202 mg, 90%) after removal of hept-1-yne in excess under reduced pressure. ¹H NMR (400 MHz, CDCl₃, ppm): $\delta_{\rm H}$ 7.40 (s, 1H), 5.10 (s, 2H), 4.24 (q, 2H, J = 7.2 Hz), 2.72 (t, 2H, J = 7.6 Hz), 1.65-1.69 (m, 2H), 1.31-1.34 (t, 3H, J = 7.1 Hz), 1.27 (m, 4H), 0.88 (t, 3H, J = 6.9 Hz). ¹³C NMR (100 MHz, CDCl₃, ppm): $\delta_{\rm C}$ 166.6, 149.0, 122.1, 62.4, 50.9, 31.5, 29.1, 25.7, 22.5, 14.1, 14.1. IR (ATR, cm⁻¹): 3136, 3088, 2956, 2922, 2862, 1742, 1554, 1462, 1403, 1371, 1340, 1224, 1139, 1050, 1025, 881, 838, 796, 753, 713. HRMS (ESI) calcd for C₁₁H₂₀N₃O₂ [M+H]⁺ 226.1550; found: 226.1546.

Ethyl 2-(4-pentyl-1H-1,2,3-triazol-1-yl)propanoate (10)

The reaction was carried out following the general experimental procedure with a higher loading of CuSO₄·5H₂O (4 mol%). Triazole **10** was isolated as a pale yellow oil (177 mg, 74%) as an inseparable mixture of 1,4- and 1,5-regioisomers in a 95/05 ratio respectively after after removal of hept-1-yne in excess under reduced pressure. ¹H NMR (400 MHz, CDCl₃, ppm): $\delta_{\rm H}$ 7.44 (s, 1H), 5.46 (q, 1H x 0.05, J = 7.4 Hz), 5.40 (q, 1H x 0.95, J = 7.4 Hz), 4.22 (q, 2H x 0.05, J = 7.2 Hz), 4.20 (q, 2H x 0.95, J = 7.2 Hz), 3.10 (t, 2H x 0.05, J = 7.5 Hz), 2.71 (t, 2H x 0.95, J = 7.6 Hz), 1.83 (d, 3H x 0.05, J = 7.4 Hz) 1.79 (d, 3H x 0.95, J = 7.4 Hz), 1.63-1.71 (m, 2H), 1.31-1.35 (m, 4H), 1.26 (t, 3H x 0.05, J = 7.2 Hz), 1.24 (t, 3H x 0.95, J = 7.1 Hz), 0.88 (t, 3H, J = 7.0 Hz). ¹³C NMR (100 MHz, CDCl₃, ppm, major regioisomer): $\delta_{\rm C}$ 169.6, 148.9, 119.8, 62.3, 58.2, 31.5, 29.1, 25.8, 22.5, 18.3, 14.1, 14.1. IR (ATR, cm⁻¹): 2955, 2931, 2861, 1748, 1553, 1457, 1379, 1303, 1224, 1197, 1099, 1072, 1046, 1023, 861. HRMS (ESI) calcd for C₁₂H₂₂N₃O₂ [M+H]⁺ 240.1707; found: 240.1700.

1-ethoxycarbonylmethyl-5-((perfluorophenoxy)methyl)-1H-1,2,3-triazole (11)

Triazole **11** was isolated as a white solid (309 mg, 88%) after removal of 1,2,3,4,5-pentafluoro-6-(prop-2-yn-1-

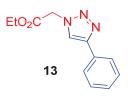
yloxy)benzene in excess under reduced pressure (75 °C, 10 mm Hg). mp 113-117 °C. 1 H NMR (400 MHz, CDCl₃, ppm): δ_{H} 7.83 (s, 1H), 5.33 (s, 2H), 5.16 (s, 2H), 4.26 (q, 2H, J = 7.2 Hz), 1.29 (t, 2H, J = 7.2 Hz) . 13 C NMR (100 MHz, CDCl₃, ppm): δ_{C} 166.1, 143.1, 142.2 (m, 2C, ^{1}J = 249.0 Hz), 138.2 (m, 2C, ^{1}J = 250.1 Hz), 132.5 (m, 1C), 125.1, 67.8, 62.7, 51.1, 14.1. IR (KBr pellet, cm⁻¹): 3125, 3082, 3003, 2960, 2661, 2455, 1745, 1649, 1516, 1427, 1421, 1384, 1345, 1313, 1227, 1183, 1151, 1115, 1034, 990, 919, 864, 809, 775, 714, 645. HRMS (ESI) calcd for $C_{13}H_{11}F_{5}N_{3}O_{3}$ [M+H]* 352.0715; found: 352.0710.

Ethyl 2-(4-((perfluorophenoxy)methyl)-1H-1,2,3-triazol-1-yl)propanoate (12)

The reaction was carried out following the general experimental procedure with a higher loading of CuSO₄.5H₂O (4 mol%). Triazole **12** was isolated as a pale yellow solid (237 mg, 65%) after removal of 1,2,3,4,5-pentafluoro-6-(prop-2-yn-1-yloxy)benzene in excess under reduced pressure (75 °C, 10 mm Hg). mp 70 °C. ¹H NMR

(400 MHz, CDCl₃, ppm): δ_H 7.87 (s, 1H), 5.45 (q, J = 7.4 Hz, 1H), 5.32 (s, 2H), 4.22 (q, 2H, J = 7.2 Hz), 1.83 (d, 3H, J = 7.4 Hz), 1.26 (t, 3H, J = 7.1 Hz). ¹³C NMR (100 MHz, CDCl₃, ppm): δ_C 169.1, 143.5, 142.9, 141.0, 139.3, 136.7, 132.5, 123.0, 67.9, 62.6, 58.5, 18.3, 14.0. IR (ATR, cm⁻¹): 2995, 2978, 2908, 1731, 1511, 1466, 1382, 1305, 1247, 1213, 1150, 1116, 1085, 1016, 989, 931, 866, 804, 770, 699, 680. HRMS (ESI) calcd for C₁₄H₁₃F₅N₃O₃ [M+H]⁺ 366.0872; found: 366.0868.

4-Phenyl-(1,2,3-triazole-1-yl)-acetic acid ethyl ester (13).



Triazole **13** was isolated as a pale yellow solid (213 mg, 92%) after removal of phenylacetylene in excess under reduced pressure. mp 100-102 °C [Lit.^[8] 100-101 °C]. ¹H NMR (400 MHz, CDCl₃, ppm): $\delta_{\rm H}$ 7.91 (s, 1H), 7.82-7.85 (m, 2H), 7.41 (t, J = 7.2 Hz, 2H), 7.30-7.34 (m,

2H), 5.18 (s, 2H), 4.26 (q, 2H, J = 7.2 Hz), 1.29 (t, 3H, J = 7.2 Hz). ¹³C NMR (100 MHz, CDCl₃, ppm): $\delta_{\rm C}$ 166.4, 148.3, 130.5, 128.9, 128.3, 125.9, 121.1, 62.5, 51.0, 14.1. IR (KBr pellet, cm⁻¹): 3135, 3079, 2985, 2960, 2901, 1748, 1558, 1470, 1448, 1418, 1374, 1225, 1119, 1077, 1049, 1023, 970, 917, 878, 814, 767, 721, 698. HRMS (ESI) calcd for $C_{12}H_{14}N_3O_2$ [M+H]⁺ 232.1081; found: 232.1081.

(2S)-(1-(4-Phenyl-1H-1,2,3-triazole-1-yl))-N-Boc-propan-2-amine (14).

BocHN N N

The reaction was carried out following the general procedure with $CuSO_4.5H_2O$ (4 mol%) for 48 hours at 70 °C. Triazole **14** was obtained as a white solid (211 mg, 70% yield) after purification by flash chromatography on silica gel (50% EtOAc-petroleum ether).

mp 146-147 °C. ¹H NMR (300 MHz, CDCl₃, ppm): $\delta_{\rm H}$ 7.79-7.83 (m, 3H), 7.39-7.44 (m, 2H), 7.29-7.35 (m, 1H), 4.78 (d, 1H, J = 6.2 Hz), 3.38-4.56 (m, 2H) 4.10 (sept, 1H, J = 6.6 Hz), 1.40 (s, 9H), 1.19 (d, 3H, J = 6.9 Hz); ¹³C NMR (75 MHz, CDCl₃, ppm): $\delta_{\rm C}$ 155.1, 147.7, 130.4, 128.8, 128.1, 125.6, 120.6, 79.9, 54.4, 46.7, 28.3, 18.0. HRMS (ESI) calcd for $C_{16}H_{23}N_4O_2$ [M+H]⁺ 303.1819; found: 303.1820.

2-(1-Benzyl-1H-1,2,3-triazol-5-yl)methoxy-cholesterol (15)

The reaction was carried out in a mixture of $t\text{-BuOH/H}_2\text{O/THF}$ (1:1:2) with CuSO₄.5H₂O (4 mol%) for 14 hours at 70 °C. Triazole **15** was obtained as a white solid (480 mg, 86%) after purification by

flash chromatography on silica gel (20% EtOAc-petroleum ether). mp 125-126 °C [Lit.^[9] 121 °C]. ¹H NMR (400 MHz, CDCl₃, ppm): $\delta_{\rm H}$ 7.37 (s, 1H), 7.28-7.30 (m, 3H), 7.19-7.21 (m, 2H), 5.43 (s, 2H), 5.25–5.26 (m, 1H), 4.58 (s, 2H), 3.19-3.26 (m, 1H), 2.28–2.33 (m, 1H), 2.11–2.18 (m, 1H), 1.65–1.94 (m, 6H), 1.17–1.48 (m, 11H), 0.91–1.10 (m, 8H), 0.91 (s, 3H), 0.84 (d, 3H, J = 6.5 Hz), 0.79 (dd, 6H, J = 1.5 Hz, 6.5 Hz), 0.60 (s, 3H). ¹³C NMR (100 MHz, CDCl₃, ppm): $\delta_{\rm C}$ 146.6, 140.8, 134.8, 129.2, 128.9, 128.3, 122.3, 121.9, 79.1, 61.9, 56.9, 56.3, 54.3, 50.3, 42.5, 39.9, 39.7, 39.2, 37.3, 37.0, 36.3, 35.9, 32.1, 32.0, 28.4, 28.3, 28.1, 24.4, 24.0, 23.0, 22.7, 21.2, 19.5, 18.9, 12.0. IR (KBr pellet, cm⁻¹): 2935, 2866, 1460, 1372, 1086, 1054, 780, 724. HRMS (ESI) calcd for C₃₇H₅₆N₃O [M+H]⁺ 558.4418; found: 558.4413.

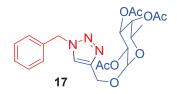
Ethyl 2-(1H-1,2,3-triazol-5-yl)methoxyacetate-cholesterol (16)

The reaction was carried out in a mixture of $t\text{-BuOH/H}_2\text{O/THF}$ (1:1:2) with CuSO₄.5H₂O (4 mol%) for 14 hours at 70 °C. Triazole **16** was obtained as a white solid (415 mg, 75%) as an inseparable

mixture of 1,4- and 1,5-regioisomers in a 9/1 ratio respectively after purification by flash chromatography on silica gel (15% EtOAc-petroleum ether). mp 128-130 °C. ¹H NMR (400 MHz, CDCl₃, ppm): $\delta_{\rm H}$ 7.67 (s, 1H x 0.9), 7.59 (s, 1H x 0.1), 5.34-5.35 (m,1H), 5.24 (s, 2H x 0.1), 5.13 (s, 2H x 0.9), 4.71 (s, 2H x 0.9), 4.63 (s, 2H x 0.1), 4.26 (q, 2H x 0.9, J = 7.2 Hz), 4.24 (q, 2H x 0.1, J = 7.2 Hz), 3.28-3.36 (m, 1H x 0.9), 3.16-3.24 (m, 1H x 0.1), 2.40 (ddd, 1H, J = 2.3 Hz, 4.7 Hz, 13.2 Hz), 2.20–2.30 (m, 1H), 1.92–2.03 (m, 3H), 1.78-1.88 (m, 3H), 1.42-1.63 (m, 8H), 1.25-1.40 (m, 5H), 1.30 (t, 3H x 0.9, J = 7.2 Hz), 1.29 (t, 3H x 0.1, J = 7.1 Hz), 0.97–1.19 (m, 10H), 1.00 (s, 3H), 0.91 (d, 3H, J = 6.6 Hz), 0.86 (dd, 6H, J = 1.8 Hz, 6.6 Hz), 0.67 (s, 3H). ¹³C NMR (100 MHz, CDCl₃, ppm, major regioisomer): $\delta_{\rm C}$ 166.4,

146.7, 140.8, 123.7, 121.9, 79.0, 62.5, 61.8, 56.9, 56.3, 51.0, 50.3, 42.5, 40.0, 39.7, 39.2, 37.3, 37.0, 36.3, 35.9, 32.1, 32.1, 28.5, 28.4, 28.2, 24.4, 24.0, 22.9, 22.7, 21.2, 19.5, 18.9, 14.2, 12.0. IR (KBr pellet, cm $^{-1}$): 2935, 2903, 2867, 2849, 1746, 1469, 1375, 1341, 1273, 1253, 1139, 1026, 845. HRMS (ESI) calcd for $C_{34}H_{56}N_3O_3$ [M+H] $^+$ 554.4316; found: 554.4318.

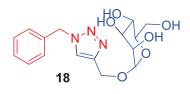
(1-Benzyl-1H-1,2,3-triazol-4-yl)methyl-α-D-tetraacetate fucopyranoside (17)



The reaction was carried out following the general experimental procedure with a higher loading of $CuSO_4.5H_2O$ (4 mol%). Triazole **17** was obtained as a colorless oil (364 mg, 79%) after purification by flash chromatography on silica

gel (40% EtOAc-petroleum ether). 1 H NMR (400 MHz, CDCl₃, ppm): $\delta_{\rm H}$ 7.33 (s, 1H), 7.26-7.28 (m, 3H), 7.17-7.19 (m, 2H), 5.42 (d, 2H, J = 3.5 Hz), 5.21 (dd, 1H, J = 3.4 Hz, 10.7 Hz), 5.15-5.16 (m, 1H), 5.04 (d, 1H, J = 3.8 Hz), 5.00 (dd, 1H, J = 3.6 Hz, 10.7 Hz), 4.69 (d, 1H, J = 12.7 Hz), 4.53 (d, 1H, J = 12.7 Hz), 4.05 (q, 1H, J = 6.4 Hz), 2.04 (s, 3H), 1.85 (d, 6H, J = 2.3 Hz). 13 C NMR (100 MHz, CDCl₃, ppm): $\delta_{\rm C}$ 170.6, 170.4, 170.0, 144.5, 134.6, 129.3, 128.9, 128.2, 122.6, 95.8, 71.2, 68.1, 68.0, 64.8, 61.5, 54.3, 20.8, 20.7, 20.7, 15.9. IR (ATR, cm⁻¹): 2985, 2940, 1739, 1497, 1454, 1435, 1369, 1220, 1165, 1130, 1048, 1013, 973, 928, 909, 821, 726, 671, 649.

(1-Benzyl-1H-1,2,3-triazol-4-yl)methyl-α-D-mannopyranoside (18)



The reaction was carried out following the general procedure with CuSO₄·5H₂O (4 mol%) for 48 hours at 70 °C. Triazole **18** was obtained as a white foam (249 mg, 71% yield) after purification by flash chromatography on silica

gel (2% H₂O-acetone). ¹H NMR (300 MHz, MeOD, ppm): $\delta_{\rm H}$ 7.99 (s, 1H), 7.30-7.41 (m, 5H), 5.59 (s, 2H), 4.83 (d, 1H, J = 1.6 Hz), 4.78 (d, 1H, J = 12.4 Hz), 4.63 (d, 1H, J = 12.4 Hz), 3.82 (dd, 1H, J = 2.1 Hz, 11.8 Hz), 3.77 (dd, 1H, J = 1.7 Hz, 3.1 Hz), 3.51-3.71 (m, 4H); ¹³C NMR (75 MHz, MeOD, ppm): $\delta_{\rm C}$ 145.7, 136.7, 130.1, 129.6, 129.2, 125.3, 100.8, 75.0, 72.5, 72.0, 68.6, 62.9, 60.7, 55.0. HRMS (ESI) calcd for $C_{16}H_{22}N_3O_6$ [M+H]⁺ 352.1505; found: 352.1508.

4-Hydroxymethyl-1H-1,2,3-triazol-1-yl)ethoxy-α-D-mannopyranoside (19)

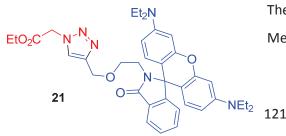
The reaction was carried out following the general procedure with CuSO₄.5H₂O (4 mol%) for 48 hours at 70 °C. Triazole **19** was obtained as a white foam (250 mg, 82% yield) after purification by flash chromatography on silica gel (5% H₂O-acetone). ¹H NMR (300 MHz,

DMSO, ppm): $\delta_{\rm H}$ 7.92 (s, 1H), 5.17 (t, 1H, J = 5.7 Hz), 4.74 (app t, 1H, J = 4.3 Hz), 4.62 (d, 1H, J = 1.5 Hz), 4.44-4.59 (m, 5H), 3.89-3.97 (m, 1H), 3.74-3.81 (m, 1H), 3.61 (dd, 1H, J = 2.0 Hz, 11.6 Hz), 3.52-3.53 (m, 1H), 3.31-3.41 (m, 5H°, 3.13 (app t, 1H, J = 6.9 Hz); 13 C NMR (75 MHz, DMSO, ppm): $\delta_{\rm C}$ 147.9, 123.0, 99.8, 74.1, 70.7, 70.0, 66.7, 65.0, 61.1, 55.0, 49.2. HRMS (ESI) calcd for $C_{11}H_{19}N_3O_7$ [M+H]⁺ 305.1220; found: 305.1224.

2-((1-Benzyl-1H-1,2,3-triazol-5-yl)methyl)-rhodamine (20)

The reaction was carried out following the general procedure with CuSO₄-5H₂O (4 mol%) for 48 hours at 70 °C. Triazole **20** was obtained as a white solid (473 mg, 70% yield) after purification by flash chromatography on silica gel (1% Et₃N-9% EtOAc-petroleum ether). mp > 250 °C (dec.). ¹H NMR (400 MHz, CDCl₃, ppm): δ_H 8.55 (dd, 1H, J = 0.9 Hz, 8.4 Hz), 8.12 (s, 1H), 7.98-8.00 (m, 1H), 7.74 (dd, J = 7.7 Hz, J = 0.9 Hz, 1H), 7.63 (dd, 1H, J = 7.7 Hz, 8.4 Hz), 7.42–7.54 (m, 7H), 7.03-7.05 (m, 1H), 6.47 (dm, 2H, J = 8.4 Hz), 6.13 (d, 1H, J = 2.6 Hz), 6.10 (m, 3H), 5.58 (s, 2H), 3.16-3.26 (m, 8H), 1.08 (t, 12H, J = 7.0 Hz); ¹³C NMR (100 MHz, CDCl₃, ppm): δ_C 168.8, 154.4, 152.5, 150.5, 148.9, 148.3, 147.9, 137.9, 135.0, 133.7, 129.6, 129.3, 128.9, 128.4, 128.1, 127.8, 124.2, 123.4, 122.7, 115.4, 115.0, 108.7, 107.8, 97.5, 65.9, 54.3, 44.3, 12.8. IR (KBr pellet, cm⁻¹): 2971, 2929, 2891, 2868, 1695, 1636, 1615, 1575, 1549, 1518, 1464, 1427, 1400, 1374, 1353, 1325, 1272, 1219, 1151, 1118, 1090, 1078, 1039, 1020, 946, 909, 860, 814, 787, 757, 734, 727, 705, 630, 608, 592. HRMS (ESI) calcd for C₄₂H₄₂N₇O₂ [M+H]⁺ 676.3400; found: 676.3400.

Ethyl 2-(1H-1,2,3-triazol-5-yl)acetate-rhodamine (21)



The reaction was carried out in a mixture of $MeOH/H_2O/CH_2Cl_2$ (1:1:3) with $CuSO_4.5H_2O$

(4 mol%) for 48 hours at 70 °C. Triazole **21** was obtained as a white solid (639 mg, 98%) after purification by flash chromatography on silica gel (4% MeOH-CH₂Cl₂). mp 98-100 °C. ¹H NMR (400 MHz, CDCl₃, ppm): $\delta_{\rm H}$ 7.87-7.89 (m, 1H), 7.61 (s, 1H), 7.39-7.43 (m, 2H), 7.05-7.07 (m, 1H), 6.42 (d, 2H, J = 8.8 Hz), 6.37 (d, 2H, J = 2.6 Hz), 6.25 (dd, 2H, J = 2.6 Hz, 8.8 Hz), 5.09 (s, 2H), 4.40 (s, 2H), 4.23 (q, 2H, J = 7.0 Hz), 3.38 (t, 2H, J = 7.2 Hz), 3.32 (q, 8H, J = 7.1 Hz), 3.20 (t, 2H, J = 7.1 Hz), 1.27 (t, 3H, J = 7.0 Hz), 1.15 (t, 12H, J = 7.0 Hz). 13 C NMR (100 MHz, CDCl₃, ppm): $\delta_{\rm C}$ 168.4, 168.3, 153.9, 153.4, 149.0, 146.1, 132.5, 131.1, 128.9, 128.0, 123.9, 123.8, 122.8, 108.3, 105.7, 98.0, 67.6, 64.9, 64.5, 62.4, 50.9, 44.5, 39.4, 14.2, 12.7. IR (KBr pellet, cm⁻¹): 2972, 2931, 2899, 2871, 1754, 1690, 1615, 1546, 1515, 1466, 1425, 1379, 1330, 1304, 1267, 1220, 1117, 1093, 1047, 1020, 915, 870, 819, 790, 759, 729, 702. HRMS (ESI) calcd for $C_{37}H_{45}N_6O_5$ [M+H] 653.3446; found: 653.3450.

7-(3-(4-(Hydroxymethyl)-1H-1,2,3-triazol-1-yl)propoxy)-2H-chromen-2-one (22)

The reaction was carried out following the general procedure with a higher loading of CuSO₄.5H₂O (4 mol%). Triazole **22** was obtained as a white solid (256 mg, 79%) after purification by flash chromatography on

silica gel (9% MeOH-EtOAc). mp 130-134 °C. ¹H NMR (400 MHz, CD₃OD, ppm): $\delta_{\rm H}$ 7.93 (s, 1H), 7.85 (d, 1H, J = 9.5 Hz), 7.51 (d, 1H, J = 8.6 Hz), 6.90 (dd, 1H, J = 2.4 Hz, 8.6 Hz), 6.85 (d, 1H, J = 2.4 Hz,), 6.23 (d, 1H, J = 9.4 Hz), 4.67 (s, 2H), 4.63 (t, 2H, J = 6.8 Hz), 4.60 (t, 2H, J = 5.9 Hz), 4.10 (t, 2H, J = 6.0 Hz), 2.42 (qt, 2H, J = 6.1 Hz). ¹³C NMR (100 MHz, CD₃OD, ppm): $\delta_{\rm C}$ 163.5, 163.2, 157.0, 149.2, 145.7, 130.5, 124.4, 114.2, 114.1, 113.5, 102.4, 66.5, 56.5, 48.3, 30.8. IR (KBr pellet, cm⁻¹): 3393, 3128, 3083, 3067, 2943, 2868, 1724, 1710, 1694, 1616, 1507, 1398, 1354, 1280, 1235, 1205, 1159, 1127, 1049, 1038, 995, 838, 791, 755. HRMS (ESI) calcd for C₁₅H₁₅N₃O₄Na [M+Na]⁺ 324.0960; found: 324.0966.

Ethyl 2-(1H-1,2,3-triazol-5-yl)propapoate-rhodamine (23)

The reaction was carried out in a mixture of MeOH/ H_2O/CH_2Cl_2 (1:1:3) with CuSO₄₋₅H₂O (4 mol%) for 48 hours at 70 °C. Triazole **23**

was obtained as a white solid (699 mg, 91% yield) after purification by flash chromatography on silica gel (9% MeOH-CH₂Cl₂). mp 85-90 °C. ¹H NMR (400 MHz, CDCl₃, ppm): $\delta_{\rm H}$ 7.86-7.89 (m, 1H), 7.60 (d, 1H, J = 9.5 Hz), 7.51 (d, 1H, J = 5.8 Hz), 7.40-7.42 (m, 2H), 7.34 (d, 1H, J = 8.5 Hz), 7.04-7.08 (m, 1H), 6.80 (dd, 1H, J = 2.4 Hz, 8.5 Hz,), 6.77 (d, 1H, J = 2.4 Hz), 6.41 (dd, 2H, J = 4.5, 8.8 Hz), 6.37 (d, 2H, J = 2.5 Hz), 6.22-6.26 (m, 3H), 4.54 (t, 2H, J = 6.8 Hz), 4.38 (s, 2H), 4.02 (t, 2H, J = 5.8 Hz), 3.29-3.38 (m, 10H), 3.19 (t, 2H, J = 6.8 Hz), 5.09 (s, 2H), 4.40 (s, 2H), 4.23 (q, 2H, J = 7.0 Hz), 3.30-3.40 (m, 10H), 3.20 (t, 2H, J = 6.8 Hz), 2.41 (qt, J = 7.0 Hz, 2H), 1.15 (t, J = 7.0 Hz, 12H). ¹³C NMR (100 MHz, CDCl₃, ppm): $\delta_{\rm C}$ 168.4, 161.7, 161.1, 155.9, 153.8, 153.4, 149.0, 145.8, 143.4, 132.5, 131.1, 129.0, 128.9, 128.1, 123.9, 122.8, 122.7, 113.5, 113.0, 112.7, 108.2, 105.6, 101.8, 98.0, 67.6, 64.9, 64.5, 47.0, 44.5, 39.4, 29.8, 12.7. IR (KBr pellet, cm⁻¹): 2970, 2930, 2871, 2242, 2099, 1735, 1687, 1614, 1547, 1514, 1466, 1427, 1394, 1355, 1329, 1300, 1268, 1225, 1120, 1093, 1045, 1019, 913, 826, 789, 759, 729, 639. HRMS (ESI) calcd for C₄₅H₄₉N₆O₆ [M+H]⁺ 769.3709; found: 769.3714.

References

- [1] I. Kosiova, S. Kovackova, P. Kois, *Tetrahedron* **2007**, *63*, 312-320.
- [2] G. M. Brooke, J. Chem. Soc., Perkin Trans. 1 1974, 233-237.
- [3] Z.-P. Yu, C.-H. Ma, Q. Wang, N. Liu, J. Yin, Z.-Q. Wu, *Macromolecules* **2016**, *49*, 1180-1190.
- [4] K. Sreenath, R. J. Clark, L. Zhu, J. Org. Chem. 2012, 77, 8268-8279.
- [5] H. Lu, S. Qi, J. Mack, Z. Li, J. Lei, N. Kobayashi, Z. Shen, J. Mater. Chem. 2011, 21, 10878-10882.
- [6] R. C. Chadwick, V. Kardelis, S. Liogier, A. Adronov, *Macromolecules* 2013, 46, 9593-9598.
- [7] F. Alonso, Y. Moglie, G. Radivoy, M. Yus, Eur. J. Org. Chem. 2010, 1875-1884.
- [8] M. d'Halluin, T. Mabit, N. Fairley, V. Fernandez, M. B. Gawande, E. Le Grognec, F.-X. Felpin, *Carbon* **2015**, *93*, 974-983.
- [9] A. M. Deobald, L. R. S. Camargo, D. Alves, J. Zukerman-Schpector, A. G. Corrêa,M. W. Paixão, *Synthesis* 2011, 4003-4010.

Chapitre 5 Préparation d'un nouveau matériau pour l'élimination de métaux dans l'eau

I <u>Introduction</u>

La dernière partie de cette thèse concerne la préparation d'une membrane de filtration capable de décontaminer des solutions aqueuses contenant des métaux lourds.

Inspiré par les travaux récents de Sakairi¹ portant sur la préparation d'un agent floculant à base de chitosan fonctionnalisé par de l'acide éthylène diamine tétraacétique (EDTA), nous avons décidé d'appliquer une stratégie similaire afin de préparer une membrane à base de papier capable de chélater les métaux.

La préparation de ce dispositif se fait *via* une réaction d'estérification entre la cellulose et le dianhydride de l'EDTA. Le matériau ainsi obtenu a par la suite été immergé dans des solutions aqueuses contenant différents métaux à une concentration initiale de 100 ppm, puis après un certain temps de contact, la solution est analysée par spectroscopie d'absorption atomique (AAS) ou par spectrométrie à plasma à couplage inductif (ICP) selon la nature du métal. Les analyses ont montré que ce matériau est capable de chélater de nombreux métaux offrant ainsi un dispositif universel pour la dépollution des eaux contaminées par des métaux lourds (Figure 1).

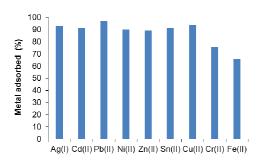


Figure 1 Capacité d'adsorption de la « membrane EDTA » vis-à-vis de différents métaux

Ce travail a fait l'objet d'une publication dans le journal ACS Sustainable Chemistry & Engineering².

- 1. S. Fujita, N. Sakairi, RSC Adv. 2016, 6, 10385–10392.
- 2. M. d'Halluin, J. Rull-Barrull, E. Le Grognec, F.-X. Felpin, Submitted to ACS Sustain. Chem. Eng. n° sc-2016-01683q*

II <u>Chemically modified cellulose filter paper for universal heavy</u> metal remediation

ABSTRACT

A chemically modified cellulose filter paper with ethylenediaminetetraacetic acid (EDTA) is described as a universal device for metal remediation. This new material was prepared by esterification of the paper with EDTA dianhydride. The high hydrophilicity of cellulose paper associated to the strong chelating properties of the EDTA moieties for metals allow the treatment of water samples containing various metal cations, including Ag(I), Ni(II), Zn(II), Cd(II), Pb(II), Sn(II) and Cu(II), with 90-95% removal efficiency. The mechanism of adsorption was deeply studied with the support of kinetic experiments and adsorption isotherms. As practical feature, one can note that the cellulose-EDTA material works on a wide range of pH and can be used either as a solid adsorbent or a membrane for continuous wastewater treatment.

Introduction

Being at the end of the food chain, humans are highly exposed to bio-accumulating contaminants such as heavy metals. From the 10 majors chemical concerns for public health identified by the World Health Organization (WHO), four of them are heavy metals, including cadmium and lead. Upon repeated exposures to pollutants including heavy metals, mainly through water supply and seafood, humans can be affected by severe disorders. For instance, in 2013, UNICEF reported that ca. 2000 children below five years die every day of diarrheal diseases due to unsafe drinking water. Therefore, the natural or anthropogenic contamination of the aquatic environment by heavy metals is a severe environmental concern for humans, animals and plants.

Physically and chemically removing heavy metals from contaminated water has been an obvious preoccupation for chemists, driven by environmental concerns and legislative pressures. In occupational settings, heavy metals have been removed from waste stream by a variety of methods including adsorption, flocculation, membrane separation, ion-exchange, precipitation, evaporation, and electrolysis. 1-3

Adsorption has been regarded as one of the most cost-effective and operationally flexible techniques for metal removal and can be used together with filtration to increase remediation efficiency. These last years, biosorption techniques involving the use of sorbents derived from renewable resources such as agricultural waste, biological materials and biopolymers, have been acknowledged as promising alternatives to methods.4-11 conventional As environmentally-friendly, biocompatible and biodegradable resources, biopolymers constitute very appealing materials for metal remediation. Chitin, consisting of N-acetyl-d-glucosamine residues, and chitosan, its Ndeacetylated derivative, have been studied for heavy metal remediation since they display inherent metal coordination properties that can be increased by chemical modifications. $\frac{12-16}{6}$ By contrast, cellulose consisting of repeating β -d-glucose units, do not form stable coordination complexes with metals and has therefore a low adsorption capacity. Yet cellulose is the most abundant biopolymer on earth and transforming this inexpensive and renewable raw material to an efficient bioadsorbent is an exciting challenge of environmental sciences. Three different approaches have been proposed for increasing the adsorption capacity of cellulose for heavy metal ions. 5 The first one involves graft copolymerization on the cellulose backbone with side chains 17 either having metal binding capacity or allowing further functionalization with chelating moieties. 18-22 The second approach focuses on the preparation of cellulose-based composites with either organic polymers 23-24 or inorganic materials. The last strategy consists in a direct chemical modification of the cellulose backbone, mainly through the functionalization of hydroxyl groups with moieties having strong metal affinities. 26-28

While the above approaches involve wood pulp, micro- and nanocellulose, the use of chemically modified cellulose filter paper for metal removing has been overlooked. Advantage of using bulk cellulose paper is twice since it can be used as either an adsorbent when immersed in solution or a membrane for purification of liquid streams. Many available evidences demonstrate that the strong chelating agent ethylenediaminetetraacetic acid (EDTA) immobilized on biopolymers acts as an efficient metal binding for water purification. Pollowing our interest for using covalently modified cellulose paper as analytical devices for pollutant detection, we report

herein the development of a chemically modified cellulose filter paper with EDTA acting as a universal device for metal remediation. We show how the same device can be used as either an immersed adsorbent or a filtration membrane allowing an unprecedented flexibility for metal remediation.

Material and methods

General remarks. All commercial solvents and reagents were used as received from Sigma-Aldrich, Fischer Scientific Ltd, Alfa Aesar. Whatman® grade 6 filter paper (42.5 mm Ø) was used as cellulose source. ¹H and ¹³C NMR, recorded at 400 MHz and 100 MHz respectively, were performed on a Bruker Advance 400. Proton chemical shifts were internally referenced to the residual proton resonance in DMSO (2.50 ppm). Carbon chemical shifts were internally referenced to the deuterated solvent signals in DMSO (39.52 ppm). Melting points were recorded on a Stuart Scientific 7SMP3 apparatus. FT-IR spectra were recorded on a Bruker Tensor 27 spectrometer with ATR technic. Scanning electron microscopy (SEM) images were recorded with a JEOL 7600 F. X-ray photoelectron spectroscopy was performed on a Thermo Fisher Scientific K-ALPHA spectrometer was used for disk surface analysis with a monochromatized AlKα source (hv = 1486.6 eV) and a 200 micron spot size. A pressure of 10^{-7} Pa was maintained in the chamber during analysis. The full spectra (0-1150eV) were obtained at a constant pass energy of 200 eV and high resolution spectra at a constant pass energy of 40 eV. Charge neutralization was required for all insulating samples. High resolution spectra were fitted and quantified using the AVANTAGE software provided by Thermo Fisher Scientific. Atomic absorption spectroscopy analyses were carried out on a THERMO SCIENTIFIC ICE 3300. ICP-AES analyses were carried out on a Thermo Fischer ICAP 6300. Elemental analyses were performed on a Thermo Fisher Scientific Flash 2000 CHNS organic elemental analyzer.

Preparation of ethylenediaminetetraacetic acid dianhydride (EDTA dianhydride) (1). Ethylenediaminetetraacetic acid dianhydride was prepared following the literature procedure.³³ To a suspension of ethylenediaminetetraacetic acid (EDTA, 30.0 g, 102.6 mmol) in pyridine (50 mL) under N₂ was added Ac₂O (40 mL). The mixture was stirred at 65 °C for 24 h and then cooled to room temperature, and filtered under a N₂ stream. The

collected solid was washed with Ac₂O (100 mL) and diethyl ether (250 mL) and dried under high vacuum to give **1** as a white solid (24 g, 91%). mp. 194-196 °C [lit. 33 194-195 °C]. 1 H NMR (400 MHz, DMSO,) δ 3.70 (s, 8H), 2.67 (s, 4H). 13 C NMR (100 MHz, DMSO) δ 165.7, 52.2, 51.2. IR (ATR) ν 2995, 2962, 2908, 2859, 1805, 1750, 1465, 1421, 1368, 1344, 1320, 1287, 1248, 1133, 1111, 1060, 998, 961, 925, 882, 818, 783, 656, 607, 550, 499, 482, 435 cm⁻¹.

General procedure for the pre-treatment of cellulose paper. Five pieces of cellulose filter papers (approx. 750 mg) were dispersed in 250 ml of a freshly prepared 10% (w/w) NaOH aqueous solution. This mixture was then shacked 24 h on an orbital agitator. The cellulose samples were washed 6 times with 50 ml of EtOH and stored in EtOH.

General procedure for the preparation of cell-EDTA. After being washed 2 times with 20 ml of DMSO, 5 pieces of pretreated cellulose papers (approx. 750 mg, 4.5 mmol) were immersed in 100 ml of dry DMSO and a solution of EDTA dianhydride **2** (3.46 g, 13.5 mmol) in dry pyridine (5 ml) was added. The mixture was shacked 20 h at 60 °C under N_2 on an orbital agitator. The pieces of paper were sonicated in EtOH, MilliQ water, acetone and CH_2Cl_2 before being dried under vacuum. The samples were analyzed by elemental analysis giving N% 2.10-2.20.

General procedure for metal adsorption. Metal solutions were freshly prepared by dissolving the desired amount of metal salt in MilliQ water in a plastic capped *via*l and a piece of EDTA-modified filter paper was immersed. The *via*l was then shacked on an orbital agitator for the required time. The piece of filter paper was then removed from the solution; the latter was analyzed either by ICP-AES or AAS. If required, the sample was diluted in order to reach the linearity of the calibration curves.

Results and discussion

Preparation of the cellulose filter paper-grafted EDTA. The covalent grafting of EDTA onto the surface of paper requires the esterification of one carboxylic function of the EDTA moieties with the hydroxyl groups of the ($\beta1 \rightarrow 4$) linked d-glucose units constituting the cellulose chains. The dense intra- and intermolecular hydrogen bond networks occurring in cellulose chains associated to the bulk nature of paper make

hydroxyl functions of glucose units weakly reactive. For instance, esterification processes under acidic conditions or using traditional coupling agents such as DCC/DMAP usually fail to give good degree of functionalization of cellulose paper and the use of more reactive acid chlorides or anhydrides are required.³⁴ Moreover, in order to break the hydrogen bond network and increase both the surface area of cellulose fibers and the reactivity of alcohols functions, the cellulose filter paper was soaked for 24 hours in 10% NaOH aqueous solution prior chemical modification.³⁵ The activated cellulose paper was functionalized with the highly reactive ethylenediaminetetraacetic acid dianhydride 1, easily obtained by treatment of commercially available EDTA with Ac₂O in pyridine (Scheme 1). The cellulose filter paper functionalized with EDTA (cell-EDTA) was copiously washed with EtOH, MilliQ water, acetone and CH₂Cl₂ to remove all trace of adsorbed compounds. The degree of functionalization was estimated to be ca. 0.2 by elemental analysis. In other words, it can be estimated that two alcohol functions were esterified with EDTA moieties every ten glucose units. We stress that all attempts to functionalize the cellulose filter paper with ethylenediaminetetraacetic acid chloride, instead of EDTA anhydride 2, failed to give a good degree of functionalization.

Scheme 1. Preparation of the cell-EDTA material.

Characterisation of the cellulose cell-EDTA. The chemical functionalization of the cellulose paper with EDTA moieties was followed by FT-IR as depicted in Figure 1. Both

spectra of pristine and chemically modified papers exhibit characteristic absorption bands of the cellulose backbone in the region of 3400, 2900 and 1100 cm⁻¹ accounting for the stretching vibrations of O-H, C-H and C-O-C bonds respectively. In pristine cellulose, the band at 1641 cm⁻¹ is assigned to the bending mode of adsorbed water. FT-IR spectrum of the chemically modified cellulose paper reveals a new band at 1726 cm⁻¹ corresponding to the stretching vibration of the carbonyl group of the newly formed ester linkage between cellulose and EDTA and providing evidence that the grafting had successfully occurred. The two absorption bands at 1591 and 1421 cm⁻¹ are characteristic of the asymmetric and symmetric OCO stretching modes of the carboxylate group, respectively, giving an additional evidence for the successful incorporation of EDTA in the cellulose backbone.

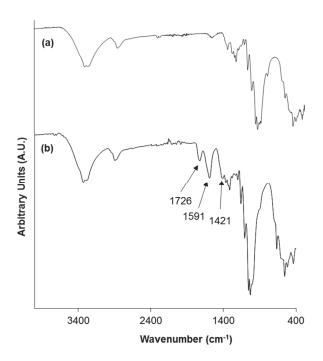


Figure 1. FT-IR spectra of (a) pristine cellulose paper and (b) cell-EDTA.

X-ray photoelectron spectroscopy analyses of both the pristine and functionalized papers give important information on the evolution of the surface composition occurring upon immobilization of the EDTA backbone (Figure 2). The high resolution spectrum of the C1s region of cell-EDTA reveals a new peak at 289.9 eV arising from the C=O photoemissions (Figure 2d). The survey scan spectra of cell-EDTA showed a peak at

399.7 eV attributed to the nitrogen atom of the EDTA moieties (Figure 2c). Photoemissions from the 1s core level nitrogen environment result in two shifted peak components, furnishing further structural insights (Figure 2e). While the peak at 399.6 eV can be attributed to the neutral form of the EDTA moieties, the peak shifted by 2.2 eV at a higher binding energy (401.8 eV) is ascribed to the protonated nitrogen atom of the zwitterionic intermediate, in good agreement with previous observations on amino acids.³⁶

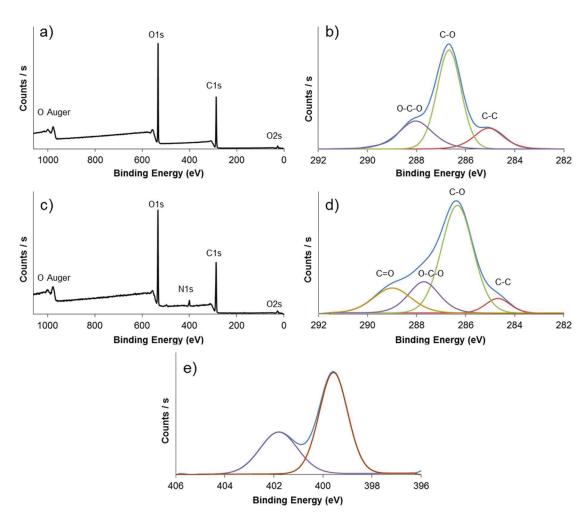


Figure 2 Survey scan spectra of (a) pristine paper, (c) cell-EDTA. High resolution C1s spectra of (b) pristine paper, (d) cell-EDTA. (d) High resolution N1s spectrum of cell-EDTA.

One of the potential issue with the chemical grafting of cellulose paper is the modification of the fibers structure resulting in altered physical properties such as resistance and structure integrity in aqueous and organic solvents. Scanning electron microscopy images depicted in Figure 3 reveal that the size of the fibers is not affected, being in the range of 10-20 μ M both the pristine and functionalized materials. This observation explains why the modified paper is not wrinkled nor weaken after the EDTA grafting. The peripheral filamentous aspect of the fibers surface can be explain by a marginal break of the hydrogen bond network upon chemical grafting but without consequence on the paper integrity.

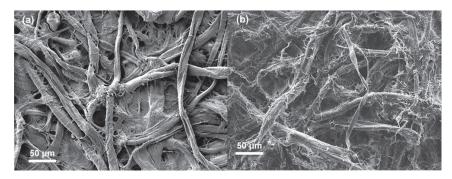


Figure 3. SEM images of (a) pristine cellulose paper and (b) cell-EDTA.

Adsorption studies. Effect of pH. The heavy metal remediation efficiency from aqueous solution by adsorption strongly depends on the pH value of the solution as the concentration of protons affects the adsorbent surface charge and the degree of ionization of the metal. The adsorption capacities of the cell-EDTA paper with respect to the pH of the solution was studied for Pb(II) and Cd(II) two highly toxic heavy metals. Two solutions containing 100 ppm of Pb(II) and Cd(II) respectively, were shacked with the cell-EDTA paper (5g/L) at room temperature for 90 min. After removal of cell-EDTA, the metal content of the solutions was analyzed by atomic absorption spectroscopy (AAS) or inductively coupled plasma atomic emission spectroscopy (ICP-AES). The results depicted in Figure 4 reveals important features. For the two metals, the maximum adsorption capacities are observed at pH ranging from 4 to 9. At higher pH values the increase of the concentration of hydroxide anions leads to the formation of metal hydroxide species precipitating in water. The adsorption capacities of the modified

paper rapidly decrease upon lowering the pH values below 4. At pH < 4, the protons compete with metal cations for binding active sites as their concentration increases. Moreover, at high proton concentration the surface of cellulose becomes positively charged and the approach of metal cations is disfavored due to electrostatic repulsions. In the conditions of this study, less than 5 ppm of Pb(II) and Cd(II) remain in solution after 90 min at pH ranging from 5 to 9 which means that ca. 95% of metal cations were adsorbed by cell-EDTA while in the presence of the unmodified cellulose paper more than 90% of metals (93% for Pb and 90% for Cd) still remain in solution at pH 7. In order to simulate real environmental conditions where the pH of water is usually in the range of 6.5-7.5, our further studies were carried out at pH 7.

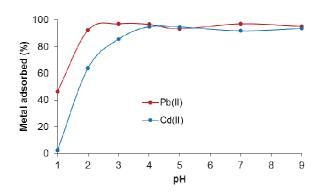


Figure 4. Effect of pH on metal adsorption by cell-EDTA.

Effect of contact time. The contact time-adsorption efficiency relationship is an important parameter as it determines the time required for the maximum removal of metals from the solution and may assess the adsorbent lifetime. As depicted in Figure 5, the static remediation of a solution containing 100 ppm of Pb(II) was fast and reached a plateau within 50 min with ca. 94% of metal adsorbed. A similar behavior was observed for the remediation of a solution containing 100 ppm of Cd(II) but the plateau was reached within 120 min with ca. 95% of metal adsorbed. For both metals a break slope was observed at 15 min, indicating that two different binding sites participate to the adsorption mechanism. Since the break slope occurred for the two metals after 15 min, it can be suggested that the cell-EDTA properties change upon extended stirring due to the swelling of fibers in water, opening regions to metal adsorption.

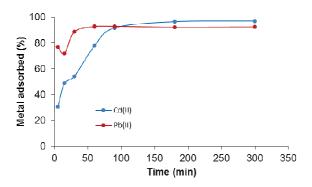


Figure 5. Effect of contact time on metal adsorption by cell-EDTA.

In order to better understand the adsorption process and predict the rate of metal removal from aqueous solutions, kinetics investigations were carried out through the evaluation of the pseudo-first-order and pseudo-second-order kinetic models. We found that the pseudo-first-order kinetics for Cd(II) and Pb(II) failed to properly explain the adsorption process. By contrast, the pseudo-second-order kinetics represented by the linear plot of t/q_t versus t describes accurately the adsorption process considering the very good correlation coefficient ($R^2 >> 0.99$) and the theoretical q_e values are in very good agreement with the experimental values (Figure 6).

The linear form of the pseudo-second-order kinetic model can be written as 37:

$$\frac{t}{q_{t}} = \frac{1}{k_{2}q_{e}^{2}} + \frac{1}{q_{e}}t$$
 (2)

where q_e and q_t (mg/g) are the adsorption capacities at equilibrium and at time t (min) respectively and k_2 (g/mg min) is the pseudo-second-order rate constant of the adsorption. From these results we can deduce that the rate of the adsorption process was controlled by chemisorption through sharing or exchange of electrons between the adsorbent and the adsorbate as covalent forces.

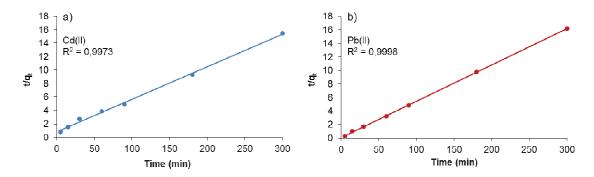


Figure 6. Pseudo-second-order plot (a) for Cd(II) and (b) for Pb(II) adsorption onto cell-EDTA (pH = 7, concentration of metal ions = 100 ppm, adsorbent dose = 5g/L).

Adsorption isotherms. Adsorption isotherms are used to understand the relationship between the amount of adsorbate on the adsorbent and the adsorbate remaining in solution at the equilibrium. Many models have been reported in the literature and their validity strongly depends on the nature of both the adsorbent and adsorbate. With the objective of describing accurately the adsorption isotherm of our cell-EDTA paper, we deeply examined the Langmuir, Freundlich and Temkin isotherms which represent the three most frequently used models.

The Langmuir model describes the formation of a saturated monolayer of adsorbate at the surface of the adsorbent. This model assumes that binding sites are energetically equivalents, each of them accommodating only one molecule of adsorbate, and interaction between adsorbed molecules are neglected. Therefore, the Langmuir model fits with adsorption processes leading to the formation of a monolayer of adsorbates onto an adsorbent containing a finite number of identical binding sites. The Langmuir isotherm model can be expressed as:

$$\frac{C_e}{q_e} = \frac{C_e}{q_m} + \frac{1}{bq_m} \tag{1}$$

where C_e (mg/L) is the equilibrium concentration of metal remaining in solution, q_e (mg/g) is the amount of metal adsorbed at the equilibrium, q_m is the maximum adsorption capacity of the adsorbent and b (L/mg) is the Langmuir constant.

The Freundlich isotherm is commonly used to describe adsorption phenomena on heterogeneous adsorbent surfaces since it assumes that a multilayer adsorption on a heterogeneous surface can be expressed with the following empirical equation:

$$q_e = K_f C_e^{1/n} \tag{2}$$

Linearizing equation (2) results in the following equation:

$$\ln q_e = \ln K_f + \frac{1}{n} \ln C_e \tag{3}$$

where C_e (mg/L) is the metal concentration remaining in solution at the equilibrium, q_e (mg/g) is the equilibrium adsorption capacity and K_f and 1/n are empirical Freundlich constant related to the adsorption capacity and intensity of adsorption respectively.

With the Temkin isotherm, adsorbate-adsorbent interactions are considered and it is assumed that the energy of adsorption is a linear function of the surface coverage. The equation implies a uniform distribution of binding energies onto the adsorbent surface and is expressed as follow:

$$q_e = \left(\frac{RT}{b_T}\right) \ln(A_T C_e) \tag{4}$$

Linearizing equation (4) results in the following equation:

$$q_e = \left(\frac{RT}{b_T}\right) \ln(A_T) + \left(\frac{RT}{b_T}\right) \ln(C_e)$$
 (5)

where q_e (mg/g) is the equilibrium adsorption capacity, C_e (mg/L) is the metal concentration remaining in solution at the equilibrium, A_T (L/g) is the Temkin isotherm equilibrium constant, b_T (J/mol) is the Temkin constant related to heat of adsorption, R (8.314 J/mol/K) is the universal gas constant and T (K) is the absolute temperature.

The regression curves were plotted for the three models and the correlation coefficients (R^2) were determined (Figure 7). As shown in Table 1, the three models correctly fit with the adsorption process of Pb(II) and Cd(II) with the cell-EDTA as good to high correlation coefficients (R^2) were calculated. The Freundlich model is the less suitable to properly describe the adsorption process, though good correlation coefficients of 0.93 and 0.92 were determined for Cd(II) and Pb(II) respectively. The Langmuir model gave very good R^2 (0.98) for Cd(II) and good correlation coefficients for Pb(II). Since the Langmuir model describes a homogeneous adsorption processes, the good R^2 calculated for the two metals indicate that the adsorption mainly occurred on adsorption sites energetically equivalents and located at the outer surface of the fibers and not inside the porous network. The linear plot of C_e/q_e versus C_e allows determining the maximum absorption capacities (q_m) for Cd(II) and Pb(II) with values of 102.04 and 227.27 mg/g respectively. These large absorption capacities are in good agreement with the experimental values

and are consistent with the Freundlich constant K_f which indicates a good adsorption capacity of the cell-EDTA for the two metals.

In the Langmuir model, the dimensionless separation factor for equilibrium parameters (R_L) , predicting the affinity between the adsorbate and the adsorbent can be defined as $R_L = 1/(1+bC_0)$, where C_0 (mg/L) is the initial concentration of metal ions. The value of R_L indicates whether the adsorption isotherm is either irreversible ($R_L = 0$), favorable ($0 < R_L < 1$) or unfavorable ($R_L > 1$). The values calculated for R_L are 0.032-0.4 for Cd(II) and 0.048-0.5 for Pb(II), indicating a favorable adsorption process. This is consistent with the results of the Freundlich model for which the n parameter in the range of 1 to 10 also indicates a favorable adsorption process. The Temkin isotherm is a very suitable model to accurately describe the adsorption of Cd(II) and Pb(II) since high R^2 values of 0.98 and 0.96 respectively were determined from linear plot of q_e versus In C_e suggesting strong adsorbate-adsorbent interactions.

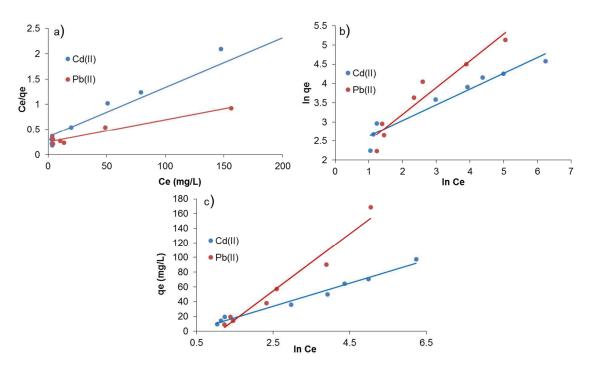


Figure 7. (a) Langmuir isotherms, (b) Freundlich isotherms and (c) Temkin isotherms for Cd(II) and Pb(II) adsorption onto cell-EDTA (pH = 7, time = 180 min, adsorbent dose = 5g/L).

Table 1. Isotherm parameters and regression data for Cd(II) and Pb(II).

Isotherm	Parameter	Cd(II)	Pb(II)
Langmuir	q _m (mg/g)	102.04	227.27
	b (L/mg)	0.03	0.02
	RL	0.032-0.4	0.048-0.5
	R ²	0.98	0.93
Freundlich	K _f	6.54	6.07
	n	2.08	1.43
	R ²	0.93	0.92
Temkin	B_{T}	15.58	38.92
	bτ	0.16	0.064
	A_T	0.65	0.33
	R ²	0.98	0.96

Adsorption of other metals. The ability of the cell-EDTA material to act as a universal adsorbent for the remediation of various heavy metals was evaluated (Figure 8). For the sake of argument, the metal ions considered in this study are recurrent environmental water pollutants damaging living systems and include Ag(I), Cd(II), Pb(II), Ni(II), Zn(II), Sn(II), Cu(II), Cr(II) and Fe(II). In order to compare the adsorption capacity of the cell-EDTA adsorbent, we used standard conditions consisting of the remediation of solutions containing 100 ppm of metal ions with 5g/L of cell-EDTA. The level of remediation was determined by atomic absorption spectroscopy or inductively coupled plasma atomic emission spectroscopy analyses of the solutions after removal of the cell-EDTA adsorbent. This study revealed the very good performance of the cell-EDTA adsorbent for Ag(I), Ni(II), Zn(II), Cd(II), Pb(II), Sn(II) and Cu(II) since more than 90% of metal ions initially introduced was adsorbed after 1h30 of soaking. The cell-EDTA material displayed a lower but still useful adsorption capacity for Cr(II) and Fe(II) with 76% and 66% of removal respectively. These results illustrate the powerful capacity of the cell-EDTA material to act as a universal adsorbent for water decontamination.

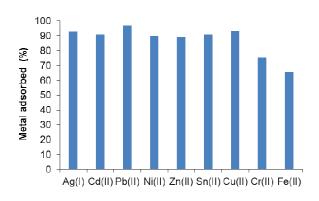


Figure 8. Adsorption efficiency of cell-EDTA for various heavy metals.

Use of cell-EDTA as membrane vs adsorbent. All the studies described above were carried out for the remediation of metal ions in water using cell-EDTA as an adsorbent. In other words, the modified cellulose paper was soaked into the contaminated solution during the required time. However, proceeding with a continuous remediation using the EDTA-grafted filter paper as a membrane would be of great interest in the industrial environment where large volumes of aqueous effluents have to be treated. With this objective in mind, we studied the purification of an aqueous solution containing 100 ppm of Cd(II) ions. After a careful flow rate optimization, we were able to remove 94% of the initial amount of Cd(II) ions with a flow rate of 4 mL/h using a small membrane of only 60 mg for the treatment of 12 mL of wastewater. This very promising result open the way for further scale-up in the industrial environment using larger membranes.

Conclusion

In summary, by exploiting the high hydrophilicity of cellulose filter paper and the excellent chelating properties of EDTA for many metal ions, we have designed a universal material for metal remediation that can be used as an adsorbent or as a simple membrane of filtration operating over a wide range of pH values. This new device for water purification was prepared by the covalent grafting of the EDTA backbone to the surface of cellulose filter paper. The properties of this very robust material were deeply evaluated through adsorption kinetic and adsorption isotherm studies. The high hydrophilicity, disposability and low toxicity of cellulose paper constitute key parameters for the design of new generations of cellulose-based adsorbents and membranes for addressing the complex issue of wastewater treatment. We believe that this work is a solid contribution in this area that will profit to a large panel of scientists working in analytical and environmental sciences.

Acknowledgements

MdH thanks the "Région des Pays de la Loire" and the CNRS for the grant. FXF is member of the "Institut Universitaire de France, IUF." Denis Loquet (University of Nantes), François-Xavier Lefèvre (University of Nantes) and Carole La (University of Nantes) are gratefully acknowledged for elemental, SEM and ICP-AES analyses respectively. SEM analyses were carried out at the "Institut des matériaux Jean Rouxel." We sincerely thank Mrs. Joanna Boucard (University of Nantes) for serving as a model for the abstract graphic.

References

- (1) Mohan, D.; Pittman Jr, C. U. Arsenic removal from water/wastewater using adsorbents—A critical review. *J. Hazard. Mater.* **2007**, *142*, 1-53.
- (2) Barakat, M. A. New trends in removing heavy metals from industrial wastewater. *Arab. J. Chem.* **2011**, *4*, 361-377.
- (3) Fu, F.; Wang, Q. Removal of heavy metal ions from wastewaters: A review. *J. Environ. Manage.* **2011,** *92*, 407-418.
- (4) Demirbas, A. Heavy metal adsorption onto agro-based waste materials: A review. *J. Hazard. Mater.* **2008**, *157*, 220-229.
- (5) O'Connell, D. W.; Birkinshaw, C.; O'Dwyer, T. F. Heavy metal adsorbents prepared from the modification of cellulose: A review. *Bioresour. Technol.* **2008**, *99*, 6709-6724.
- (6) Sud, D.; Mahajan, G.; Kaur, M. P. Agricultural waste material as potential adsorbent for sequestering heavy metal ions from aqueous solutions A review. *Bioresour. Technol.* **2008**, *99*, 6017-6027.
- (7) Wan Ngah, W. S.; Hanafiah, M. A. K. M. Removal of heavy metal ions from wastewater by chemically modified plant wastes as adsorbents: A review. *Bioresour. Technol.* 2008, 99, 3935-3948.
- (8) Bilal, M.; Shah, J. A.; Ashfaq, T.; Gardazi, S. M. H.; Tahir, A. A.; Pervez, A.; Haroon, H.; Mahmood, Q. Waste biomass adsorbents for copper removal from industrial wastewater—A review. J. Hazard. Mater. 2013, 263, Part 2, 322-333.
- (9) Hegazi, H. A. Removal of heavy metals from wastewater using agricultural and industrial wastes as adsorbents. *HBRC Journal* **2013**, *9*, 276-282.
- (10) Nguyen, T. A. H.; Ngo, H. H.; Guo, W. S.; Zhang, J.; Liang, S.; Yue, Q. Y.; Li, Q.; Nguyen, T. V. Applicability of agricultural waste and by-products for adsorptive removal of heavy metals from wastewater. *Bioresour. Technol.* **2013**, *148*, 574-585.
- (11) Wang, X.; Lü, S.; Gao, C.; Feng, C.; Xu, X.; Bai, X.; Gao, N.; Yang, J.; Liu, M.; Wu, L. Recovery of ammonium and phosphate from wastewater by wheat straw-based amphoteric adsorbent and reusing as a multifunctional slow-release compound fertilizer. *ACS Sustainable Chem. Eng.* **2016**, *4*, 2068-2079.

- (12) Zhou, D.; Zhang, L.; Zhou, J.; Guo, S. Cellulose/chitin beads for adsorption of heavy metals in aqueous solution. *Water Res.* **2004**, *38*, 2643-2650.
- (13) Zhou, D.; Zhang, L.; Guo, S. Mechanisms of lead biosorption on cellulose/chitin beads. *Water Res.* **2005**, *39*, 3755-3762.
- (14) Wang, X.; Bai, H.; Yao, Z.; Liu, A.; Shi, G. Electrically conductive and mechanically strong biomimetic chitosan/reduced graphene oxide composite films. *J. Mater. Chem.* **2010**, *20*, 9032-9036.
- (15) Aliabadi, M.; Irani, M.; Ismaeili, J.; Piri, H.; Parnian, M. J. Electrospun nanofiber membrane of PEO/Chitosan for the adsorption of nickel, cadmium, lead and copper ions from aqueous solution. *Chem. Eng. J.* **2013**, *220*, 237-243.
- (16) Aliabadi, M.; Irani, M.; Ismaeili, J.; Najafzadeh, S. Design and evaluation of chitosan/hydroxyapatite composite nanofiber membrane for the removal of heavy metal ions from aqueous solution. *J. Taiwan Inst. Chem. Eng.* **2014**, *45*, 518-526.
- (17) Roy, D.; Semsarilar, M.; Guthrie, J. T.; Perrier, S. Cellulose modification by polymer grafting: a review. *Chem. Soc. Rev.* **2009**, *38*, 2046-2064.
- (18) Güçlü, G.; Gürdağ, G.; Özgümüş, S. Competitive removal of heavy metal ions by cellulose graft copolymers. *J. Appl. Polym. Sci.* **2003**, *90*, 2034-2039.
- (19) Yu, X.; Tong, S.; Ge, M.; Wu, L.; Zuo, J.; Cao, C.; Song, W. Synthesis and characterization of multi-amino-functionalized cellulose for arsenic adsorption. *Carbohydr. Polym.* **2013**, *92*, 380-387.
- (20) Tian, Y.; Wu, M.; Liu, R.; Wang, D.; Lin, X.; Liu, W.; Ma, L.; Li, Y.; Huang, Y. Modified native cellulose fibers—A novel efficient adsorbent for both fluoride and arsenic. J. Hazard. Mater. 2011, 185, 93-100.
- (21) Zheng, Y. Q.; Deng, S.; Niu, L.; Xu, F. J.; Chai, M. Y.; Yu, G. Functionalized cotton *via* surface-initiated atom transfer radical polymerization for enhanced sorption of Cu(II) and Pb(II). *J. Hazard. Mater.* **2011**, *192*, 1401-1408.
- (22) O'Connell, D. W.; Birkinshaw, C.; O'Dwyer, T. F. A chelating cellulose adsorbent for the removal of Cu(II) from aqueous solutions. *J. Appl. Polym. Sci.* **2006**, *99*, 2888-2897.
- (23) Li, N.; Bai, R. Copper adsorption on chitosan–cellulose hydrogel beads: behaviors and mechanisms. *Sep. Purif. Technol.* **2005**, *42*, 237-247.

- (24) Yang, R.; Aubrecht, K. B.; Ma, H.; Wang, R.; Grubbs, R. B.; Hsiao, B. S.; Chu, B. Thiol-modified cellulose nanofibrous composite membranes for chromium (VI) and lead (II) adsorption. *Polymer* **2014**, *55*, 1167-1176.
- (25) Choi, S.; Jeong, Y. The removal of heavy metals in aqueous solution by hydroxyapatite/cellulose composite. *Fiber. Polym.* **2008**, *9*, 267-270.
- (26) Hokkanen, S.; Repo, E.; Sillanpää, M. Removal of heavy metals from aqueous solutions by succinic anhydride modified mercerized nanocellulose. *Chem. Eng. J.* **2013**, *223*, 40-47.
- (27) Yu, X.; Tong, S.; Ge, M.; Wu, L.; Zuo, J.; Cao, C.; Song, W. Adsorption of heavy metal ions from aqueous solution by carboxylated cellulose nanocrystals. *J. Environ. Sci.* **2013**, *25*, 933-943.
- (28) Li, Y.; Wen, Y.; Wang, L.; He, J.; Al-Deyab, S. S.; El-Newehy, M.; Yu, J.; Ding, B. Simultaneous visual detection and removal of lead(ii) ions with pyromellitic dianhydride-grafted cellulose nanofibrous membranes. *J. Mat. Chem. A* **2015**, *3*, 18180-18189.
- (29) Fujita, S.; Sakairi, N. Water soluble EDTA-linked chitosan as a zwitterionic flocculant for pH sensitive removal of Cu(ii) ion. *RSC Adv.* **2016**, *6*, 10385-10392.
- (30) Kahovec, J.; Matějka, Z.; Štamberg, J. EDTA ester of bead cellulose a fast-kinetics chelating sorbent. *Polym. Bull.* **1980,** *3*, 13-17.
- (31) Rull-Barrull, J.; d'Halluin, M.; Le Grognec, E.; Felpin, F.-X. A paper-based biomimetic device for the reduction of Cu(ii) to Cu(i) application to the sensing of Cu(ii). *Chem. Commun.* **2016**, *52*, 6569-6572.
- (32) Rull-Barrull, J.; d'Halluin, M.; Le Grognec, E.; Felpin, F.-X. Chemically-modified cellulose paper as smart sensor device for colorimetric and optical detection of hydrogen sulfate in water. *Chem. Commun.* **2016**, *52*, 2525-2528.
- (33) Capretta, A.; Maharajh, R. B.; Bell, R. A. Synthesis and characterization of cyclomaltoheptaose-based metal chelants as probes for intestinal permeability. *Carbohydr. Res.* **1995**, *267*, 49-63.
- (34) d'Halluin, M.; Rull-Barrull, J.; Le Grognec, E.; Jacquemin, D.; Felpin, F.-X. Writing and erasing hidden optical information on covalently modified cellulose paper. *Chem. Commun.* **2016**, *52*, 7672-7675.

- (35) Goldmann, A. S.; Tischer, T.; Barner, L.; Bruns, M.; Barner-Kowollik, C. Mild and modular surface modification of cellulose *via* hetero Diels–Alder (HDA) cycloaddition. *Biomacromolecules* **2011**, *12*, 1137-1145.
- (36) Nolting, D.; Aziz, E. F.; Ottosson, N.; Faubel, M.; Hertel, I. V.; Winter, B. pH-Induced protonation of lysine in aqueous solution causes chemical shifts in X-ray photoelectron spectroscopy. *J. Am. Chem. Soc.* **2007**, *129*, 14068-14073.
- (37) Ho, Y.-S. Review of second-order models for adsorption systems. *J. Hazard. Mater.* **2006**, *136*, 681-689.

Conclusion générale et perspectives

Les objectifs de cette thèse ont été de développer de nouveaux matériaux à base de papier grâce à des méthodes de fonctionnalisations covalentes de ce dernier.

La première partie de ce travail a été consacrée au développement d'une nouvelle méthode d'écriture à la surface du papier permettant le stockage d'information à la surface de celui-ci via le greffage covalent et la photodimérisation spatialement résolue de coumarines. Cette méthodologie a permis d'inscrire à la surface du papier des motifs complexes tel que des QRCodes. Les informations ainsi stockées à la surface du matériau sont invisibles à l'œil nu mais peuvent être révélées grâce à l'utilisation d'une lampe UV.

Par la suite, nous nous sommes intéressés à la préparation de nouvelles sondes moléculaires greffées à la surface du papier permettant ainsi de préparer des dispositifs de détection de polluants tel que les ions HSO₄⁻ et Cu²⁺. De manière analogue au papier pH, ces outils peuvent être utilisés pour détecter de manière colorimétrique la présence du polluant après immersion d'une bandelette de papier modifié dans une solution aqueuse. Des analyses par spectrométrie UV-Visible permettent de déterminer la concentration en analyte dans la solution analysée (après réalisation d'une courbe d'étalonnage) avec des limites de détection de 11,6 ppm (HSO₄⁻) et 2 ppm (Cu²⁺). Ce type d'outil facile d'utilisation, transportable et ne nécessitant pas de compétences pointues pourront certainement trouver une utilité dans le domaine des sciences environnementales.

A la suite du travail sur la détection du Cu(II) dans l'eau, nous nous sommes rendus compte qu'outre la capacité de réduire le Cu (II) en Cu (I), cet outil permet également de séquestrer le cuivre à la surface du matériau. Ces capacités ont été mises à profit dans la réaction click de Huisgen où notre dispositif a été utilisé comme agent réducteur et séquestrant du cuivre. Cette stratégie sans précédent dans la littérature apporte un nouvel outil pour la synthèse organique et permet d'obtenir des produits de réactions quasiment exempts de cuivre ce qui est un atout majeur dans le cas par exemple de synthèse de principes actifs pour la chimie pharmaceutique où les taux de contaminants métalliques sont très réglementés.

La dernière partie de ce travail a porté sur la préparation d'une membrane pour la décontamination des eaux contenant des métaux lourds. Cet outil a été préparé en greffant à la surface du papier de l'acide éthylène diamine tétraacétique (EDTA). Les tests réalisés par la suite ont montré que cette membrane a la capacité d'éliminer de nombreux métaux comme l'Ag(I), le Ni(II), le Zn(II), le Cd(II), le Pb(II), l'Sn(II) ou encore le Cu(II) avec une efficacité supérieure à 90%.

Ces différents travaux ouvrent de nombreuses perspectives pour le développement de nouveaux matériaux à base de cellulose fonctionnalisée de manière covalente. La preuve de concept que nous avons apportée au sujet de la photoimpression peut certainement être améliorée en utilisant d'autres types de molécules et pourquoi pas un mélange de plusieurs molécules. La préparation de sondes moléculaires greffées à la surface du papier offre des outils de détection des polluants pratiques et simples d'utilisation. Afin de pouvoir analyser la présence d'autres polluants dans l'eau (métaux ou polluants organiques) il est nécessaire de développer de nouvelles sondes. Enfin, la préparation d'une membrane pour la dépollution de l'eau a montré de bons résultats pour les métaux lourds, il est possible d'envisager la préparation de membranes capable d'éliminer d'autres types de polluants notamment des composés organiques.

Annexes

En annexes, se trouvent des travaux réalisés aux cours de ma première année thèse qui ont porté sur la multicatalyse hétérogène en flux continu. L'objectif initial de ces travaux était de développer en flux une méthodologie d'arylation des pyrroles basée sur la réaction de Meerwein précédemment étudiée au sein de l'équipe¹. Cependant, nous nous sommes retrouvés confrontés à divers problèmes lors du passage de cette réaction en flux avec notamment des problèmes de stabilité du catalyseur et d'autres problèmes techniques inhérents à l'appareillage de flux continu. Ces différentes raisons nous ont poussés à réorienter le sujet de cette thèse après un an de travail.

Ce travail de première année n'a pour autant pas été infructueux puisqu'avec l'aide d'un stagiaire de Master 1 au laboratoire, nous avons développé un nouveau catalyseur à base de nanoparticules de cuivre supporté sur du graphite qui a été employé dans la réaction de Huisgen et la réaction d'arylation de Meerwein du pyrrole².

Enfin, au cours de cette première année nous avons rédigé au sein de l'équipe une revue portant sur l'utilisation plus sûre des sels de diazonium en synthèse pallado-catalysée avec notamment l'apport des méthodologies en flux continu et la génération *in situ* des espèces réactives à partir de précurseurs stables³.

155

- 1. A. Honraedt, M.-A. Raux, E. Le Grognec, D. Jacquemin, F.-X. Felpin, *Chem. Commun.* 2014, **50**, 5236-5238.
- 2. M. d'Halluin, T. Mabit, N. Fairley, V. Fernandez, M. B. Gawande, E. Le Grognec, F.-X. Felpin, *Carbon*, 2015, **93**, 974-983.
- 3. N. Oger, M. d' Halluin, E. Le Grognec, F.-X. Felpin, *Org. Process Res. Dev.* 2014, **18**, 1786–1801.



Available at www.sciencedirect.com

ScienceDirect





Graphite-supported ultra-small copper nanoparticles – Preparation, characterization and catalysis applications



Martin d'Halluin ^a, Thibaud Mabit ^a, Neal Fairley ^b, Vincent Fernandez ^c, Manoj B. Gawande ^d, Erwan Le Grognec ^a, François-Xavier Felpin ^{a,e,*}

- a Université de Nantes; UFR des Sciences et des Techniques, CNRS UMR 6230, CEISAM, 2 rue de la Houssinière, 44322 Nantes Cedex 3, France
- ^b Casa Software Ltd, Bay House, 5 Grosvenor Terrace, Teignmouth TQ14 8NE, United Kingdom
- ^c Université de Nantes, UFR Sciences et Techniques, UMR CNRS 6502, IMN, 2 rue de la Houssinière, BP 32229, 44322 Nantes Cedex 3, France
- ^d Regional Centre of Advanced Technologies and Materials, Faculty of Science, Department of Physical Chemistry, Palacky University, Šlechtitelů 11, 783 71 Olomouc, Czech Republic
- e Institut Universitaire de France, 103 blud St Michel, 75005 Paris Cedex 5, France

ARTICLEINFO

Article history: Received 30 March 2015 Accepted 7 June 2015 Available online 12 June 2015

ABSTRACT

A convenient preparation of graphite-supported ultra-small copper nanoparticles (Cu NPs) has been developed. Ultra-small Cu NPs, generated by reduction of $\text{Cu}(\text{OAc})_2$ with H_2 , were well dispersed onto the graphite support and possess a very narrow distribution in size, ranging from 1.6 to 2.6 nm. The catalytic activity of these ultra-small graphite-supported Cu NPs was evaluated for the Meerwein arylation of pyrroles and the multicomponent synthesis of 1,2,3-triazoles via click reaction.

© 2015 Elsevier Ltd. All rights reserved.

1. Introduction

Metallic nanoparticles (NPs) at the nanometer scale can be seen as a bridge between atomic and bulk metal, exhibiting unique physical, electronic and chemical properties. The peculiar profile of metallic nano-objects has been exploited for many applications in various scientific areas including catalysis [1]. The challenges associated with NPs, used as catalysts, concern the preparation of highly reactive nano-object having a size in the range of 1–2 nm and their removal from the reaction mixture in an efficient way in order to avoid unwanted contaminations. In the vast family of metallic NPs, Cu NPs have attracted considerable attention from the chemical community as efficient nanocatalysts in a myriad

of important chemical transformations [2,3]. For the clean removal of Cu NPs from the reaction mixture, nanofiltration has proven to be useful for specific applications [4–6], but the adsorption of Cu NPs on a support is certainly the preferred approach to efficiently address this issue through filtration or magnetic separation [7,8]. While metal oxides are arguably the most common support for Cu NPs [9–16], the use of polymers [17–19], silica [20–22] and graphene [23–28] have also been reported.

By contrast, inexpensive carbon materials such as activated charcoal and graphite have been much less used as support for Cu NPs [29–35], while they have been widely used with other transition metals because of their chemical inertness and commercial availability at low cost [36]. For instance,

E-mail address: fx.felpin@univ-nantes.fr (F.-X. Felpin). http://dx.doi.org/10.1016/j.carbon.2015.06.017 0008-6223/© 2015 Elsevier Ltd. All rights reserved.

^{*} Corresponding author at: Université de Nantes; UFR des Sciences et des Techniques, CNRS UMR 6230, CEISAM, 2 rue de la Houssinière, 44322 Nantes Cedex 3, France.

activated charcoal has been widely used as an adsorbent and a support for palladium NPs because of its high surface area (up to 1500 m²/g), low cost and weak toxicity [37-41]. Amongst others [42], we have contributed to this area for the preparation of activated charcoal-supported Pd, Pd-Au and Pd-Cu catalysts for cross-coupling reactions [43-51]. However, one of the recurrent inconvenience regarding the use of commercially available activated charcoal is the complexity of its textural properties that are characterized by a disorganized porous structure containing aromatic sheets and strips having three different groups of pores: micropores (up to 2 nm), mesopores (2-50 nm) and macropores (>50 nm). The pore distribution as well as the chemical composition of the carbon surface (mainly oxygen, hydrogen and mineral matter) depend on the nature of the pyrolyzed material (mainly wood, coconut shell or fruit pets), the carbonization process and various chemical treatments. The texture of activated charcoal strongly influences the metal-support interaction and thereby, reproducibility issues are frequently observed in catalysis applications [49]. The confusion between charcoal-supported Cu NPs and Cu molecular species has also been recently pointed out by Buckley et al. [52].

By contrast, graphite is a highly ordered and crystalline material composed of aromatic sheets with a constant interlayer spacing of 0.335 nm. Graphite is an essentially non porous material having a low active surface area (~10 m²/g), but atoms and small molecules can slip between the layers, resulting in a confinement effect. Surprisingly, graphite has been nearly unexplored as support for Cu NPs and the only studies reported so far showed the formation of Cu NPs of uncontrolled size [53]. The low active surface area could be detrimental for catalytic applications due to a poor dispersion of NPs, however, we believe that this issue could be circumvented by preparing ultra-small NPs.

Therefore, efficient procedures for preparing graphitesupported ultra-small Cu NPs are clearly appealing for applications in catalysis. In this paper we report successful applications for the Meerwein arylation of pyrroles and 1,3-dipolar cycloadditions of azides with alkynes catalyzed by ultra-small Cu NPs supported on graphite.

2. Experimental

2.1. Apparatus and reagents

All commercial solvents and reagents were used as received from Sigma–Aldrich, Fischer Scientific Ltd, Alfa Aesar and TCI Europe companies and were degased with argon before use. Silica gel (40–63 μm) used in flash column chromatography was obtained from Merck. Analytical thin-layer chromatography (TLC) was performed on silica gel plates (TLC silica gel 60 F254 purchased from Merck), visualized with a Spectroline UV254 lamp, and stained with a basic solution of KMnO₄. ¹H and ¹³C, recorded at 400 MHz or 300 MHz, 100 MHz or 75 MHz, respectively, were performed on Bruker Advance 400 and Bruker Advance 300 spectrometers. Proton chemical shifts were internally referenced to the residual proton resonance in CDCl₃ (7.26 ppm) or DMSO (2.50 ppm). Carbon chemical shifts were internally referenced to the

deuterated solvent signals in CDCl3 (77.2 ppm) or DMSO (39.52 ppm). Melting point were recorded on a Stuart Scientific 7SMP3 apparatus. FT-IR spectra were recorded on a Bruker Tensor 27 spectrometer with ATR technic or KBr plates. HRMS in ESI mode were recorded on a LTQ-Orbitrap (ThermoFisher Scientific) at the ENV of Nantes. Transmission electron microscopy (TEM) images were recorded on a Hitachi HF-2000 FEG-TEM. X-ray diffraction (XRD) patterns were recorded on a Bruker D8 Advance X-ray Diffractometer. The X-ray photoelectron spectra were recorded on a Kratos Nova using an monochromatic X-ray source at 20 mA 15 kV (300 W) to confirm the chemical state of Cu. The surface analyzed was about 700 μm by 300 $\mu m.$ High resolution spectrum were done with a 0.1 eV step at Pass energy 10 eV corresponding to an overall instrument resolution of 0.33 ± 0.02 eV on Silver Fermi edge. All samples were maintained on conductive adhesive double side tape.

2.2. Preparation of graphite-supported ultra-small Cu NPs (5% CuNPs/Gr)

Copper acetate monohydrate (0.1 g, 0.5 mmol) was dissolved in degased methanol (60 mL) at 25 °C. Graphite (0.5 g, <20 μm particle size, Aldrich 282863) was added and the solution was degased 5 min with H_2 . The solution was stirred for 16 h under H_2 atmosphere at 25 °C. The solid was collected by filtration, washed with distilled methanol (3 × 5 mL), deionized water (3 × 5 mL), acetone (3 × 5 mL) then dried under vacuum overnight to give a black solid. ICP-MS analysis determined that the content of copper onto graphite was ca. 4.8–5 wt.%.

2.3. General procedure for the C-H arylation of N-Boc pyrrole

To a mixture of aniline and MeSO $_3$ H (65 μ L, 1.0 mmol) in H $_2$ O (1 mL) at 25 °C was added t-BuONO (180 μ L, 1.35 mmol, 90% purity). The reaction mixture was stirred for 30 min at 25 °C. Then, CaCO $_3$ (100 mg, 1.0 mmol), N-Boc pyrrole 2 (0.67 mL, 4.0 mmol), 5% Cu NPs/Gr (130 mg, 10 mol%) and acetone (2.5 mL) were successively added. After being stirred for the required time the crude was purified by flash chromatography on silica gel to give the pure product.

$2.3.1. \quad \hbox{N-tert-butoxycarbonyl-2-(4-nitrophenyl)-1} \\ \hbox{H-pyrrole 3a}$

Yellow solid (208 mg, 72%). mp 122–123 °C [lit. [54] 120–121 °C]; 1 H NMR (400 MHz, CDCl₃,) 3 8.21 (d, 2H, 1 9 = 8.9 Hz), 7.51 (d, 2H, 1 9 = 8.9 Hz), 7.40 (dd, 1H, 1 9 = 3.3 Hz, 1 9 = 1.7 Hz), 6.32 (dd, 1H, 1 9 = 3.3 Hz, 1 9 = 1.7 Hz), 6.27 (app t, 1H, 1 9 = 3.3 Hz), 1.43 (s, 9H); 1 9 C NMR (100 MHz, CDCl₃) 3 149.1, 146.9, 140.9, 133, 129.7 (2C), 124.5, 123.1 (2C), 116.7, 111.3, 84.7, 27.9 (3C); IR (KBr) v 3147, 2982, 1742, 1596, 1506, 1331, 1304, 1142 cm 1 9; HRMS (ESI) calcd for 1 9 C 1 15 C 1 16 C 1 17 C 1 17 C 1 17 C 1 18 C 1 18 C 1 18 C 1 19 C 1 1

2.3.2. N-tert-butoxycarbonyl-2-(2-methoxy-4-nitrophenyl)-1H-pyrrole 3b

Yellow oil (182 mg, 57%). ¹H NMR (300 MHz, CDCl₃,) δ 7.88 (dd, 1H, J = 2.1, 8.4 Hz), 7.72 (d, 1H, J = 2.1 Hz), 7.42 (d, 1H, J = 8.4 Hz),

7.38 (dd, 1H, J = 1.8, 3.3 Hz), 6.29–6.23 (m, 2H), 3.86 (s, 3H), 1.40 (s, 9H). 13 C NMR (75 MHz, CDCl₃) δ 157.7, 149.1, 148.3, 131.2, 130.1, 129.1, 123.2, 116, 115.5, 110.9, 105.1, 83.8, 56, 27.8 (3C). IR (neat) v 2977, 1740, 1526, 1320, 1148 cm $^{-1}$. HRMS (ESI) calcd for $C_{16}H_{19}O_5N_2$ [M+H $^+$]: 319.1288, found: 319.1285.

2.4. General procedure for the "click" reaction with phenylacetylene

A 15 mL sealed tube was charged with benzyl bromide 4 (171 mg, 1.0 mmol), sodium azide (65 mg, 1.0 mmol), phenylacetylene (153 mg, 1.5 mmol), Cu NPs/Gr (65 mg, 5 mol%) and 2.5 mL of $\rm H_2O/MeOH$ (4/1). The mixture is degased for 2 min with N₂, then the tube is sealed and the reaction mixture is heated at 70 °C for 12 h. After this time, the mixture was diluted with EtOAc (10 mL) and $\rm H_2O$ (5 mL). The aqueous phase was extracted with EtOAc (3×10 ml). The collected organic extracts were dried on Na₂SO₄, filtered and evaporated to dryness. The crude was purified either by flash chromatography on silica gel or by precipitation to give the pure product.

2.4.1. 1-Benzyl-4-phenyl-1H-1,2,3-triazole **6a** White solid (213 mg, 91%). mp 129–130 °C [lit. [55] 132–133 °C]; ^1H NMR (400 MHz, CDCl $_3$) δ 7.81–7.79 (m, 2H), 7.66 (s, 1H), 7.42–7.30 (m, 8H), 5.58 (s, 2H); ^{13}C NMR (100 MHz, CDCl $_3$) δ 148.4, 134.8, 130.7, 129.4, 129, 128.4, 128.3, 125.9, 119.7, 54.5. IR (neat) v 3145, 1495, 1469, 1452, 1428, 1362, 1354, 1222, 1140, 1075, 1046, 973, 808, 768, 729, 696 cm $^{-1}$. HRMS (ESI) calcd for C $_{15}\text{H}_{14}\text{N}_3$ [M+H*]: 236.1182, found: 236.1174.

2.4.2. 1-Cinnamyl-4-phenyl-1H-1,2,3-triazole **6b** White solid (214 mg, 82%). mp 132–134 °C [lit. [56] 134 °C]; 1 H NMR (400 MHz, CDCl₃), 3 7.85–7.82 (m, 3H), 7.44–7.40 (m, 4H), 7.37–7.27 (m, 4H), 6.72 (d, 1H, J=15.8 Hz), 6.40 (dt, 1H, J=6.7 Hz, J=15.8 Hz), 6.19 (dd, 2H, J=1.3 Hz, J=6.7 Hz); 13 C NMR (100 MHz, CDCl₃) 3 148.3, 135.7, 135.6, 130.7, 129, 128.9, 128.8, 128.4, 126.9, 125.9, 122, 119.5, 52.7. IR (neat) v 3052, 1465, 1440, 1355, 1222, 1190, 1138, 1075, 1043, 980, 913, 805, 760, 730, 6 94 cm $^{-1}$ HRMS (ESI) calcd for 6 C₁₇H₁₆N₃ [M+H*]: 262.1338, found: 262.1338.

2.4.3. 1-Phenyl-2-(4-phenyl-1H-1,2,3-triazol-1-yl)ethan-1-one 6c

White solid (195 mg, 74%). mp 166–169 °C [lit. [57] 172–175 °C];

¹H NMR (400 MHz, CDCl₃), δ 8.02 (t, 2H, J = 7.7 Hz), 7.95 (s, 1H),
7.86 (d, 2H, J = 7.7 Hz), 7.68 (t, 1H, J = 7.4 Hz), 7.55 (t, 2H, J = 7.7 Hz), 7.43 (t, 2H, J = 7.7 Hz), 7.34 (t, 1H, J = 7.4 Hz), 5.89 (s, 2H); 13 C NMR (100 MHz, CDCl₃) δ 190.4, 148.4, 134.8, 134.1,
130.7, 129.4, 129, 128.4, 126, 55.7. IR (neat) v 3091, 2933, 1703,
1582, 1484, 1447, 1352, 1227, 1050, 980, 768, 752, 688,
641 cm $^{-1}$. HRMS (ESI) calcd for $C_{16}H_{14}ON_3$ [M+H $^{+}$]: 264.1131,
found: 264.1123.

2.4.4. Ethyl 2-(4-phenyl-1H-1,2,3-triazol-1-yl)acetate **6d** White solid (210 mg, 91%). mp 100–101 °C [lit. [55] 94–95 °C]; 1 H NMR (400 MHz, CDCl₃,) δ 7.90 (s, 1H), 7.86–7.84 (m, 2H), 7.45–7.41 (m, 2H), 7.36–7.32 (m, 1H), 5.20 (s, 2H), 4.29 (q, 2H, J = 7.1 Hz), 1.32 (t, 3H, J = 7.1 Hz); 13 C NMR (100 MHz, CDCl₃) δ 166.4, 148.5, 130.6, 129, 128.5, 126, 121, 62.7, 51.2, 14.3. IR

(neat) v 3137, 3000, 2949, 1755, 1473, 1445, 1348, 1218, 1198, 1079, 1019, 766, 695 cm $^{-1}$. HRMS (ESI) calcd for $C_{12}H_{14}O_2N_3$ [M+H $^{+}$]: 232.1080, found: 232.1075.

2.4.5. 2-Phenyl-2-(4-phenyl-1H-1,2,3-triazol-1-yl)ethan-1-ol

White solid (142 mg, 54%). mp 124–125 °C [lit. [33] 125–127 °C];

¹H NMR (400 MHz, DMSO) δ 8.79 (s, 1H), 7.88–7.85 (m, 2H), 7.47–7.31 (m, 8H), 5.83 (dd, 1H, J = 4.9 Hz, J = 9.2 Hz), 5.33 (t, 1H, J = 5.4 Hz), 4.36–4.29 (m, 1H), 4.05 (dt, 1H, J = 4.9 Hz, J = 11.6 Hz);

¹³C NMR (100 MHz, DMSO) δ 146.1, 137.3, 130.8, 128.8, 128.6, 128.2, 127.7, 127.1, 125.1, 120.8, 66.4, 63.1. IR (neat) v 3388, 3125, 3098, 3027, 2973, 2932, 1492, 1463, 1428, 1227, 1188, 1077, 1050, 1028, 762, 727, 695 cm $^{-1}$. HRMS (ESI) calcd for C₁₆H₁₆ON₃ [M+H $^{+}$]: 266.1287, found: 266.1283.

3. Discussion

A number of preparative procedures have been described for the synthesis of supported-transition-metal NPs [58–60]. The most common procedures require a succession of steps which can be roughly described as: (1) impregnation, coprecipitation or deposition-precipitation of the metal precursor as a molecular complex onto the support; (2) calcination or drying; (3) formation of NPs by reduction. Another widespread approach consists in preparing metal NPs in solution before adsorbing them on the support.

While coprecipitation and deposition–precipitation methods are well-suited with metal oxides as supports, they are mostly unsuitable with carbon support due to the formation of large aggregates [61]; the hydrophobic nature of carbons and the low density of surface hydroxyl groups being responsible of this behavior. On the other hand, the preparation of metal NPs in solution before adsorption on the support requires the use of stabilizers covering NPs as a protecting barrier to prevent aggregation and control the crystallite growth. In the absence of stabilizers, small NPs are thermodynamically unstable with respect to agglomeration and the adsorption step on the support can dramatically modify their size, shape and properties.

As previously mentioned, activated charcoal has not been extensively used as support for copper NPs. Yus and coworkers prepared CuNPs (size distribution of ca. 3.0 ± 1.5 nm) by reduction of CuCl₂ with lithium metal and 4,4'-di-tert-butylbiphenyl (DTBB) as electron carrier in THF [30]. Addition of activated charcoal to the suspension of Cu NPs, furnished the copper-on-activated charcoal catalyst (Cu NPs/C). Extensive characterization showed that particle size increased to 6 ± 2 nm and Cu(0) NPs were oxidized into a mixture of Cu₂O and CuO NPs. Sharghi et al. developed a simple method to prepare Cu NPs/C by refluxing CuI in EtOH in the presence of activated charcoal [30]. However, this procedure generated large Cu NPs with a wide particle size distribution of ca. 80-300 nm. Similarly, graphite has been mostly overlooked as a support for Cu NPs. Lopez-Ruiz et al. described the synthesis of graphite-supported copper(I) oxide NPs by reduction of CuSO₄·5H₂O in water. However, this procedure led to a wide range of nanoparticles size distribution, up to 200 nm [53].

3.1. Catalyst preparation

With these literature precedents in hand, we embarked in an evaluation of several strategies for the synthesis of Cu NPs/Gr. The goal of this study was to design a robust and reproducible procedure leading to size-controlled Cu NPs supported on graphite. In order to avoid the use of organic stabilizers, we anticipated that the NPs formation should occur in the presence of graphite. To this end, we roughly designed a standard procedure whereby an inexpensive molecular source of Cu was transformed into Cu NPs that were simultaneously adsorbed on graphite. To fill these specifications we selected water and MeOH as solvent, NaBH4, hydrazine and H2 as reducing agent, and Cu(OAc)2 as copper source. Concerning the support, graphite (<20 µm particle size) was used as received without any pre-treatment step. By taking advantage of transmission electron microscopy (TEM), we determined the influence of the reaction conditions on the nanoparticles size.

We started our study with water as solvent and studied the formation of Cu NPs from a suspension of Cu(OAc)2 and graphite in the presence of NaBH4, hydrazine and H2 (Fig. 1). The concentration of Cu was adjusted in order to prepare catalysts with ~5 wt.% of Cu on graphite. The use of NaBH4 led to grapes of poorly dispersed aggregated Cu NPs (Fig. 1a), while with hydrazine, polydisperse cubic NPs having a size ranging from 100 to 400 nm were observed (Fig. 1b). On the other hand, TEM analysis revealed that with H2 as reducing agent, an uncontrolled growth of nanoparticles occurred on the surface of graphite (Fig. 1c). These disappointing results, leading to poorly dispersed crystallites having a wide distribution in size, were attributed to the hydrophobic nature of graphite which readily agglomerated in water. Thereby, the very low dispersion of graphite in water, led to a random growth of Cu NPs.

In order to address this issue, we changed water for MeOH as solvent since graphite readily dispersed in alcoholic solvents upon vigorous stirring. Surprisingly, the reduction of copper(II) acetate in MeOH with NaBH₄, led to the formation of needle-like Cu NPs (Fig. 2a). This unexpected observation could result from the combination of the low concentration of copper species solubilized in MeOH and the strong reductive properties of NaBH₄ leading to a fast crystal growth. This hypothesis was reinforced by the observation of a mixture of needle-like and spherical nanoparticles at a 4-fold higher concentration of copper. With hydrazine in MeOH,

significantly smaller spherical Cu NPs were observed compared to those obtained in water, but the wide distribution in the diameter of the crystallites, ranging from 50 to 150 nm, was still unsatisfactory (Fig. 2b).

By contrast, small spherical Cu NPs with a crystallite size <3.8 nm were obtained using ${\rm H_2/MeOH}$ as reaction conditions. The NPs were well-dispersed onto the graphite support. Despite a high local concentration of Cu NPs, no aggregate was observed and a closest analysis on more than 200 NPs revealed a very narrow distribution in size with 80% of NPs ranging from 1.6 to 2.6 nm and an average diameter of 2.1 nm (Fig. 3). Importantly, the concentration of the copper(II) acetate significantly influenced the NPs growth since a twofold more concentrated solution gave 50% larger graphite-supported Cu NPs with an average size of 3.1 nm.

Cu 2p, O 1s, C 1s, Cu 3p photoemission peaks have been studied by X-ray photoelectron spectroscopy (XPS). Unlike traditional XPS spectra fitting procedures using purely synthetic spectral components, we used XPS data processing method based on vector analysis that allows creating XPS spectral components by incorporating key information, obtained experimentally [62]. The nanocrystal surface composition, investigated by XPS analysis on the Cu 2p region, revealed the presence of Cu2+ as major species with the characteristic binding energies for CuO and Cu(OH)2 at respectively 933.7 eV and 934.4 eV, and the satellite shake-up detected near 938-946 eV, along with a smaller amount of Cu_2O with the Cu $2p_{3/2}$ peak at 932.3 eV (Fig. 4, top). This result indicates that the catalyst mainly consisted of graphitesupported Cu(OH)2 and CuO NPs. While the data from the Cu 2p region offer obvious shape differences between the oxidation states, the relatively low kinetic energy for emission of Cu 2p electrons and the wide range of energies required to obtain the full doublet coupled with the proximity of the oxygen KLL Auger peaks represents a source for uncertainty in the true XPS background signal to these doublet data. While invaluable when interpreting copper spectra, the Cu 2p doublet adds to the complexity when attempting to measure relative proportions of distinct oxidation states. For these reasons, we also studied the Cu 3p doublet to measure the relative proportions of copper species using background subtracted components derived from Cu 3p (Fig. 4, bottom). Both Cu 2p and Cu 3p data in Fig. 4 are derived simultaneously by vector transformations of raw spectra. These components are fully constrained in terms of position and shape, allowing

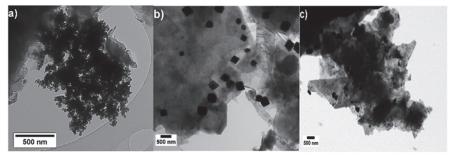


Fig. 1 - TEM micrographs of Cu NPs/graphite from (a) NaBH₄/H₂O, (b) NH₂NH₂/H₂O, (c) H₂/H₂O systems.

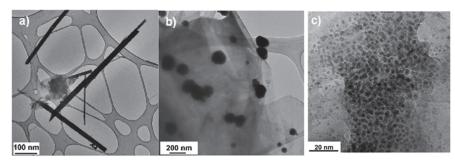


Fig. 2 - TEM micrographs of Cu NPs/graphite from (a) NaBH₄/MeOH, (b) NH₂NH₂/MeOH, (c) H₂/MeOH systems.

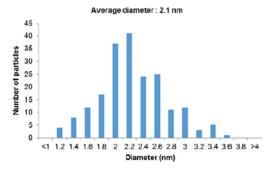


Fig. 3 – Distribution of the crystallite size on 200 NPs. (A color version of this figure can be viewed online.)

the component area as the only adjustable parameter for fitting these data. A two-parameter universal cross-section was defined and consistently applied to all data considered [63]. When repeatedly measured, the sample resulted in a reduction of Cu(II) to Cu(I). Thereby, the initial state of the sample and all subsequence measurements could be fitted using the same component model, validated against a small library of eight graphite-supported Cu NPs catalysts, and provided logically correct trends for the Cu(II) and Cu(I) intensities. The component model in Fig. 4 was capable of reproducing all Cu 3p spectra from a total of twenty-seven measurements without relaxation of any fitting constrains. From these studies we determined that the catalyst mainly consisted of Cu(II) species (c.a. 96%) as CuO and Cu(OH)2 NPs in a 1/3 ratio, with the corresponding binding energies at respectively 76.7 and 79.0 eV, along with Cu2O NPs (c.a. 4%) with the Cu 3p peak at 74.9 eV. Importantly, our data processing method allowed us to differentiate between Cu(I) and Cu(0) using Cu 2p and Cu 3p core level data, while using standard XPS spectra fitting procedures in limited energy windows render impossible this task [64]. Both Auger and valence band spectra were measured from the twenty-seven samples. The valence bands, in particular, were used to construct Cu 3p lineshapes and, more importantly, confirmed the correlation of the Cu 3p lineshapes with Cu(I) as the valence band spectra for Cu(I) and Cu (0) are very different in position and shape [65]. From these studies, it is clear that no Cu(0) contributed to the Cu 2p and Cu 3p spectra depicted in Fig. 4. The presence of residual

Cu(OAc)₂·H₂O that could be impregnated onto the surface of graphite was discarded due to absence of ester peaks. To explain the formation of Cu₂O and CuO NPs in the H₂/MeOH reducing mixture, it was assumed that Cu(OAc)₂·H₂O was reduced to Cu(O) or Cu₂O which rapidly oxidized to CuO and Cu(OH)₂ during the catalyst treatment upon exposition to air and moisture. This assumption was supported by the drastic change of the surface composition showing crystals of copper(II) acetate in the μ m range, when H₂ was omitted.

The X-ray diffraction (XRD) pattern of the solid did not show signal for Cu species, confirming the presence of highly dispersed ultra-small Cu NPs [15]. The textural properties of the 5% Cu NPs/Gr catalyst, provided by low temperature (77 K) nitrogen adsorption-desorption isotherms, revealed the weak influence of Cu NPs since low Langmuir and BET surface area of respectively 13 and 8 m²/g were calculated. The material is weakly porous with pore volume of 0.026 cm³/g and pore size distribution of 12.8 nm.

3.2. Catalyst activity

The catalytic activity of Cu NPs/Gr was evaluated for the Meerwein arylation of N-Boc-pyrrole 2 with anilines, via insitu generated diazonium salts (Fig. 5). This coppercatalyzed reaction was recently optimized in our laboratory using copper(II) acetate as a homogeneous catalyst and acetone/water as solvent system [66]. We were pleased to find that the use of Cu NPs/Gr indeed promoted the coupling of 4-nitroaniline 1a and 2-methoxy-4-nitroaniline 1b with N-Boc-pyrrole 2 at room temperature in synthetically useful yields. Although the yields recorded for these examples dropped by \sim 10% compared to the homogeneous version, this work constitutes a remarkable example of the Meerwein arylation catalyzed by a heterogeneous catalyst. To the best of our knowledge, this is the first example of the Meerwein arylation of heterocycles using a heterogeneous catalyst. The advantage of graphite compared to other carbon-material such as activated charcoal and graphene oxide, is its high inertness with aryl radicals generated for diazonium salts. Indeed, aryl radicals extensively react with activated charcoal and graphene oxide, leading to unwanted covalently grafted and modified material.

Furthermore, the catalytic performances of 5% Cu NPs/Gr catalyst were investigated for the Huisgen 1,3-dipolar cycloaddition of organic azides with alkynes [67,68],

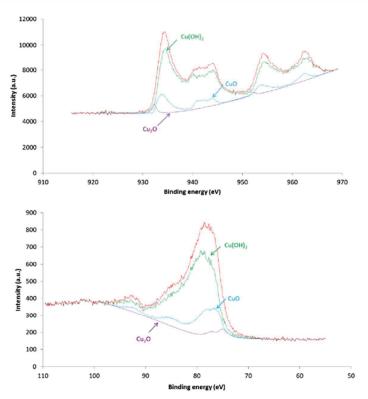


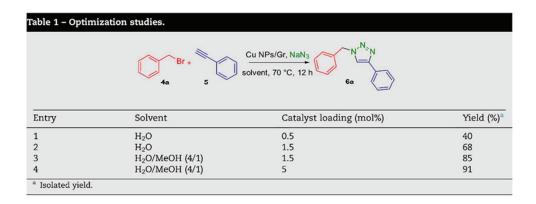
Fig. 4 – X-ray photoelectron spectra of Cu NPs/Gr catalyst showing the Cu 2p (top) and Cu 3p (bottom) regions. (A color version of this figure can be viewed online.)

Fig. 5 - Meerwein arylation of N-Boc-pyrrole. (A color version of this figure can be viewed online.)

independently discovered by Medal and Sharpless [69,70]. This reaction is a leading transformation in the arsenal of synthetic chemists that found numerous applications in chemical-biology [71] and material chemistry [72]. Owing to its synthetic prevalence, especially for the synthesis of biologically active compounds, several strategies have been devoted to the immobilization of the copper catalyst allowing an easy recovery by a simple filtration. Several materials including zeolite [73,74], silica [75], guar-gum [76], iron oxides [77–79], acetylene black [80] and charcoal [29–34,53,81] have been successfully used as support. One of the drawbacks of this reaction concerns the use of hazardous organic azides which are thermally sensitive compounds. To circumvent this issue, the multicomponent synthesis of 1,2,3-triazoles involving the generation of organic azides in situ from organic halides and

sodium azide has been first proposed by Fokin and Van der Eycken [82,83]. In continuation of our research interest in the development of methodologies involving very reactive intermediates in safe conditions [84,85], we investigated the multicomponent synthesis of 1,2,3-triazoles using Cu NPs/Gr as catalyst (Table 1). Initially, the reaction of benzyl bromide 4, sodium azide and phenylacetylene 5 was optimized with regard to the solvent system and the catalyst loading. We initially selected water as solvent for the multicomponent reaction carried out at 70 °C with 0.5 mol% Cu. The modest yield obtained in these conditions (40%) prompted us to increase threefold the catalyst loading at 1.5 mol% Cu. As expected a significant improved yield (68%) was obtained for the expected triazole 6a. However, in these conditions, we observed a poor dispersion of the catalyst due to the high hydrophobicity of graphite. The use of H₂O/MeOH (4/1) as solvent system significantly enhanced the catalyst dispersion, resulting in an improved yield (85%) for the triazole 6a. Eventually, the catalyst loading could be increased to 5 mol% in order to reach an excellent yield for 6a (91%).

This optimized procedure was further applied to other electrophiles as depicted in Table 2. The multicomponent reaction allowed the use of various bromides, leading to triazoles 6a—e in good to excellent yields (74–91%). Remarkably,



the mild conditions developed in this study were compatible with hydrolysable ester functions (compound 6d). The use of styrene oxide 7 as electrophile was also investigated and we were pleased to find that the opening of epoxide by NaN_3 selectively occurred at the benzylic carbon to give the corresponding β -hydroxy-1,4-disubstituted triazole 6e in 54% yield. The regioselectivity of this reaction was determined by 1H NMR carried out in DMSO-d6 whereby the signal for the OH group appeared as a triplet, indicating the formation of a primary alcohol. This result is in agreement with the extensive study provided by the group of Yus [33]. It must be noted that no other regioisomer was detected in the crude mixture. The heterogeneous 5% Cu NPs/Gr catalyst was easily recovered from the crude mixture by filtration over a nylon

membrane. ICP-MS analysis of the crude mixture containing triazole 6a, revealed only 6 ppb of solubilized copper species after a single filtration. This very low contamination is remarkable since triazoles are usually considered as good ligands for Cu, leading to extensive leaching phenomena. The high affinity of Cu NPs for graphite likely explains this very low leaching that qualifies our catalyst for applications requiring low Cu contamination, for instance in medicinal chemistry [71].

4. Conclusion

In summary, we have developed a very convenient synthesis of graphite-supported ultra-small Cu NPs under mild conditions by reduction of copper(II) acetate in MeOH at room temperature, under an atmosphere of hydrogen. The procedure developed does not require specific equipment nor extensive knowledge in material chemistry. This very simple procedure furnished well dispersed ultra-small Cu NPs with a very narrow distribution in size, ranging from 1.6 to 2.6 nm. This heterogeneous catalyst was successfully evaluated for the copper-catalyzed arylation of pyrroles with aryl diazonium salts and the 1,3-dipolar cycloaddition of organic azides with phenylacetylene. A three-component click procedure was developed in aqueous condition allowing the generation of hazardous organic azides in situ. The catalyst was easily recovered by filtration leaving the crude mixture virtually free of copper residues, as evidenced by ICP-MS analyses. We believe that this work provides significant insights for heterogeneous copper catalysis that should be of interest for synthetic chemists concerned by the metallic contamination of their products.

Acknowledgments

We gratefully acknowledge the University of Nantes, the "Centre National de la Recherche Scientifique" (CNRS), the "Région Pays de la Loire" in the framework of a "recrutement sur poste stratégique". F.-X.F. is a member of the "Institut Universitaire de France" (IUF). The authors thanks Prof. T. Toupance (University of Bordeaux) for the determination of BET and Langmuir surface area and J. Hémez (University of Nantes) for HRMS analyses. We gratefully acknowledge Mrs

Emily Smith (Nottingham University) for fruitful discussions on XPS data and Dr Jérôme Majimel (University of Bordeaux) and Mr Uli Castanet (University of Bordeaux) for their assistance in DRX analyses.

REFERENCES

- Astruc D, Lu F, Aranzaes JR. Nanoparticles as recyclable catalysts: the frontier between homogeneous and heterogeneous catalysis. Angew Chem Int Ed 2005:44:7852-72.
- [2] Ranu BC, Dey R, Chatterjee T, Ahammed S. Copper nanoparticle-catalyzed carbon-carbon and carbonheteroatom bond formation with a greener perspective. ChemSusChem 2012;5:22–44.
- [3] Allen SE, Walvoord RR, Padilla-Salinas R, Kozlowski MC. Aerobic copper-catalyzed organic reactions. Chem Rev 2013;113:6234–458.
- [4] Al-Rashdi BAM, Johnson DJ, Hilal N. Removal of heavy metal ions by nanofiltration. Desalination 2013;315:2–17.
- [5] Wei XZ, Kong X, Wang SX, Xiang H, Wang JD, Chen JY. Removal of heavy metals from electroplating wastewater by thin-film composite nanofiltration hollow-fiber membranes. Ind Eng Chem Res 2013;52:17583–90.
- [6] Chen JJ, Ahmad AL, Ooi BS. Thermo-responsive properties of poly(n-isopropylacrylamide-co-acrylic acid) hydrogel and its effect on copper ion removal and fouling of polymerenhanced ultrafiltration. J Membr Sci 2014;469:73–9.
- [7] Campelo JM, Luna D, Luque R, Marinas JM, Romero AA. Sustainable preparation of supported metal nanoparticles and their applications in catalysis. ChemSusChem 2009:2:18–45.
- [8] White RJ, Luque R, Budarin VL, Clark JH, Macquarrie DJ. Supported metal nanoparticles on porous materials. methods and applications. Chem Soc Rev 2009;38:481–94.
- [9] Lin JH, Guliants VV. Supported copper catalysts prepared from colloidal copper for the water-gas shift reaction. ChemCatChem 2011;3:1426–30.
- [10] Wang XH. Chemical and morphological characterization of mesoporous material supported copper oxide nanoparticles for potential application. J Porous Mater 2011;18:623–30.
- [11] Fuku K, Takakura S, Kamegawa T, Mori K, Yamashita H. Preparation of size-controlled copper-nanoparticlesupported catalyst using rapid and uniform heating under microwave irradiation. Chem Lett 2012;41:614–6.
- [12] Lin JH, Guliants VV. Hydrogen production through water-gas shift reaction over supported Cu, Ni, and Cu-Ni nanoparticle catalysts prepared from metal colloids. ChemCatChem 2012:4:1611-21.
- [13] Sun WJ, Wang Y, Wu X, Yao XQ. Palladium-, ligand-, and solvent-free synthesis of ynones by the coupling of acyl chlorides and terminal alkynes in the presence of a reusable copper nanoparticle catalyst. Green Chem 2013;15:2356–60.
- [14] Mikami Y, Ebata K, Mitsudome T, Mizugaki T, Jitsukawa K, Kaneda K. Reversible dehydrogenation-hydrogenation of tetrahydroquinoline-quinoline using a supported copper nanoparticle catalyst. Heterocycles 2011;82:1371–7.
- [15] Baig RBN, Varma RS. A highly active and magnetically retrievable nanoferrite-dopa-copper catalyst for the coupling of thiophenols with aryl halides. Chem Commun 2012;48:2582–4.
- [16] Shelke SN, Bankar SR, Mhaske GR, Kadam SS, Murade DK, Bhorkade SB, et al. Iron oxide-supported copper oxide nanoparticles (Nanocat-Fe-Cuo): magnetically recyclable

- catalysts for the synthesis of pyrazole derivatives, 4-methoxyaniline, and Ullmann-type condensation reactions. ACS Sust Chem Eng 2014;2:1699–706.
- [17] Huang ZJ, Li FB, Chen BF, Xue F, Chen GC, Yuan GG. Nitrogenrich copolymeric microsheets supporting copper nanoparticles for catalyzing arylation of N-heterocycles. Appl Catal A Gen 2011;403:104–11.
- [18] Papageorgiou SK, Favvas EP, Sapalidis AA, Romanos GE, Katsaros FK. Facile synthesis of carbon supported copper nanoparticles from alginate precursor with controlled metal content and catalytic no reduction properties. J Hazard Mater 2011;189:384–90.
- [19] Pham LQ, Sohn JH, Kim CW, Park JH, Kang HS, Lee BC, et al. Copper nanoparticles incorporated with conducting polymer: effects of copper concentration and surfactants on the stability and conductivity. J Colloid Interface Sci 2012;365:103–9.
- [20] Gonzalez-Arellano C, Luque R, Macquarrie DJ. Microwave efficient s-arylation of thiols with aryl iodides using supported metal nanoparticles. Chem Commun 2009:1410–2.
- [21] Gonzalez-Arellano C, Balu AM, Luque R, Macquarrie DJ. Catalytically active self-assembled silica-based nanostructures containing supported nanoparticles. Green Chem 2010;12:1995–2002.
- [22] Yoshida K, Gonzalez-Arellano C, Luque R, Gai PL. Efficient hydrogenation of carbonyl compounds using low-loaded supported copper nanoparticles under microwave irradiation. Appl Catal A Gen 2010;379:38–44.
- [23] Gotoh K, Kinumoto T, Fujii E, Yamamoto A, Hashimoto H, Ohkubo T, et al. Exfoliated graphene sheets decorated with metal/metal oxide nanoparticles: simple preparation from cation exchanged graphite oxide. Carbon 2011;49:1118–25.
- [24] Mondal P, Sinha A, Salam N, Roy AS, Jana NR, Islam SM. Enhanced catalytic performance by copper nanoparticlegraphene based composite. RSC Adv 2013;3:5615–23.
- [25] Fakhri P, Jaleh B, Nasrollahzadeh M. Synthesis and characterization of copper nanoparticles supported on reduced graphene oxide as a highly active and recyclable catalyst for the synthesis of formamides and primary amines. J Mol Catal A: Chem 2014;383–384:17–22.
- [26] Guo X, Hao C, Jin G, Zhu H-Y, Guo X-Y. Copper nanoparticles on graphene support: an efficient photocatalyst for coupling of nitroaromatics in visible light. Angew Chem Int Ed 2014;53:1973-7.
- [27] Huang Q, Zhou L, Jiang X, Zhou Y, Fan H, Lang W. Synthesis of copper graphene materials functionalized by amino acids and their catalytic applications. ACS Appl Mater Inter 2014;6:13502-9.
- [28] Xie G, Forslund M, Pan J. Direct electrochemical synthesis of reduced graphene oxide (RGO)/copper composite films and their electrical/electroactive properties. ACS Appl Mater Inter 2014;6:7444-55.
- [29] Alonso F, Moglie Y, Radivoy G, Yus M. Copper nanoparticles in click chemistry: an alternative catalytic system for the cycloaddition of terminal alkynes and azides. Tetrahedron Lett 2009;50:2358–62.
- [30] Sharghi H, Khalifeh R, Doroodmand MM. Copper nanoparticles on charcoal for multicomponent catalytic synthesis of 1,2,3-triazole derivatives from benzyl halides or alkyl halides, terminal alkynes and sodium azide in water as a "Green" solvent. Adv Synth Catal 2009;351:207–18.
- [31] Alonso F, Moglie Y, Radivoy G, Yus M. Multicomponent synthesis of 1,2,3-triazoles in water catalyzed by copper nanoparticles on activated carbon. Adv Synth Catal 2010;352:3208–14.
- [32] Alonso F, Moglie Y, Radivoy G, Yus M. Click chemistry from organic halides, diazonium salts and anilines in water

- catalysed by copper nanoparticles on activated carbon. Org Biomol Chem 2011;9:6385–95.
- [33] Alonso F, Moglie Y, Radivoy G, Yus M. Multicomponent click synthesis of 1,2,3-triazoles from epoxides in water catalyzed by copper nanoparticles on activated carbon. J Org Chem 2011;76:8394–405.
- [34] Sharghi H, Khalifeh R, Mansouri S, Aberi M, Eskandari M. Simple, efficient, and applicable route for synthesis of 2aryl(heteroaryl)-benzimidazoles at room temperature using copper nanoparticles on activated carbon as a reusable heterogeneous catalyst. Catal Lett 2011;141:1845–50.
- [35] Albaladejo MJ, Alonso F, Yus M. Synthesis of indolizines and heterocyclic chalcones catalyzed by supported copper nanoparticles. Chem Eur J 2013;19:5242–5.
- [36] Rodríguez-reinoso F. The role of carbon materials in heterogeneous catalysis. Carbon 1998;36:159–75.
- [37] Zapf A, Beller M. Fine chemical synthesis with homogeneous palladium catalysts: examples. Status Trend Top Catal 2002:19:101–9.
- [38] Felpin F-X, Ayad T, Mitra S. Pd/C: an old catalyst for new applications – its use for the Suzuki-Miyaura reaction. Eur J Org Chem 2006:2679–90.
- [39] Seki M. Recent advances in Pd/C-catalyzed coupling reactions. Synthesis 2006:2975–92.
- [40] Yin L, Liebscher J. Carbon—carbon coupling reactions catalyzed by heterogeneous palladium catalysts. Chem Rev 2006;107:133–73.
- [41] Pal M. Palladium-catalyzed alkynylation of aryl and heteroaryl halides: a journey from conventional palladium complexes or salts to palladium/carbon. Synlett 2009;2896–912.
- [42] Toebes ML, van Dillen JA, de Jong KP. Synthesis of supported palladium catalysts. J Mol Catal A: Chem 2001;173:75–98.
- [43] Felpin F-X, Ibarguren O, Nassar-Hardy L, Fouquet E. Synthesis of oxindoles by tandem Heck-reduction-cyclization (Hrc) from a single bifunctional, in situ generated Pd/C catalyst. J Org Chem 2009;74:1349–52.
- [44] Ibarguren O, Zakri C, Fouquet E, Felpin F-X. Heterogeneous palladium multi-task catalyst for sequential Heck-reductioncyclization (Hrc) reactions: influence of the support. Tetrahedron Lett 2009;50:5071–4.
- [45] Felpin F-X, Fouquet E. A useful, reliable and safer protocol for hydrogenation and the hydrogenolysis of O-benzyl groups: the in situ preparation of an active Pd(0)/C catalyst with welldefined properties. Chem Eur J 2010;16:12440-5.
- [46] Felpin F-X, Miqueu K, Sotiropoulos J-M, Fouquet E, Ibarguren O, Laudien J. Room-temperature, ligand- and base-free heck reactions of aryl diazonium salts at low palladium loading: sustainable preparation of substituted stilbene derivatives. Chem Eur J 2010;16:5191–204.
- [47] Naturale G, Lamblin M, Commandeur C, Felpin F-X, Dessolin J. Direct C-H alkylation of naphthoquinones with amino acids through a revisited Kochi-Anderson radical decarboxylation: trends in reactivity and applications. Eur J Org Chem 2012;2012:5774–88.
- [48] Rossy C, Majimel J, Fouquet E, Delacôte C, Boujtita M, Labrugère C, et al. Stabilisation of carbon-supported palladium nanoparticles through the formation of an alloy with gold: application to the Sonogashira reaction. Chem Eur J 2013;19:14024–9.
- [49] Felpin F-X. Ten years of adventures with Pd/C catalysts: from reductive processes to coupling reactions. Synlett 2014;25:1055–67.
- [50] Rossy C, Majimel J, Delapierre MT, Fouquet E, Felpin F-X. Palladium and copper-supported on charcoal: a heterogeneous multi-task catalyst for Sequential Sonogashira-Click and Click-Heck Reactions. J Organomet Chem 2014;755:78–85.

- [51] Rossy C, Majimel J, Delapierre MT, Fouquet E, Felpin F-X. On the peculiar recycling properties of charcoal-supported palladium oxide nanoparticles in Sonogashira reactions. Appl Catal A Gen 2014;482:157–62.
- [52] Buckley BR, Butterworth R, Dann SE, Heaney H, Stubbs EC. "Copper-in-Charcoal" revisited: delineating the nature of the copper species and its role in catalysis. ACS Catal 2014;5:793-6.
- [53] Lopez-Ruiz H, Cerda-Pedro JE, Rojas-Lima S, Pérez-Pérez I, Rodriguez-Sanchez BV, Santillan R, et al. Cuprous oxide on charcoal-catalyzed ligand-free, synthesis of 1,4-disubstituted 1,2,3-triazoles via click chemistry. ARKIVOC 2013:139–64.
- [54] Groenendaal L, Bruining MJ, Hendrickx EHJ, Persoons A, Vekemans JAJM, Havinga EE, et al. Synthesis and (non)linear optical properties of a series of donor—oligopyrrole—acceptor molecules. Chem Mater 1998;10:226–34.
- [55] Alonso F, Moglie Y, Radivoy G, Yus M. Unsupported copper nanoparticles in the 1,3-dipolar cycloaddition of terminal alkynes and azides. Eur J Org Chem 2010:1875–84.
- [56] Campbell-Verduyn LS, Mirfeizi L, Dierckx RA, Elsinga PH, Feringa BL. Phosphoramidite accelerated copper(I)-catalyzed 3+2 cycloadditions of azides and alkynes. Chem Commun 2009;2139–41.
- [57] Reddy PS, Sreedhar B. Tandem oxidative A-tosyloxylation of alcohols/nucleophilic addition of azide/copper-catalyzed 1,3dipolar cycloaddition. Synthesis 2009:4203–7.
- [58] Gates BC. Supported metal clusters: synthesis, structure, and catalysis. Chem Rev 1995:95:511–22.
- [59] Pinna F. Supported metal catalysts preparation. Catal Today 1998;41:129–37.
- [60] Mondloch JE, Bayram E, Finke RG. A review of the kinetics and mechanisms of formation of supported-nanoparticle heterogeneous catalysts. J Mol Catal A: Chem 2012;355: 1–38
- [61] Corma A, Garcia H. Supported gold nanoparticles as catalysts for organic reactions. Chem Soc Rev 2008;37:2096–126.
- [62] Baltrusaitis J, Mendoza-Sanchez B, Fernandez V, Veenstra R, Dukstiene N, Roberts A, et al. Generalized molybdenum oxide surface chemical state Xps determination via informed amorphous sample model. Appl Surf Sci 2015;326:151–61.
- [63] Briggs D, Grant JT. Surface Analysis by Auger and X-Ray Photoelectron Spectroscopy. IMPublications; 2003.
- [64] Cao J-L, Shao G-S, Ma T-Y, Wang Y, Ren T-Z, Wu S-H, et al. Hierarchical meso-macroporous titania-supported cuo nanocatalysts: preparation, characterization and catalytic co oxidation. J Mater Sci 2009;44:6717–26.
- [65] Scanlon DO, Morgan BJ, Watson GW. Modeling the polaronic nature of p-type defects in Cu₂O: The failure of Gga and Gga+U. J Chem Phys 2009;131:124703.
- [66] Honraedt A, Raux M-A, Le Grognec E, Jacquemin D, Felpin F-X. Copper-catalyzed free-radical C-H arylation of pyrroles. Chem Commun 2014;50:5236–8.
- [67] Gil MV, Arévalo MJ, López Ó. Click chemistry What's in a name? Triazole synthesis and beyond. Synthesis 2007;1589–620.
- [68] Meldal M, Tornøe CW. Cu-catalyzed azide—alkyne cycloaddition. Chem Rev 2008;108:2952–3015.
- [69] Rostovtsev VV, Green LG, Fokin VV, Sharpless KB. A stepwise Huisgen cycloaddition process: copper(I)-catalyzed regioselective "Ligation" of azides and terminal alkynes. Angew Chem Int Ed 2002;41:2596–9.
- [70] Tornøe CW, Christensen C, Meldal M. Peptidotriazoles on solid phase: [1,2,3]-triazoles by regiospecific copper(I)catalyzed 1,3-dipolar cycloadditions of terminal alkynes to azides. J Org Chem 2002;67:3057–64.
- [71] Thirumurugan P, Matosiuk D, Jozwiak K. Click chemistry for drug development and diverse chemical-biology applications. Chem Rev 2013;113:4905–79.

- [72] Lutz J-F. 1,3-Dipolar cycloadditions of azides and alkynes: a universal ligation tool in polymer and materials science. Angew Chem Int Ed 2007;46:1018–25.
- [73] Chassaing S, Sani Souna Sido A, Alix A, Kumarraja M, Pale P, Sommer J. "Click Chemistry" in zeolites: copper(I) zeolites as new heterogeneous and ligand-free catalysts for the Huisgen [3+2] cycloaddition. Chem Eur J 2008;14:6713–21.
- [74] Boningari T, Olmos A, Reddy BM, Sommer J, Pale P. Zeo-click chemistry: copper(I)–zeolite-catalyzed cascade reaction; onepot epoxide ring-opening and cycloaddition. Eur J Org Chem 2010;6338–47.
- [75] Veerakumar P, Velayudham M, Lu K-L, Rajagopal S. Highly dispersed silica-supported nanocopper as an efficient heterogeneous catalyst: application in the synthesis of 1,2,3triazoles and thioethers. Catal Sci Technol 2011;1:1512–25.
- [76] Kumar A, Aerry S, Saxena A, de A, Mozumdar S. Copper nanoparticulates in guar-gum: a recyclable catalytic system for the huisgen [3+2]-cycloaddition of azides and alkynes without additives under ambient conditions. Green Chem 2012;14:1298–301.
- [77] Moghaddam FM, Ayati SE. Copper immobilized onto a triazole functionalized magnetic nanoparticle: a robust magnetically recoverable catalyst for "Click" reactions. RSC Adv 2015;5:3894–902.
- [78] Anil Kumar BSP, Harsha Vardhan Reddy K, Satish G, Uday Kumar R, Nageswar YVD. Synthesis of β-hydroxy-1,4disubstituted-1,2,3-triazoles catalyzed by copper ferrite

- nanoparticles in tap water using click chemistry. RSC Adv 2014:4:60652-7.
- [79] Anil Kumar BSP, Harsha Vardhan Reddy K, Madhav B, Ramesh K, Nageswar YVD. Magnetically separable CuFe₂O₄ nano particles catalyzed multicomponent synthesis of 1,4disubstituted 1,2,3-triazoles in tap water using 'Click Chemistry'. Tetrahedron Lett 2012;53:4595–9.
- [80] Kang H, Jung HS, Kim JY, Park JC, Kim M, Song H, et al. Immobilized Cuo hollow nanospheres catalyzed alkyneazide cycloadditions. J Nanosci Nanotechnol 2010;10:6504–9.
- [81] Alonso F, Moglie Y, Radivoy G, Yus M. Multicomponent click synthesis of potentially biologically active triazoles catalysed by copper nanoparticles on activated carbon in water. Heterocycles 2012;84:1033–44.
- [82] Appukkuttan P, Dehaen W, Fokin VV, Van der Eycken E. A microwave-assisted click chemistry synthesis of 1,4disubstituted 1,2,3-triazoles via a copper(I)-catalyzed threecomponent reaction. Org Lett 2004;6:4223–5.
- [83] Hassan S, Müller TJJ. Multicomponent syntheses based upon copper-catalyzed alkyne-azide cycloaddition. Adv Synth Catal 2015;357:617–66.
- [84] Oger N, d'Halluin M, Le Grognec E, Felpin F-X. Using aryl diazonium salts in palladium-catalyzed reactions under safer conditions. Org Process Res Dev 2014;18:1786–801.
- [85] Oger N, Le Grognec E, Felpin F-X. Continuous-flow heck-matsuda reaction: homogeneous versus heterogeneous palladium catalysts. J Org Chem 2014;79:8255–62.

Using Aryl Diazonium Salts in Palladium-Catalyzed Reactions under Safer Conditions

Nicolas Oger, Martin d'Halluin, Erwan Le Grognec, and François-Xavier Felpin*, Felpin*

[†]Université de Nantes; UFR des Sciences et des Techniques, CNRS UMR 6230, CEISAM, 2 rue de la Houssinière, 44322 Nantes Cedex 3, France

ABSTRACT: In this review, we give a concise but complete overview of methods describing the use of aryl diazonium salts in palladium-catalyzed reactions under safe conditions from a laboratory scale to a multikilogram scale. The approaches summarized herein are critically discussed, highlighting strengths and weaknesses.

■ INTRODUCTION

Aryl diazonium salts are a class of very reactive electrophiles displaying a large spectrum of reactivities from free-radical chemistry to organometallic synthesis. They have been widely used in industry in colour chemicals and in the manufacture of intermediates.³ More specifically, they have proved to be efficient and more reactive aryl halide and aryl sulfonate surrogates in palladium-catalyzed coupling reactions. 4 The "superelectrophile" properties of aryl diazonium salts have been successfully exploited for Suzuki- and Heck-type reactions, ultimately allowing processes at room temperature in hydrophilic solvents (alcohols and water) and without ligand or base.

With this picture, one could imagine that aryl diazonium salts are ideal electrophilic partners for palladium-catalyzed coupling reactions. Unfortunately, the high nucleofugic properties of the diazonium function, giving N2 release, make these compounds rather unstable and potentially explosive.⁵ The hazardous behavior of aryl diazonium salts can be largely controlled through the nature of the counterion. While chloride and carboxylate counterions usually give very unstable diazonium salts, very good stability of diazonium salts bearing tetrafluoroborate, sulfonate, or disulfonimide anions has been reported. As an illustration of this, Filimonov et al.7 reported the preparation of aryl diazonium tosylates displaying high thermal stability (up to 600 °C). Moreover, the stability of the salts is also governed by the nature of the substituents decorating the aromatic ring. For instance, strongly electron-withdrawing groups enhance the redox potential of the salts, leading to uncontrolled homolytic dediazonization pathways. While most palladium-catalyzed coupling reactions involve the use of purified crystalline salts, safer strategies are still appealing, especially when working on multigram or even multikilogram scales.5

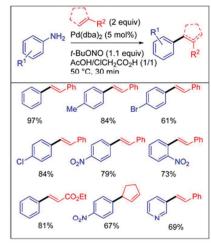
In this review, we aim to get an overview of strategies that do not involve the use of isolated salts in palladium-catalyzed reactions. Each approach is presented and critically discussed with the support of selected relevant examples. Ultimately, we anticipate that this contribution will serve as a textbook for synthetic chemists, engineers, and process chemists designing chemical pathways involving palladium-catalyzed reactions using aryl diazonium salts as aryl halide surrogates. Importantly, we stress that this review does not address safety investigations of

diazonium salts, since they largely depend on their structure; we have focused the discussion only on ways to generate and react these species under safer conditions. This review does not cover the general use of aryl diazonium salts in organic processes, and the reader can further refer to recently published reviews. ^{1b,2b,10}

DIAZONIUM SALTS GENERATED IN SITU FROM **ANILINES**

The diazotization of readily available anilines in situ is an obvious and straightforward way to generate aryl diazonium salts under safe conditions. In their pioneering studies, Matsuda and coworkers already noticed that the palladium-catalyzed arylation of olefins they discovered in the late 1970s was limited by the instability of diazonium salts even at room temperature. 11 In this

Table 1. Pioneering studies by Matsuda et al.



Special Issue: Safety of Chemical Processes 14

Received: September 16, 2014 Published: November 3, 2014

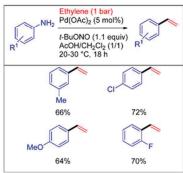
ACS Publications © 2014 American Chemical Society

1786

dx.doi.org/10.1021/op500299t | Ora. Process Res. Dev. 2014, 18, 1786-1801

[‡]Institut Universitaire de France, 103 blvd St Michel, 75005 Paris Cedex 5, France

Table 2. Arylation of ethylene with aryl diazonium salts generated in situ



event, they showed that the use of acetic acid and chloroacetic acid as solvents and proton donors for the diazonium formation in combination with t-BuONO as the nitrosating agent resulted in a safer procedure for the (hetero)arylation of styrene, ethyl acrylate, and aliphatic alkenes on a multigram scale (Table 1). Interestingly, this methodology allowed the olefination of pyridine at C3, which was unattainable otherwise since the 3-pyridine diazonium salt is highly unstable even at room temperature and cannot be isolated.

The low cost and weakly corrosive properties of acetic acid prompted other research groups to adapt such an approach to various palladium-catalyzed coupling reactions. For instance, Beller et al.¹³ described, on only four examples, a tandem diazotization/palladium-catalyzed olefination of anilines with ethylene, working on a multigram scale (Table 2). The reaction proceeded in a mixture of acetic acid and CH₂Cl₂ in the presence of t-BuONO as the diazotizing agent and Pd(OAc)₂ as the catalyst. Remarkably, the coupling was carried out at room

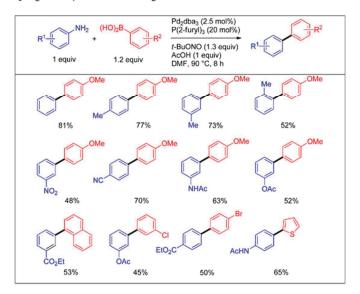
temperature under ethylene at atmospheric pressure and was not sensitive to the electronic nature of the aromatic substrate.

The studies by Matsuda and Beller showed that an excess of acetic acid as a proton donor is required to efficiently promote Heck-type reactions. Although the reason for this behavior still remains unclear, it is likely related to the low pKa of acetic acid, slowing the formation of the diazonium salt. A solution addressing this issue consisted of using a highly polar solvent such as DMF or DMSO, in which the rate of the diazonium salt formation is considerably enhanced. This strategy has been applied by Wang and co-workers for the one-pot diazotization/ Suzuki cross-coupling of anilines with aryl boronic acids (Table 3).14 Thanks to the use of DMF as the solvent, the coupling proceeded with only 1 equiv of acetic acid in the presence of t-BuONO as the diazotizing agent and Pd2(dba)2/P(2-furyl)3 as the catalyst system. The cross-coupling proceeded in modest to good yields with a variety of substrates and was relatively insensitive to the electronic nature of both the boronic acid and

A very similar catalytic system was simultaneously reported by Beller and co-workers for the copper-free alkynylation of anilines near room temperature (Table 4). Extensive optimization studies resulted in the development of a very efficient coupling of both aliphatic and aromatic alkynes with diazonium salts generated from anilines and a stoichiometric amount of $\mathrm{CH_3CO_2H}/\mathrm{t-BuONO}$ as diazotizing agents. For this Sonogashira coupling, $\mathrm{Pd}(\mathrm{OAc)_2/P(2-furyl)_3}$ was used as the catalyst and DMSO was preferred over DMF. The protocol proved to be general since anilines bearing electron-releasing and electron-withdrawing groups reacted with similar efficiencies with a very large selection of both aromatic and aliphatic alkynes.

Interestingly, a carbonylative variant of this methodology was subsequently developed that proceeds under similar conditions in the presence of carbon monoxide (10 bar) (Table 5). ¹⁶ For some reasons, the carbonylative Sonogashira reaction proceeded in higher yields in a mixture of DMSO and THF. As already

Table 3. Suzuki cross-coupling with aryl diazonium salts generated in situ



1787

dx.doi.org/10.1021/op500299t | Org. Process Res. Dev. 2014, 18, 1786–1801

Table 4. Selected examples of Sonogashira couplings with aryl diazonium salts generated in situ

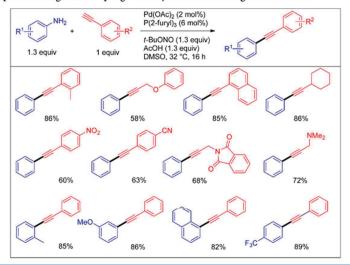
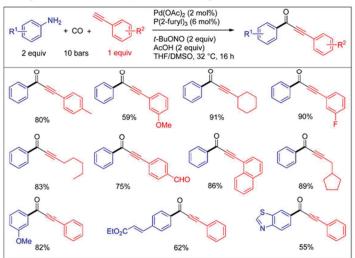


Table 5. Carbonylative Sonogashira reaction with aryl diazonium salts generated in situ



observed for the Sonogashira reaction, this very convenient carbonylative variant was rather insensitive to the electronic nature of the partners, and excellent yields were consistently obtained.

However, the intrinsic low stability of aryl diazonium acetate salts sometimes led to degradation products, especially upon heating, decreasing the reaction yields. By contrast, aryl diazonium cations involved in an ion pair with tetrafluoroborate anions are usually very stable salts. Isolated crystalline diazonium tetrafluoroborate salts are usually prepared by diazotization of the corresponding aromatic amines with NaNO₂ in 40–50% aqueous fluoroboric acid followed by precipitation in aqueous media. However, this procedure, which requires an excess of HBF4 $_{4}$ is not convenient for tandem diazotization/Pd-catalyzed coupling reactions with acid-sensitive compounds. Moreover, the

presence of large amount of water can be problematic with substrates prone to hydrolysis. Therefore, the anhydrous preparation of aryl diazonium tetrafluoroborate salts in ethereal solvents (THF, Et₂O) or $\mathrm{CH_2Cl_2}$ by diazotization of the corresponding anilines with an alkyl nitrite and boron trifluoride through the transient formation of nitrosyl fluoride as a diazotating reactive intermediate, described in the 1970s by Doyle and Bryker, was preferred in palladium-catalyzed reactions.

Andrus and co-workers adapted this procedure to palladium—imidazolium carbene-catalyzed Heck¹⁹ and Suzuki²⁰ reactions with diazonium ions formed in situ. In this event, they developed very convenient one-pot sequential procedures in which the diazonium salts were initially formed from the corresponding anilines with equimolar amounts of t-BuONO and BF₃·Et₂O in

1788

dx.doi.org/10.1021/op500299t | Org. Process Res. Dev. 2014, 18, 1786–1801

Table 6. Heck and Suzuki couplings with aryl diazonium salts generated in ${\rm situ}^a$

"Yields in parentheses correspond to couplings carried out with isolated diazonium tetrafluoroborate salts.

THF at 0 °C (Table 6). Upon completion of the diazotization, the palladium acetate—imidazolium catalyst system and the coupling partner (styrene or boronic acid) were added dropwise, and the reaction was continued until completion at room temperature. Although these procedures were very convenient from an experimental point of view, they suffered from much lower yields, typically 20–30% lower than analogous couplings

Scheme 1. Key Heck–Matsuda reaction toward the total synthesis of ecteinascidin 743

carried out using isolated diazonium salts (see the yields in parentheses in Table 6).

A spectacular application of sequential diazotization/Heck-Matsuda coupling reactions for the construction of an advanced intermediate of ecteinascidin 743 was described by the group of Fukuyama (Scheme 1).²¹ The treatment of the highly decorated aniline 1 with t-BuONO and BF3·Et2O in THF at -15 °C produced the expected diazonium salt, which was reacted with a solution of cyclic enamide 2 in CH3CN in the presence of Pd2(dba)3 and NaOAc. The coupling occurred regio- and stereoselectively from the less hindered face of the enamide, producing the desired compound 3 in high yield. The Heck-Matsuda reaction is particularly well suited for such an application in the total synthesis of complex natural products since the mild conditions and short reaction times allow one to work with architectures bearing sensitive functional groups. This example is an impressive testimony to the efficient introduction of diazonium chemistry into the field of highly complex molecule synthesis and would serve as a model for medicinal chemists.

Doyle's procedure for generating dry diazonium salts in situ from the t-BuONO/BF₃·Et₂O couple has also been successfully implemented in Sonogashira cross-coupling reactions. In this event, Sarkar and co-workers reported Sonogashira-type crosscouplings of aryl diazonium salts with terminal alkynes using an unusual Pd-Au dual catalytic system (Table 7).22 The dry diazonium salt, prepared at 0 °C in THF for 1 h, was reacted with phenylacetylene as the coupling partner in the presence of PdCl₂ and AuCl as catalysts, IPr NHC as the ligand, and 2,6-di-tertbutyl-4-methylpyridine as the base. The coupling proceeded at room temperature in half an hour with correct yields. However, as already observed by Andrus et al., much greater yields were obtained with a procedure starting from isolated aryl diazonium salts (see the yields in parentheses in Table 7). Cacchi and coworkers also contributed to this area for the Sonogashira reaction with a one-pot diazotization/coupling sequence. However, the solvent used for the diazotizing step (THF) was unsuitable for the subsequent coupling and had to be hazardously removed in vacuo and replaced by MeCN.23

Interestingly, dry aryl diazonium salts can also be generated in protic solvents such as methanol. This approach has been explored by Sun, Jiang, and co-workers for the Suzuki coupling of diazonium salts with boronic acids in the presence of magnetic

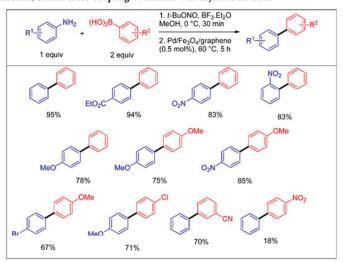
1789

dx.doi.org/10.1021/op500299t | Org. Process Res. Dev. 2014, 18, 1786–1801

Table 7. Dual catalytic Sonogashira reaction with aryl diazonium salts generated in situ a

"Yields in parentheses correspond to couplings carried out with isolated diazonium tetrafluoroborate salts.

Table 8. Tandem diazotization/Suzuki cross-coupling of anilines with arylboronic acids



Scheme 2. Intramolecular Heck—Matsuda reaction onto an $\alpha\beta$ -unsaturated ester

palladium nanoparticles (Table 8).²⁴ Good to excellent yields were usually obtained with a variety of unchallenging substrates,

but the use of strongly electron-deficient arylboronic acids severely compromised the reaction efficiency.

Acid-sensitive substrates usually do not tolerate the presence of BF₃·Et₂O. In such cases, nitrosyl cations have been successfully used. For instance, the group of Correia reported that the diazotization of aniline 4 failed with standard protocols as a result of extensive decomposition.²⁵ Therefore, a neutral diazotization of 4 using NOBF₄ was conducted, furnishing the required diazonium tetrafluoroborate salt in solution in CH₃CN, which reacted in situ to give the targeted cyclized compound 5 in 53–67% yield (Scheme 2). Importantly, the reaction was conducted under an atmosphere of carbon monoxide to generate Pd(0) from Pd(OAc)₂.

Sefkow and co-workers described an ingenious diastereoselective synthesis of *trans*-dihydrobenzofurans using a palladiumcatalyzed oxyarylation as a key step. ²⁶ In the optimization studies,

1790

dx.doi.org/10.1021/op500299t | Org. Process Res. Dev. 2014, 18, 1786-1801

Table 9. Tandem diazotization/oxyarylation for the synthesis of *trans*-dihydrobenzofurans

Scheme 3. Heck-Matsuda reaction through a double catalytic cycle

$$\begin{array}{c} R_1 \stackrel{\text{ii}}{=} \\ R_1 \stackrel{\text{ii}}{=} \\ \end{array} \begin{array}{c} R_2 \\ \end{array} \begin{array}{c} R_1 \stackrel{\text{ii}}{=} \\ \end{array} \begin{array}{c} R_2 \\ \end{array} \begin{array}{c} R_1 \stackrel{\text{ii}}{=} \\ \end{array} \begin{array}{c} R_2 \\ \end{array} \begin{array}{c} R_1 \stackrel{\text{ii}}{=} \\ \end{array} \begin{array}{c} R_2 \\ \end{array} \begin{array}{c} R_1 \stackrel{\text{ii}}{=} \\ \end{array} \begin{array}{c} R_2 \\ \end{array} \begin{array}{c} R_1 \stackrel{\text{ii}}{=} \\ \end{array} \begin{array}{c} R_2 \\ \end{array} \begin{array}{c} R_1 \stackrel{\text{ii}}{=} \\ \end{array} \begin{array}{c} R_2 \\ \end{array} \begin{array}{c} R_1 \stackrel{\text{ii}}{=} \\ \end{array} \begin{array}{c} R_2 \\ \end{array} \begin{array}{c} R_1 \stackrel{\text{ii}}{=} \\ \end{array} \begin{array}{c} R_2 \\ \end{array} \begin{array}{c} R_1 \stackrel{\text{ii}}{=} \\ \end{array} \begin{array}{c} R_2 \\ \end{array} \begin{array}{c} R_1 \stackrel{\text{ii}}{=} \\ \end{array} \begin{array}{c} R_2 \\ \end{array} \begin{array}{c} R_1 \stackrel{\text{ii}}{=} \\ \end{array} \begin{array}{c} R_2 \\ \end{array} \begin{array}{c} R_1 \stackrel{\text{ii}}{=} \\ \end{array} \begin{array}{c} R_2 \\ \end{array} \begin{array}{c} R_1 \stackrel{\text{ii}}{=} \\ \end{array} \begin{array}{c} R_2 \\ \end{array} \begin{array}{c} R_1 \stackrel{\text{ii}}{=} \\ \end{array} \begin{array}{c} R_2 \\ \end{array} \begin{array}{c} R_1 \stackrel{\text{ii}}{=} \\ \end{array} \begin{array}{c} R_2 \\ \end{array} \begin{array}{c} R_1 \stackrel{\text{ii}}{=} \\ \end{array} \begin{array}{c} R_2 \\ \end{array} \begin{array}{c} R_1 \stackrel{\text{ii}}{=} \\ \end{array} \begin{array}{c} R_2 \\ \end{array} \begin{array}{c} R_1 \stackrel{\text{ii}}{=} \\ \end{array} \begin{array}{c} R_1 \stackrel{\text{ii}}{=} \\ \end{array} \begin{array}{c} R_2 \\ \end{array} \begin{array}{c} R_1 \stackrel{\text{ii}}{=} \\ \end{array} \begin{array}{c} R_2 \\ \end{array} \begin{array}{c} R_1 \stackrel{\text{ii}}{=} \\ \end{array} \begin{array}{c} R_1 \stackrel{\text{ii}$$

the authors observed that the formation of the diazonium salt from 2-aminophenol occurred in low yields with standard procedures. Accordingly, they opted for a one-pot diazotization/oxyarylation sequence through the use of nitrosyl hexafluor-ophosphate (NOPF₆) as a neutral diazotizing agent (Table 9). The whole process was developed in CH₃CN as the solvent and

required the use of ZnCO₃ as a base for the oxyarylation. After the diazotization was achieved (30 min at 0 °C), the remaining reactants, including Pd₂(dba)₃ as the catalyst, ZnCO₃, and the phenylpropene derivative as the coupling partner, were added to the reaction mixture, providing the desired *trans*-dihydrobenzofurans. The methodology was compatible with electron-rich phenylpropenes and a range of 2-aminophenols bearing electron-withdrawing or electron-releasing groups. Unfortunately, heteroaromatic diazonium salts were incompatible with the process and failed to give the desired products.

Our group recently introduced a new concept for handling palladium-catalyzed Heck reactions involving aryl diazonium salts under safer and greener conditions. In 2011, we reported an unprecedented substoichiometric use of hazardous aryl diazonium salts for the Heck-Matsuda reaction in MeOH as solvent via a double catalytic cycle, as depicted in Scheme 3. treatment of a mixture of aniline A and t-BuONO with a catalytic amount of MeSO₃H produces a substoichiometric amount of diazonium salt B with the simultaneous release of t-BuOH and H₂O. The introduction of Pd(OAc)₂ to the reaction mixture starts the cooperative catalysis, ultimately leading to the coupling product E. Our cooperative bicatalysis features a number of key advances: (1) at any time of the process, only a catalytic amount of diazonium salt is produced in situ; (2) the reaction is experimentally very simple without any ligand nor base; (3) t-BuOH, N2, and H2O are the only benign byproducts produced; and (4) MeOH acts as a solvent and as a potent reducing agent to convert $Pd(OAc)_2$ into Pd(0) species.

While our first-generation procedure was successful only with anilines bearing electron-withdrawing substituents, we recently reported an improved methodology covering the complete electronic range of anilines.²⁸ Indeed, with our first-generation procedure, the use of electron-rich anilines quantitatively led to triazenes, which rapidly degraded into a collection of unidentified side-products. The triazene formation resulted from the coexistence in the flask of the diazonium salts in catalytic amounts with the unreacted nucleophilic free aniline. Therefore, we devised an alternative procedure wherein the concentration of the aniline was maintained low via slow addition to the reaction mixture using a syringe pump (Table 10). With such an advanced procedure, a large electronic range of anilines were successfully coupled to methyl acrylate. Even 3,4,5-trimethoxyaniline, usually a poor substrate for palladium catalysis, furnished the coupling product in good yield (73%). Interestingly, the methodology was also extended to other olefinic partners such as cyclopentene derivatives and acrylonitrile.

Unfortunately, this double catalytic process could not be extended to Suzuki cross-coupling because of a distinct mechanism. However, we instead developed a new concept that proceeds through the formation of an arylpalladium alkoxo complex generated in situ from Pd(OAc), and a diazonium salt.²⁹ This concept was elaborated by taking into consideration the impressive work of Jutand and Amatore on the mechanism of the transmetalation step in the Suzuki-Miyaura reaction. 30 The major key feature is that the process was carried out under neutral conditions with an acid-free diazonium salt formation and a basefree transmetalation step. The concept was based on the following catalytic cycle (Scheme 4). Our strategy started with the observation by 1H NMR spectroscopy that treatment of aniline F with t-BuONO in MeOH led to the formation of a small amount of the corresponding diazonium hydroxide (5%) along with the remaining aniline. With this information in mind, we elaborated a strategy wherein the diazonium hydroxide reacted

1791

dx.doi.org/10.1021/op500299t | Org. Process Res. Dev. 2014, 18, 1786-1801

Table 10. Heck-Matsuda reactions using a cooperative bicatalytic strategy

Scheme 4. Strategy for ligand-, base-, and acid-free Suzuki-type reactions. The catalytic cycle was reprinted with permission from ref 29. Copyright 2013 John Wiley & Sons.

with the palladium catalyst to give palladium alkoxo intermediate H. The latter was engaged in the transmetalation step with the boronic acid without any base to give complex J, which upon

reductive elimination furnished the desired biphenyl compound K. We observed that in the absence of any ligand or additive the transmetalation step dramatically slowed down, leading to rapid

1792

dx.doi.org/10.1021/op500299t | Org. Process Res. Dev. 2014, 18, 1786–1801

Scheme 5. Synthesis of the herbicide Prosulfuron (10)

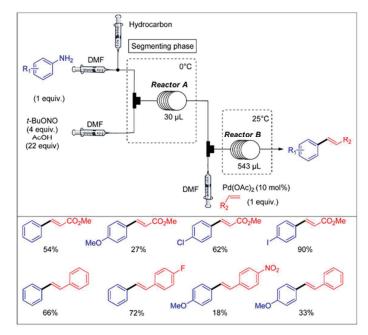
precipitation of the catalyst as palladium black. We addressed this issue with the use of an ortho-coordinating group, leading to a chelation-assisted cross-coupling reaction. With such a strategy, we described the coupling of various ortho-substituted anilines bearing both electron-releasing and electron-withdrawing groups with aryl- or alkenylboronic acids. From a general perspective, a large number of coordinating groups are compatible with this process, including halogen, ether, nitro, and carbonyl functions. In the absence of an ortho-coordinating group on the aniline, a very poor yield of the corresponding biphenyl was obtained. The formation of the palladium alkoxo complex was detected by ESI-MS in the form of a trimeric palladium complex.

An impressive multiton-scale synthesis of an early intermediate of Prosulfuron (10), a well-known herbicide, was produced at Syngenta (formerly Ciba-Geigy) using a Heck–Matsuda coupling as key step. 9b,31 While a Friedel–Crafts alkylation of benzenesulfonic acid was initially envisaged,

manufacturing costs and environmental concerns convinced process chemists to develop a more efficient strategy. To this end, they developed a diazotization/Heck-Matsuda coupling/ hydrogenation sequence starting with 2-aminobenzenesulfonic acid (6) and ending with sodium 2-(3,3,3-trifluoropropyl)benzenesulfonate (9) (Scheme 5). The process produces 2 kg of waste/kg of product for the sequential three steps, corresponding to an impressive E-factor of 2. Each chemical was carefully and judiciously selected in order to make this integrated approach as cost-effective as possible. Thus, pentan-1-ol was selected as the solvent for its compatibility with the three steps and its harmless nature, while Pd(dba)2 as the catalyst, generated in situ from dibenzylideneacetone and PdCl2, proved to be the best compromise between cost and efficiency. In this work, an impressively efficient sequence was optimized, leading to an overall yield of 93% over the three steps (i.e., an average yield of 98% per step). A rather low turnover number (100-200) was achieved because of a rather high loading of palladium (0.5-1.5 mol %), but the addition of charcoal in the last hydrogenation step allowed the complete recovery of palladium species with a single filtration. This work, one of the few examples of a Pdcatalyzed coupling reaction working on an industrial scale,³² highlights the power of diazonium chemistry for process chemists.

The diazotization of aniline is usually a fast exothermic reaction, rendering the precise temperature control required on bulk scale extremely challenging. A modern and still-underused strategy to enhance the safety of diazonium handling is the use of continuous-flow reactors. ^{94,33} Indeed, the high surface-to-volume ratio of the reactor considerably improves the heat transfer, decreasing the risk of formation of hot spots. Moreover, continuous-flow processes are usually much more reproducible because of the precise control of the reaction parameters, and

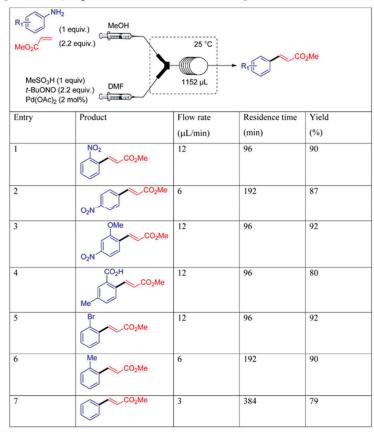
Table 11. Flow setup described by Wirth and co-workers and selected examples



1793

dx.doi.org/10.1021/op500299t | Org. Process Res. Dev. 2014, 18, 1786–1801

Table 12. Flow setup described by Organ and co-workers and selected examples



increasing the number or size of the flow reactors allow readily achievable scale-up. All these features provide the workers with a safe environment. For instance, o-difluorobenzene can be produced on a multikilogram scale through a continuous-flow Balz–Schiemann reaction. 9d

Wirth and co-workers developed a process for Heck-Matsuda reactions working in a segmented flow.³⁴ The main difference between laminar and segmented flow is the use of an immiscible inert solvent segmenting the laminar flow. With such a flow regime, more efficient mixing due to internal circulation in the segments was expected. Thereby, sequential diazotization/ Heck-Matsuda reactions were carried out with a four-stream flow device using syringe pumps, as depicted in Table 11. The whole sequence was conducted in a mixture of DMF and AcOH using a hydrocarbon such as heptane as the segmenting phase. The diazonium salt was produced in a first microreactor (30 μ L) immersed in an ice bath and then reacted with an alkene at 25 °C (methyl acrylate or a styrene) in the presence of Pd(OAc)₂ (10 mol %). This methodology gave arylated alkenes in moderate to high yields (18-90%) in a short reaction time (total retention time = 27 min). Interestingly, similar yields were obtained when commercially available p-nitrobenzenediazonium tetrafluoroborate was used, suggesting that the in situ production of diazonium

salts under segmented flow is a promising approach for safer use of such hazardous compounds.

Intrigued by the moderate yields obtained by Wirth and coworkers with some anilines, the group of Organ hypothesized that the diazonium salt underwent rapid hydrodediazotization that competed with the coupling reaction.³⁵ After extensive optimization studies, Organ and co-workers provided evidence that DMF indeed promoted unwanted hydrodediazotization and that this reaction was suppressed in MeOH at 0 °C. This observation was in line with our previous studies conducted in batch, which showed that MeOH was the solvent of choice for palladium-catalyzed reactions involving aryl diazonium salts.30 With these preliminary results in hand, they subsequently developed multicomponent diazotization/Heck-Matsuda reactions using only one flow reactor. They anticipated that the diazonium produced could be directly consumed in the coupling reaction, thereby inhibiting the unwanted hydrodediazotization, even at room temperature. The optimized flow setup was established with a two-stream flow reactor (Table 12). The first syringe pump was fed with a solution of the aniline and methyl acrylate in MeOH, while the second syringe pump was fed with a solution of t-BuONO, MeSO₃H, and Pd(OAc)₂ in DMF. The two streams met at a mixing chamber and entered into an FEP coil reactor (1152 μ L) at room temperature. According to their

1794

dx.doi.org/10.1021/op500299t | Org. Process Res. Dev. 2014, 18, 1786-1801

Scheme 6. Comparison of kinetics in two-step versus multicomponent processes

Two-step one-pot process

electronic nature, the anilines were reacted at flow rates ranging from 3 to 12 μ L/min, corresponding to residence times of 6.4 and 1.6 h, respectively. With this methodology, the authors obtained styrene compounds in good to excellent yields (51–98%), especially with anilines bearing electron-withdrawing groups.

At the time Organ and co-workers published their results, we were conducting independent studies that led to a significantly different flow setup.³⁷ Actually, while the reaction yields achieved with Organ's procedure were excellent, the very low flow rates led to long residence times (up to 6.4 h) and consequently to rather low throughput. In this event, we studied the coupling of 4-bromoaniline (11) with methyl acrylate in order to determine whether a two-step procedure involving sequential diazotization/coupling or a multicomponent process wherein the diazotization and the coupling occur in the same reaction chamber is the most efficient way by considering reaction rates (Scheme 6). Interestingly, we observed that the two-step procedure required a total of 120 min to reach >91% ¹H NMR yield of 13, while a similar yield was obtained only after more than 18 h in the case of a multicomponent process.

Although the reason for such a difference was uncertain, we considered these preliminary results to develop a three-stream flow setup that consisted of a first reactor for the diazonium salt formation and a second for the coupling reaction (Table 13). The first PEEK tubing reactor ($100 \, \mu L$ or $5 \, \text{mL}$) was fed with a first stream containing a solution of the anilinium in MeOH, obtained from the corresponding aniline and MeSO₃H, and a second stream contained a solution of t-BuONO in MeOH. Then the diazonium salt solution met a solution of methyl acrylate and $Pd(OAc)_2$ ($0.5 \, \text{mol}$ %) in THF in a T-shaped mixer and entered a second PEEK tubing reactor ($5 \, \text{mL}$). We observed that the use of THF as a cosolvent was required to avoid the MeOH-induced precipitation of palladium, leading to issues with clogging of the tubing reactor. Both reactors were placed in an oven to accurately control the reaction temperature ($40-60 \, ^{\circ}\text{C}$). While anilines

bearing electron-withdrawing groups were coupled to methyl acrylate with a short total residence time (17.2 min), electron-neutral and electron-rich anilines required longer residence times (41.7–116.7 min).

With the aim of developing a more environmentally friendly version of this process, we set up a new flow reactor working with a heterogeneous palladium catalyst (Table 14). To this end, we used Pd EnCat 30, which consists of palladium acetate encapsulated in a polyurea matrix. While the reaction yields were in the same range as those obtained with the homogeneous process, a number of decisive improvements have to be mentioned: (1) the residence times were significantly shortened to 225 s with electron-deficient anilines; (2) the concentration of reagents was increased 2-fold; (3) the palladium content in the crude mixture was 100 times lower than under homogeneous conditions; (4) a single green solvent (MeOH) was used throughout the process. It should be noted that Heck-Matsuda reactions catalyzed by heterogeneous palladium catalysts were not known with flow reactors at the time we reported our studies, although examples in batch had previously been reported. 36b,

■ ACETANILIDES AS LATENT DIAZONIUM SALTS

Although the methods described above proved to be successful, the use of free anilines can occasionally be impractical because

Scheme 7. One-flask deacetylation/diazotization sequence

they are sometimes prone to oxidation and need to be freshly purified before use. Moreover, the nucleophilic amino groups of anilines may also be problematic when the aromatic core needs to be functionalized before generation of the diazonium salt.

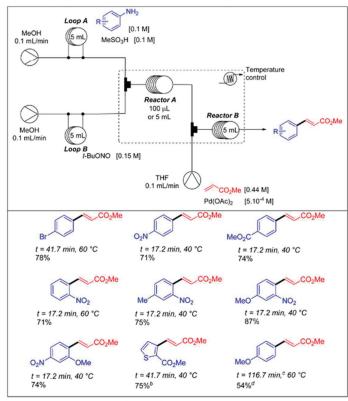
Schmidt and co-workers judiciously addressed these issues by the use of acetanilides, which can be easily deacetylated under acidic conditions and converted into the corresponding arenediazonium salts in the presence of a nitrite source by a one-flask deacetylation/diazotization sequence (Scheme 7). According to the nature of the acetanilide substrate, the deprotection step was preferably achieved with either BF₃·Et₂O or HCl/NH,BF₁ as the acid. However, they later privileged the use of BF₃·Et₂O in more complex sequences (vide infra).

This strategy was extended to one-flask deacetylation/diazotization/Heck—Matsuda reactions (Table 15). 40 The one-pot process occurred sequentially and started with cleavage of the acetanilide functions by BF₃·Et₂O in MeOH at 65 °C, followed by the addition of *t*-BuONO at 0 °C to trigger the diazotization step. The diazonium salt was then reacted in situ with acrylates or styrenes in the presence of Pd(OAc)₂ (5 mol %). This three-step one-flask sequential process proved to be particularly efficient with methyl acrylate, while the use of styrenes gave more erratic results, especially with electron-rich acetanilides. During this work, Schmidt noticed the adverse effect of excess *t*-BuONO on certain substrates, likely due to its strong oxidizing properties. Application of this strategy to a straightforward preparation of a key fragment of aripiprazole, 41 an approved drug for the treatment of psychotic disorders, demonstrated the usefulness

1795

dx.doi.org/10.1021/op500299t | Org. Process Res. Dev. 2014, 18, 1786-1801

Table 13. Flow setup described by Felpin and co-workers and selected examples^a



 a Isolated yields (averages of at least two runs) are shown. $^{b}1 \times 10^{-3}$ M Pd(OAc)₂. c Flow rate/stream: 0.025 mL min⁻¹. $^{d}4 \times 10^{-3}$ M Pd(OAc)₂.

of this chemistry. A related strategy toward the preparation of the same key intermediate was described by our group, but our approach suffered from the use of an isolated diazonium salt. 42

Interestingly, acetanilide can serve as an ortho-directing group for oxidative Heck reactions with methyl acrylate before sequential deacetylation/diazotization/Heck—Matsuda reactions (Table 16).⁴³ The oxidative Heck step was rather insensitive to the electronic nature of the acetanilide, although the presence of halogens was detrimental to the reaction yield. The subsequent three-step one-pot olefination of acetanilides gave dienic arenes in modest to good yields (14–66%).

ARYL TRIAZENES AS STABLE LATENT ARYL DIAZONIUM SALTS

Another strategy that avoids the isolation and purification of hazardous aryl diazonium salts consists of the use of aryl triazenes. Indeed, the nucleophilic addition of secondary aliphatic amines onto diazonium functions is reversible and pH-dependent. As a consequence, aryl triazenes can be considered as a latent source of aryl diazonium salts. Aryl triazenes are stable toward many reagents, including aqueous bases, alkoxides, and alkyllithium and Grignard reagents. By contrast, they are unstable under acidic conditions and in the presence of strong electrophiles such as Br₂, MeI, and Me₃SiI.⁴⁴ Under neutral conditions, most triazenes are stable toward air,

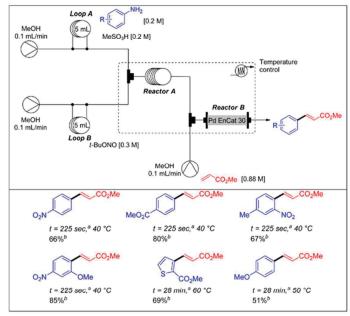
typically up to 140 °C, and can be stored for years in a refrigerator. Moreover, aryl triazenes bearing electron-releasing groups or bulky ortho substituents are usually less stable than triazenes decorated with electron-withdrawing groups. This trend can be explained by the less nucleophilic and therefore less reactive nitrogen lone pair with electron-deficient triazenes.

Typically, aryl triazenes are prepared by in situ trapping of aryl diazonium salts with secondary aliphatic amines such as morpholine and pyrrolidine.45 They can be back-converted into their corresponding diazonium salt congeners upon addition of Brønsted or Lewis acids. This strategy was pioneered by the group of Sengupta, who described palladium-catalyzed Heck reactions with morpholinyl diazenes as latent aryl diazonium salts that were unmasked in situ with a Brønsted acid (Table 17).46 While the use of acetic acid or acidic Dowex resins failed to give the expected coupling products, a variety of acids including TFA, HBF4, HF, HClO4, and MeSO3H were compatible, with an efficiency comparable to that when the process was carried out in MeOH or EtOH as the solvent. Aryl triazenes decorated with halogen, methoxy, and methyl substituents reacted smoothly in refluxing EtOH or MeOH with acrylates, styrene, and cyclopentene, leading to the coupling products in good yields (>73%). However, very electron-deficient aryl triazenes, bearing for instance a nitro group, failed to participate in the coupling whatever the acid used. This behavior is the result of the strong

1796

dx.doi.org/10.1021/op500299t | Org. Process Res. Dev. 2014, 18, 1786–1801

Table 14. Flow setup with an immobilized palladium catalyst described by Felpin and co-workers and selected examples



"Total residence time including reactor A and reactor B. "Isolated yield.

Table 15. One-flask deacetylation/diazotization/Heck-Matsuda sequence

deactivation of the nitrogen lone pair, which cannot be protonated by the acid.

Even more impressively, the strategy worked for the double Heck coupling on a bis(triazene) with styrene as the olefinic

Scheme 8. Olefination of a bis(triazene) compound

partner, giving the expected compound in 63-70% yield according to the acid used (Scheme 8).

A similar strategy has also been described by the groups of Tamao⁴⁷ and Luo⁴⁸ for Suzuki cross-coupling reactions. Both groups studied the coupling of pyrrolidinyl diazene with arylboronic acids, using BF₃·Et₂O as the Lewis acid to liberate the diazonium tetrafluoroborate function. While Tamao and coworkers privileged the use of Pd₂(dba)₃ and P(fBu)₃ in DME as the catalytic system, the group of Luo reported the use of a polymer-supported NHC–Pd catalyst in dioxane. Both strategies were successful with a variety of aryl triazenes and arylboronic acids bearing either electron-poor or electron-

1797

dx.doi.org/10.1021/op500299t | Org. Process Res. Dev. 2014, 18, 1786–1801

Table 16. Acetanilides as an ortho-directing group for oxidative Heck reactions

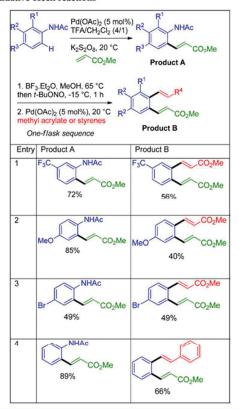


Table 17. Selected examples from the work of Sengupta and co-workers

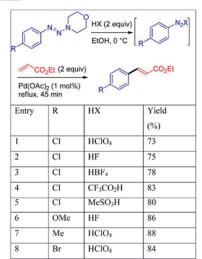


Table 18. Selected examples from the groups of Tamao and Luo

R ¹ -II					
(1 equiv)			DME, rt, <1 h		R1_[
BF ₃ .Et ₂ O — (1 equiv)			Polymer-supported NHC-Pd catalyst		R ² -L
B(OH) ₂ dioxane, rt, 8-12 h					
R ² (2 equiv)					
Entry	R ¹	R ²		Yield A	Yield B
				(%) ^a	(%) ^a
1	2-Me	4-OMe		72	1
2	3-Me	4-OMe		80	1
3	4-Me	4-OMe		91	82
4	Н	3-NO ₂		/	74
5	4-Cl	4-OMe		68	1
6	4-Br	Н		/	71
7	3-NO ₂	Н	3	1	92 (78) ^b
8	4-NO ₂	4-	Me	/	93
9	4-NO ₂	4-OMe		/	96

"Isolated yields. "Yield after seven reuses.

Scheme 9. Sequential Sonogashira/Heck reactions on a bifunctional iodotriazene

releasing substituents (Table 18). The catalytic system described by Tamao exhibited good catalytic activity with short reaction times (<1 h) at room temperature, while the heterogeneous catalyst reported by Luo required longer reaction times (8–12 h) but was recyclable on at least eight runs.

However, aryl triazenes are synthetically useful only if they serve as a stable latent diazonium function in multistep syntheses. In this event, Sengupta and Sadhukhan reported⁴⁹ a single example of a Sonogashira/Heck reaction sequence on a bifunctional iodotriazene, as depicted in Scheme 9. The Sonogashira alkynylation proceeded first at the iodine atom, while in a second reaction the latent diazonium function was uncovered with 2 equiv of HBF₄ for the Heck coupling with methyl acrylate in MeOH.

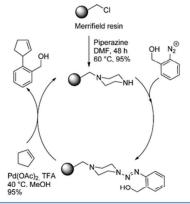
In a very elegant work, Knochel also exploited the high stability of triazenes under basic conditions for the preparation of new bifunctional coupling reagents bearing a boronic ester group and a triazene function (Table 19). ⁵⁰ These donor—acceptor

1798

dx.doi.org/10.1021/op500299t | Org. Process Res. Dev. 2014, 18, 1786-1801

Table 19. Orthogonal Suzuki cross-coupling reactions

Scheme 10. Solid-phase Heck coupling from triazenes



coupling reagents formed the central aromatic ring of new dissymmetrical terphenyls. The triazene function proved to be remarkably stable under basic conditions since the bifunctional reagents were prepared from bromo- or iodotriazenes through halogen—magnesium exchange followed by borylation. Several donor—acceptor-substituted coupling reagents were prepared in good overall yields and engaged in a first Suzuki coupling at the boron atom. In the presence of Pd(Ph₃P)₄ and K₃PO₄ in dioxane/water at 100 °C, all of the triazene-substituted arylboronic esters underwent Suzuki cross-coupling reactions with bromo- and iodo(hetero)arenes in good yields without affecting the triazene function. The second Suzuki cross-couplings were carried out through BF₃·Et₂O-mediated decomposition of the triazene function in a mixture of MeOH and Et₂O

as the solvent at 0 °C. Through this methodology, highly decorated terphenyls were prepared in good overall yields with complete chemo- and regioselectivity. This work perfectly illustrates the power of triazenes in masking on demand hazardous aryl diazonium salts, especially in multistep sequences.

The acid-mediated decomposition of triazenes into the corresponding diazonium salts generates an aliphatic secondary amine as a byproduct, contaminating the coupling product. In order to facilitate the purification step, a solid-phase approach with a piperazine bound to the Merrifield resin allowed the linkage of the triazene to a solid support. Cleavage of this traceless linker to generate the aryl diazonium salt proceeded upon addition of 2 equiv of TFA. This strategy has been applied to palladium-catalyzed Heck, Suzuki, and Sonogashira reactions with good overall efficiency (Scheme 10). ⁵¹

■ CONCLUSION

Although the palladium-catalyzed chemistry of diazonium salts has been known for more than 30 years, it has remained confidential until recently. This feature could be explained, at least in part, by the hazardous behavior of some aryl diazonium salts, heaping opprobrium on this class of extremely useful reagents, although many salts are very stable under suitable conditions. While diazonium salts can help chemists in designing more sustainable methodologies, especially for palladiumcatalyzed coupling reactions, they are much often overlooked. However, chemists have at their disposal many tools to predict or evaluate the hazardous behavior of diazonium salts, as is the case for azides and nitrated aryl compounds. One of the primary rules to avoid some drawbacks of these species is to avoid their handling as crystalline salts, privileging methodologies involving their formation in situ. In this review, we have provided an overview of the most reliable strategies that allow the use of

1799

dx.doi.org/10.1021/op500299t | Org. Process Res. Dev. 2014, 18, 1786-1801

nonisolated diazonium salts for palladium-catalyzed reactions, while related approaches have also been successfully implemented to copper chemistry by our group. ⁵² We believe that this contribution could serve as a useful textbook for chemists hesitant to make these powerful reagents an everyday tool for the design of synthetic routes.

AUTHOR INFORMATION

Corresponding Author

*E-mail: fx.felpin@univ-nantes.fr.

Notes

The authors declare no competing financial interest.

Biographies



Nicolas Oger was born in Tours, France, in 1987. After a University Program (two years) leading to a Technical Science Degree in Chemistry at Poitiers (France), he moved to Heriot-Watt University (Edinburgh, United Kingdom) and graduated with his B.Sc. in 2008. He completed his M.Sc. in Organic Chemistry from the University of Nantes (France) in 2012. He is currently performing his doctoral studies at the University of Nantes under the supervision of Prof. F.-X. Felpin and Dr. E. Le Grognec. His research interests are in the fields of heterogeneous catalysis and flow chemistry.



Martin d'Halluin was born in Lille, France, in 1989. He earned his M.Sc. in Chemistry from the University of Bordeaux (France) in 2013. He is currently a Ph.D. student in the team of Prof. F.-X. Felpin at the University of Nantes, working on cellulose modification. His research interests are in the fields of organometallic chemistry, catalysis, and nanosciences.



Erwan Le Grognec was born in Lorient, France, in 1972. He received his undergraduate degree at the University of Nantes in 1996 and earned a Ph.D. in Organometallic Chemistry from the University of Burgundy (Dijon, France) in 2000 under the supervision of Prof. Rinaldo Poli. After a postdoctoral stay at Shell Chemical in Amsterdam (The Netherlands) as a Marie Curie Fellow, he was appointed CNRS Researcher at the University of Nantes in 2001. His current interests concern the development of synthetic methods based on organometallic reactions, polymer-supported chemistry, and asymmetric synthesis.



François-Xavier Felpin was born in Villefranche-sur-Saône, France, in 1977. He received his Ph.D. degree in 2003 from the University of Nantes under the supervision of Professor Jacques Lebreton, working on the synthesis of alkaloids. After earning his Ph.D., he was engaged in a postdoctoral position with Professor Robert S. Coleman at The Ohio State University (Columbus, Ohio, United States), working on the synthesis of Mitomycin. In 2004 he joined the University of Bordeaux as an Assistant Professor, and he received his habilitation in 2009. In Autumn 2011 he moved to the University of Nantes, where he was promoted Full Professor. Prof. Felpin is a junior member of the Institut Universitaire de France, and he recently received the 2014 Young Researcher Award from the French Chemical Society. His research interests include heterogeneous and homogeneous sustainable catalysis, new technologies, and materials chemistry.

ACKNOWLEDGMENTS

We gratefully acknowledge the University of Nantes, the Centre National de la Recherche Scientifique (CNRS), and the Région Pays de la Loire in the framework of a "recrutement sur poste stratégique". F.-X.F. is a member of the Institut Universitaire de France (IUF). We gratefully acknowledge Mrs. Ingrid Ciliberti for her technical assistance with the manuscript preparation.

1800

dx.doi.org/10.1021/op500299t | Org. Process Res. Dev. 2014, 18, 1786–1801

REFERENCES

- (1) (a) Galli, C. Chem. Rev. 1988, 88, 765. (b) Hari, D. P.; König, B. Angew. Chem., Int. Ed. 2013, 52, 4734.
- (2) (a) Roglans, A.; Pla-Quintana, A.; Moreno-Mañas, M. Chem. Rev. 2006, 106, 4622. (b) Mo, F.; Dong, G.; Zhang, Y.; Wang, J. Org. Biomol. Chem. 2013, 11, 1582.
- (3) Patai, S. The Chemistry of Diazonium and Diazo Groups; John Wiley & Sons: Chichester, U.K., 1978.
- (4) (a) Taylor, J. G.; Moro, A. V.; Correia, C. R. D. Eur. J. Org. Chem. 2011, 1403. (b) Felpin, F.-X.; Nassar-Hardy, L.; Le Callonnec, F.; Fouquet, E. Tetrahedron 2011, 67, 2815. (c) Bonin, H.; Fouquet, E.; Felpin, F.-X. Adv. Synth. Catal. 2011, 353, 3063.
- (5) Saunders, K. H. The Aromatic Diazonium Compounds and their Technical Applications; Edward Arnold and Co.: London, 1949.
- (6) Flood, D. T. Org. Synth. 1933, 13, 46.
- (7) Filimonov, V. D.; Trusova, M.; Postnikov, P.; Krasnokutskaya, E. A.; Lee, Y. M.; Hwang, H. Y.; Kim, H.; Chi, K.-W. Org. Lett. 2008, 10, 3961.
- (8) (a) Barbero, M.; Crisma, M.; Degani, I.; Fochi, R.; Perracino, P. Synthesis 1998, 1171. (b) Artuso, E.; Barbero, M.; Degani, I.; Dughera, S.; Fochi, R. Tetrahedron 2006, 62, 3146. (c) Barbero, M.; Cadamuro, S.; Dughera, S. Synthesis 2006, 3443.
- (9) (a) Nielsen, M. A.; Nielsen, M. K.; Pittelkow, T. Org. Process Res. Dev. 2004, 8, 1059. (b) Baumeister, P.; Meyer, W.; Oertle, K.; Seifert, G.; Steiner, H. Chimia 1997, S.I, 144. (c) Molinaro, C.; Mowat, J.; Gosselin, F.; O'Shea, P. D.; Marcoux, J.-F.; Angelaud, R.; Davies, I. W. J. Org. Chem. 2007, 72, 1856. (d) Yu, Z.; Lv, Y.; Yu, C. Org. Process Res. Dev. 2012, 16, 1669. (e) Colleville, A. P.; Horan, R. A. J.; Tomkinson, N. C. O. Org. Process Res. Dev. 2014, 18, 1128.
- (10) He, L.; Qiu, G.; Gao, Y.; Wu, J. Org. Biomol. Chem. 2014, 12, 6965.
- (11) Kikukawa, K.; Matsuda, T. Chem. Lett. 1977, 159.
- (12) (a) Kikukawa, K.; Maemura, K.; Nagira, K.; Wada, F.; Matsuda, T. Chem. Lett. 1980, 551. (b) Kikukawa, K.; Maemura, K.; Kiseki, Y.; Wada, F.; Matsuda, T.; Giam, C. S. J. Org. Chem. 1981, 46, 4885.
- (13) Beller, M.; Fischer, H.; Kühlein, K. Tetrahedron Lett. 1994, 35, 8773.
- (14) Mo, F.; Qiu, D.; Jiang, Y.; Zhang, Y.; Wang, J. Tetrahedron Lett. 2011, 52, 518.
- (15) Wu, X.-F.; Neumann, H.; Beller, M. Chem. Commun. 2011, 47, 7959.
- (16) Wu, X.-F.; Neumann, H.; Beller, M. Angew. Chem., Int. Ed. 2011, 50, 11142.
- (17) (a) Hanson, P.; Rowell, S. C.; Taylor, A. B.; Walton, P. H.; Timms, A. W. J. Chem. Soc., Perkin Trans. 2 2002, 1126. (b) Hanson, P.; Jones, J. R.; Taylor, A. B.; Walton, P. H.; Timms, A. W. J. Chem. Soc., Perkin Trans. 2 2002, 1135.
- (18) Doyle, M. P.; Bryker, W. J. J. Org. Chem. 1979, 44, 1572.
- (19) Andrus, M. B.; Song, C.; Zhang, J. Org. Lett. 2002, 4, 2079.
- (20) Andrus, M. B.; Song, C. Org. Lett. 2001, 3, 3761.
- (21) Kawagishi, F.; Toma, T.; Inui, T.; Yokoshima, S.; Fukuyama, T. J. Am. Chem. Soc. 2013, 135, 13684.
- (22) Panda, B.; Sarkar, T. K. Chem. Commun. 2010, 46, 3131.
- (23) Fabrizi, G.; Goggiamani, A.; Sferrazza, A.; Cacchi, S. Angew. Chem., Int. Ed. 2010, 49, 4067.
- (24) Zong, Y.; Hu, J.; Sun, P.; Jiang, X. Synlett **2012**, 23, 2393.
- (25) Siqueira, F. A.; Taylor, J. G.; Correia, C. R. D. Tetrahedron Lett. 2010, 51, 2102.
- (26) Coy B., E. D.; Jovanovic, L.; Sefkow, M. Org. Lett. 2010, 12, 1976.
- (27) (a) Le Callonnec, F.; Fouquet, E.; Felpin, F.-X. *Org. Lett.* **2011**, *13*, 2646. (b) Susperregui, N.; Miqueu, K.; Sotiropoulos, J.-M.; Le Callonnec, F.; Fouquet, F.; Falpin, F. Y. Chem.—Eur. **12012**, *18*, 7210.
- Callonnec, F.; Fouquet, E.; Felpin, F.-X. Chem.—Eur. J. 2012, 18, 7210. (28) Oger, N.; Le Callonnec, F.; Jacquemin, D.; Fouquet, E.; Le Grognec, E.; Felpin, F.-X. Adv. Synth. Catal. 2014, 356, 1065.
- (29) Joncour, R.; Susperregui, N.; Pinaud, N.; Miqueu, K.; Fouquet, E.; Sotiropoulos, J.-M.; Felpin, F.-X. Chem.—Eur. J. 2013, 19, 9291.
- (30) (a) Amatore, C.; Jutand, A.; Le Duc, G. Chem.—Eur. J. 2011, 17, 2492. (b) Carrow, B. P.; Hartwig, J. F. J. Am. Chem. Soc. 2011, 133, 2116.
- (31) Baumeister, P.; Seifert, G.; Steiner, H. Process for the preparation of substituted benzenes and benzene sulfonic acid and derivatives

- thereof and a process for the preparation of N,N'-substituted ureas. EP0584043, 1992.
- (32) (a) Zapf, A.; Beller, M. Top. Catal. 2002, 19, 101. (b) Blaser, H.-U.; Indolese, A.; Naud, F.; Nettekoven, U.; Schnyder, A. Adv. Synth. Catal. 2004, 346, 1583. (c) Magano, J.; Dunetz, J. R. Chem. Rev. 2011, 111, 2177.
- (33) (a) Fortt, R.; Wootton, R. C. R.; de Mello, A. J. Org. Process Res. Dev. 2003, 7, 762. (b) Malet-Sanz, L.; Madrzak, J.; Ley, S. V.; Baxendale, I. R. Org. Biomol. Chem. 2010, 8, 5324. (c) Chernyak, N.; Buchwald, S. L. Am. Chem. Soc. 2012, 134, 12466. (d) Hu, D. X.; O'Brien, M.; Ley, S. V. Org. Lett. 2012, 14, 4246. (e) Salice, P.; Fenaroli, D.; De Filippo, C. C.; Menna, E.; Gasparini, G.; Maggini, M. Chem. Today 2012, 30, 37. (f) Chen, M.; Buchwald, S. L. Angew. Chem., Int. Ed. 2013, 52, 4247. (g) Wang, X.; Cuny, G. D.; Noël, T. Angew. Chem., Int. Ed. 2013, 52, 426. (h) Yu, Z.-Q.; Lv, Y.-W.; Yu, C.-M.; Su, W.-K. Tetrahedron Lett. 2013, 54, 1261. (i) Wootton, R. C. R.; Fortt, R.; de Mello, A. J. Lab Chip 2002, 2, S. (j) Malet-Sanz, L.; Madrzak, J.; Holvey, R. S.; Underwood, T. Tetrahedron Lett. 2009, 50, 7263. (k) Li, B.; Widlicka, D.; Boucher, S.; Hayward, C.; Lucas, J.; Murray, J. C.; O'Neil, B. T.; Pfisterer, D.; Samp, L.; VanAlsten, J.; Xiang, Y.; Young, J. Org. Process Res. Dev. 2012, 16, 2031. (l) Jacq, J.; Pasau, P. Chem.—Eur. J. 2014, 20, 12223.
- (34) Ahmed-Omer, B.; Barrow, D. A.; Wirth, T. Tetrahedron Lett. 2009, 50, 3352.
- (35) Nalivela, K. S.; Tilley, M.; McGuire, M. A.; Organ, M. G. Chem.— Eur. J. 2014, 20, 6603.
- (36) (a) Felpin, F.-X.; Fouquet, E. Adv. Synth. Catal. 2008, 350, 863. (b) Felpin, F.-X.; Fouquet, E.; Zakri, C. Adv. Synth. Catal. 2008, 350, 2559. (c) Felpin, F.-X.; Miqueu, K.; Sotiropoulos, J.-M.; Fouquet, E.; Ibarguren, O.; Laudien, J. Chem.—Eur. J. 2010, 16, 5191. (d) Rossy, C.; Fouquet, E.; Felpin, F.-X. Synthesis 2012, 44, 37.
- (37) Oger, N.; Le Grognec, E.; Felpin, F.-X. J. Org. Chem. 2014, 79, 8255.
- (38) (a) Beller, M.; Kühlein, K. Synlett 1995, 441. (b) Brunner, H.; Le Cousturier de Courcy, N.; Genêt, J.-P. Tetrahedron Lett. 1999, 40, 4815. (c) Felpin, F.-X.; Ibarguren, O.; Nassar-Hardy, L.; Fouquet, E. J. Org. Chem. 2009, 74, 1349. (d) Ibarguren, O.; Zakri, C.; Fouquet, E.; Felpin, F.-X. Tetrahedron Lett. 2009, 50, 5071. (e) Gholinejad, M. Appl. Organomet. Chem. 2013, 27, 19. (f) Li, X.; Wang, L.-C.; Chang, H.-H.; Zhang, C.-X.; Wei, W.-L. Appl. Catal., A 2013, 462–463, 15. (g) Singh, A. S.; Shendage, S. S.; Nagarkar, J. M. Tetrahedron Lett. 2013, 54, 6319. (39) (a) Schmidt, B.; Berger, R.; Holter, F. Org. Biomol. Chem. 2010, 8, 1406. (b) Schmidt, B.; Elizarov, N.; Berger, R.; Petersen, M. H. Synthesis 2013, 45, 1174.
- (40) Schmidt, B.; Berger, R. Adv. Synth. Catal. 2013, 355, 463.
- (41) Schmidt, B.; Hölter, F.; Berger, R.; Jessel, S. Adv. Synth. Catal. 2010, 352, 2463.
- (42) Felpin, F.-X.; Coste, J.; Zakri, C.; Fouquet, E. Chem.—Eur. J. 2009, 15, 7238.
- (43) Schmidt, B.; Elizarov, N. Chem. Commun. 2012, 48, 4350.
- (44) Lazny, R.; Poplawski, J.; Köbberling, J.; Enders, D.; Bräse, S. Synlett 1999, 1304.
- (45) Sengupta, S.; Sadhukhan, S. K. Org. Synth. 2002, 79, 52.
- (46) (a) Sengupta, S.; Sadhukhan, S. K.; Bhattacharyya, S. *Tetrahedron* 1997, 53, 2213. (b) Bhattacharya, S.; Majee, S.; Mukherjee, R.; Sengupta, S. *Synth. Commun.* 1995, 25, 651.
- (47) Saeki, T.; Son, E.-C.; Tamao, K. Org. Lett. 2004, 6, 617.
- (48) Nan, G.; Ren, F.; Luo, M. Beilstein J. Org. Chem. 2010, 6, 70.
- (49) Sengupta, S.; Sadhukhan, S. K. Tetrahedron Lett. 1998, 39, 715.
 (50) Liu, C.-Y.; Gavryushin, A.; Knochel, P. Chem.—Asian J. 2007, 2,
- (51) Bräse, S.; Schroen, M. Angew. Chem., Int. Ed. 1999, 38, 1071.
- (52) (a) Honraedt, A.; Le Callonnec, F.; Le Grognec, E.; Fernandez, V.; Felpin, F.-X. J. Org. Chem. 2013, 78, 4604. (b) Honraedt, A.; Raux, M.-A.; Grognec, E. L.; Jacquemin, D.; Felpin, F.-X. Chem. Commun. 2014, 50, 5236.

1020.

Résumé étendu en Français

Introduction

Depuis des siècles la cellulose (Schéma 1), un polymère linéaire composé d'unité anhydrocellobiose, est utilisée par l'Homme comme source d'énergie, support pour l'écriture ou matériau de base pour la fabrication du textile.

Schéma 1 Structure de la cellulose avec comme motif de répétition l'anhydrocellobiose

Ce biomatériau renouvelable et durable; sa production annuelle par les plantes est estimée à 1,5x10¹² tonnes (plus de 50% de la biomasse); continue de susciter un vif intérêt dans de nombreux domaines d'application. La modification chimique de la cellulose permet d'obtenir des matériaux dotés de nouvelles propriétés. Si la modification par des procédés de physisorption a été massivement étudiée et permet d'apporter de nouvelles fonctionnalités à ce matériau, ces procédés présentent l'inconvénient d'être sensible à la désorption. C'est pourquoi le développement de matériaux cellulosiques plus robustes reste un enjeu considérable. C'est dans ce contexte que ce travail de thèse s'inscrit, *via* la fonctionnalisation covalente de la cellulose, afin de préparer de nouveaux dispositifs à base de papier.

Les résultats obtenus au cours de cette thèse ont été divisés en 4 chapitres :

- Le premier traite du développement d'une nouvelle méthode d'écriture covalente à la surface du papier permettant le stockage d'information.
- Le deuxième concerne la préparation d'une sonde moléculaire greffée à la surface du papier permettant la détection de l'ion HSO₄-
- Le troisième traite de la mise au point d'un outil de détection du Cu²⁺ et de l'application de cet outil comme réducteur supporté pour la réaction click de Huisgen
- Le dernier concerne la préparation d'une membrane de décontamination des eaux contenant des métaux lourds.

I. <u>Préparation d'un nouveau matériau pour le stockage d'informations</u>

Les premiers travaux réalisés au cours de cette thèse traitent du développement d'une nouvelle méthode d'écriture invisible à la surface de la cellulose permettant ainsi le stockage d'information à la surface de ce matériau.

Ceci a été rendu possible *via* le greffage covalent de coumarines à la surface de la cellulose. Sous l'effet d'un rayonnement de longueur d'onde contrôlée ces molécules peuvent subir une réaction de dimérisation réversible (Schéma 2).

Schéma 2 Dimérisation réversible des coumarines

Dans un premier temps, nous avons réalisé des études de chimie théorique afin de valider la possibilité de réaliser la dimérisation des coumarines à la surface de la cellulose (Figure 1).

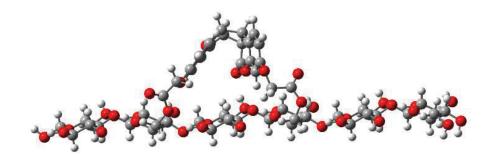


Figure 1 Représentation de la géométrie du dimère obtenu après irradiation

Afin de fonctionnaliser la cellulose, un dérivé de la coumarine comportant une fonction chlorure d'acide a été synthétisé en deux étapes en partant de la 7-Hydroxycoumarine commerciale. Ce dérivé est greffé de manière covalente à la surface de la cellulose *via* une réaction d'estérification (Schéma 3).

Paper-grafted coumarins

Schéma 3 Stratégie de fonctionnalisation du papier

Les propriétés optiques du matériau obtenues ont été analysées par spectrométrie UV-Visible (Figure 2). Ces analyses ont permis de vérifier la faisabilité et l'efficacité de la réaction de dimérisation à la surface du papier

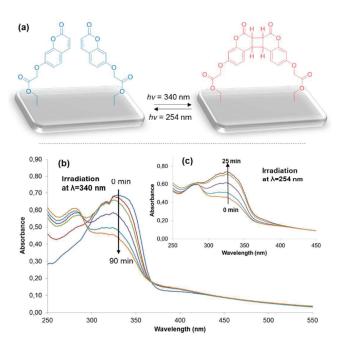


Figure 2 (a) Cycloaddition [2+2] réversible des coumarines. (b) Décroissance de l'absorbance du papier greffé après irradiation à 340nm (c) Réaction inverse après irradiation à 254nm.

Afin de s'assurer de la stabilité de notre système, plusieurs cycles de dimérisation/rétrocyclisation ont été réalisés (Figure 3). Les résultats indiquent une bonne stabilité de notre matériau puisque même après trois cycles il n'y a pas de baisse significative de l'absorbance de notre système.

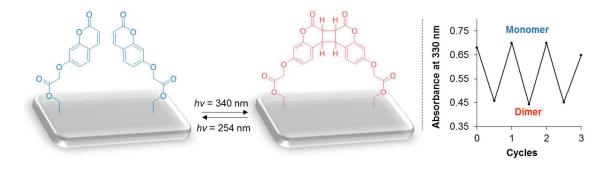


Figure 3 Test de résistance à la fatigue du matériau avec plusieurs cycles d'irradiation à 340 nm et 254 nm.

Enfin, l'utilisation d'un photomasque a permis de réaliser la réaction de dimérisation des coumarines de manière spatialement controlée permettant ainsi l'encodage d'informations à la surface du matériau. Dans un premier temps, nous avons réalisé la photoimpression covalente du logo de notre université puis nous avons inscrit à la surface de ce matériau un motif plus complexe, un QRCode (Figure 4).

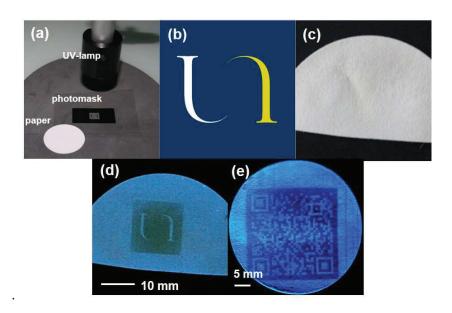


Figure 4 Illustration du système de photoimpression covalente

Invisible à l'œil nu, les informations ainsi encodées à la surface du papier peuvent être révélées en utilisant une lampe UV.

En conclusion, ce travail apporte une nouvelle méthode d'écriture invisible à la surface du papier reposant sur les propriétés de dimérisation des coumarines greffées de manière covalente à la surface du matériau ce qui apporte une stabilité plus importante au système puisque les molécules photosensibles ne sont pas sujettes à la désorption.

II. Préparation d'un outil de détection de l'ion HSO₄ dans l'eau

Le deuxième chapitre présente la préparation et le greffage à la surface du papier d'une sonde organique sélective de l'ion HSO₄⁻ fournissant ainsi un outil de détection sous la forme de bandelette de papier (analogue au papier pH).

Le développement de sondes organiques pour la détection d'ions dans l'eau est un champ de recherche très important, notamment pour la détection de polluants. Pour réaliser cette étude, nous avons décidé de travailler avec des dérivés de la rhodamine B, une famille de molécules déjà décrite pour la détection d'ions en solution. La détection est due à la formation de liaison hydrogène entre la sonde et l'analyte, ce qui induit une délocalisation des électrons au sein de la rhodamine passant alors de sa forme spirolactame incolore à une forme zwitterionique ouverte fortement colorée (Schéma 4).

Schéma 4 Représentation du principe de détection d'un ion par une rhodamine

Ici, la fonctionnalisation du papier est réalisée en deux étapes, une première réaction d'estérification permet de greffer à la surface de la cellulose un aldéhyde qui subit par la suite une réaction d'amination réductrice avec un dérivé de la rhodamine B portant un bras éthylène diamine préalable préparé au laboratoire (Schéma 5).

Schéma 5 Préparation et greffage de la sonde à la surface du papier

Le papier ainsi obtenu a ensuite été immergé dans des solutions aqueuses contenant différents anions afin d'étudier sa sélectivité. Seul l'anion HSO_4^- a été détecté de manière colorimétrique par notre dispositif comme en témoigne la photo ci-dessous (Figure 5a).

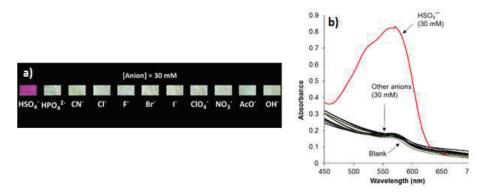


Figure 5 (a) Détection colorimétrique de HSO₄- dans l'eau (b) Spectres UV-Visibles correspondants

Afin de vérifier cette sélectivité, des analyses par spectrométrie UV-Visible ont été réalisées, elles permettent de confirmer les observations faîtes de manière colorimétriques, puisque seul le papier immergé dans la solution contenant l'anion HSO₄- possède une absorbance caractéristique de la forme ouverte de la rhodamine (Figure 5b).

Par la suite, les limites de détection colorimétrique (à l'œil nu) et optique (par UV-Visible) ont été évaluées. A l'œil nu, la limite de détection semble se situer entre 0,1 et 0,5 mM (Figure 6a) à en juger par le dégradé de couleur obtenu. Cette observation a été validée par les études UV-Visibles qui donnent une limite de détection de 0,12 mM (Figure 6b et 6c).

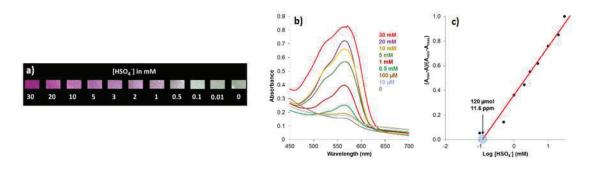


Figure 6 (a) Influence de la concentration sur la détection colorimétrique (b) Spectres

UV-Visibles correspondants (c) Détermination de la limite de détection

De manière remarquable, ce dispositif peut être réutilisé après une simple immersion dans une solution de soude 1M reformant la rhodamine sous sa forme spirolactame incolore.

En conclusion, nous avons développé un nouvel outil de détection de l'ion HSO₄ en milieu aqueux. Ce dispositif a l'avantage d'être simple d'utilisation, peu encombrant et offre une bonne sélectivité et limite de détection même à l'œil nu.

III. <u>Préparation d'un dispositif à base de papier capable de réduire le Cu(II)</u> en Cu(I) : Application à la détection et la catalyse

Ce chapitre traite de la préparation d'un dispositif bioinspiré à base de papier capable de détecter le Cu(II) dans l'eau et de l'utilisation de ce matériau comme réducteur supporté pour la réaction click de cycloaddition 1,3-dipolaire de Huisgen.

De nouveau, la fonctionnalisation du papier a été réalisée *via* une réaction d'estérification permettant d'introduire une fonction thiol à la surface de la cellulose (Schéma 6).

Schéma 6 Préparation du papier modifié comportant une fonction thiol

Le matériau ainsi obtenu a ensuite été mis en contact avec différents ions métalliques et a montré une grande sélectivité envers l'ion Cu(II) (Figure 7a).

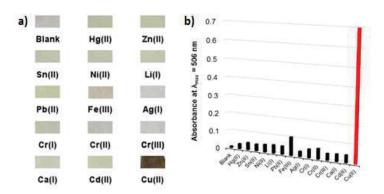


Figure 7 (a) Détection colorimétrique de Cu^{2+} (b) Intensité de l'absorbance à λ_{max} =506 nm pour les différents métaux

Comme dans le chapitre précédent cette détection colorimétrique a été confirmée par une détection optique à l'aide d'analyses UV-Visible (Figure 7b).

Dans le cas présent, la détection a lieu grâce à la formation d'un complexe thiol-cuivre induisant un transfert de charge S->Cu entraînant une coloration du papier.

Comme pour le travail précédent, la limite de détection a également été déterminée de manière colorimétrique (Figure 8a) et de manière optique (Figure 8b et 8c).

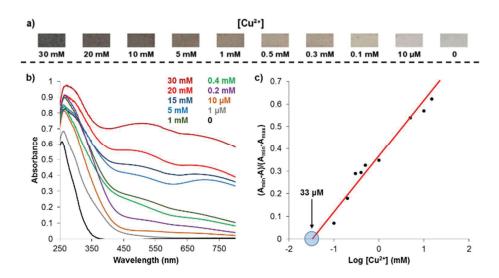


Figure 8 (a) Influence de la concentration sur la détection colorimétrique (b) Spectres UV-Visibles correspondants (c) Détermination de la limite de détection

La limite de détection obtenue par analyses UV-Visible est de 33 µmol/L soit 2 ppm de cuivre. De plus, grâce à l'utilisation d'une technique d'analyse d'image, il a été possible de déterminer la concentration d'un échantillon inconnu en étudiant la coloration du papier (coordonnées de couleurs) et en comparant ces résultats avec une courbe de calibration préalablement établie (Figure 9).

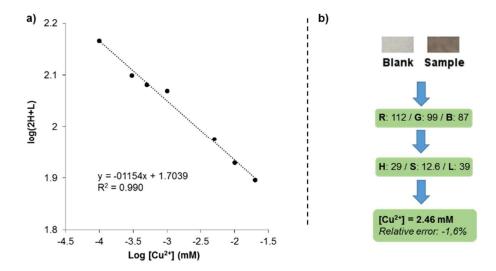


Figure 9 Analyse d'un échantillon inconnu *via* l'étude des coordonnées de couleurs de l'échantillon

Des analyses par spectrométrie photoélectronique X (XPS) ont révélé que le cuivre présent à la surface de ce matériau se trouve au degré d'oxydation +1 sous la forme de nanoparticules d'oxyde de cuivre Cu₂O.

Ce résultat nous a donné l'idée d'utiliser ce dispositif comme réducteur supporté pour la réaction click de formation de triazole. Cette stratégie inédite de réducteur immobilisé sur un support a été appliquée pour la préparation de plus de 19 produits différents avec de bons rendements (Figure 10).

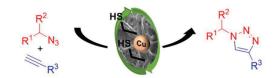


Figure 10 Illustration de la stratégie de synthèse

De manière intéressante, ce dispositif possède également la capacité de retenir le cuivre à la surface de la cellulose permettant ainsi de récupérer après une simple filtration un brut réactionnel quasiment exempt de cuivre.

En conclusion, nous avons développé un nouveau dispositif capable de détecter de manière colorimétrique et optique la présence de Cu(II) dans une solution aqueuse *via* la formation de nanoparticule d'oxyde de cuivre Cu₂O où le cuivre se retrouve au degré d'oxydation +1. Nous avons par la suite utilisé ce matériau comme réducteur supporté pour la réaction click de Huisgen.

IV. <u>Préparation d'un nouveau matériau pour la remédiation de métaux dans</u> l'eau

La dernière partie de cette thèse concerne la préparation d'une membrane capable de décontaminer des solutions aqueuses contenant des métaux lourds.

Inspiré par des travaux récents portant sur la préparation d'un agent floculant à base de chitosan fonctionnalisé par de l'acide éthylène diamine tétraacétique (EDTA) nous avons décidé d'appliquer une stratégie similaire afin de préparer une membrane à base de papier capable de chélater les métaux.

La préparation de ce dispositif se fait *via* une réaction d'estérification entre la cellulose et le dianhydride de l'EDTA (Schéma 7).

$$\begin{array}{c} \text{CO}_2\text{H} \\ \text{HO}_2\text{C} \\ \text{HO}_2\text{C} \\ \text{EDTA} \\ \end{array} \begin{array}{c} \text{Ac}_2\text{O, pyridine} \\ \text{65 °C, 24 h} \\ \end{array} \begin{array}{c} \text{OH} \\ \text{OH} \\ \text{OH} \\ \end{array} \begin{array}{c} \text{OH} \\ \end{array} \begin{array}{c} \text{OH} \\ \text{OH} \\ \end{array} \begin{array}{c} \text{OH} \\ \end{array} \begin{array}{c} \text{OH} \\ \text{OH} \\ \end{array} \begin{array}{c} \text{OH} \\ \text{OH} \\ \end{array} \begin{array}{c} \text{$$

Schéma 7 Stratégie de synthèse de la « membrane EDTA »

Le matériau ainsi obtenu a par la suite été immergé dans des solutions aqueuses contenant différents métaux à une concentration initiale de 100 ppm, puis après un certain temps de contact, la solution est analysée par spectroscopie d'absorption atomique (AAS) ou par spectrométrie à plasma à couplage inductif (ICP) selon la nature du métal. Les analyses ont montré que ce matériau est capable de chélater de nombreux métaux offrant ainsi un dispositif universel pour la dépollution des eaux contaminées par des métaux lourds (Figure 11).

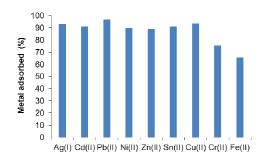


Figure 11 Capacité d'adsorption de la « membrane EDTA » vis-à-vis de différents métaux

Ce dispositif a l'avantage de pouvoir fonctionner sur une large gamme de pH (de 3 à 9) comme l'attestent les analyses réalisées sur le plomb et le cadmium (Figure 12)

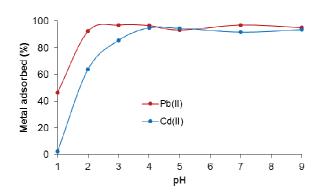


Figure 12 Influence du PH sur l'adsorption du plomb et du cadmium

Les caractéristiques d'adsorption de cette membrane ont également été évaluées, les études de cinétique révèlent que l'adsorption suit une cinétique du pseudo-second-ordre (Figure 13a).

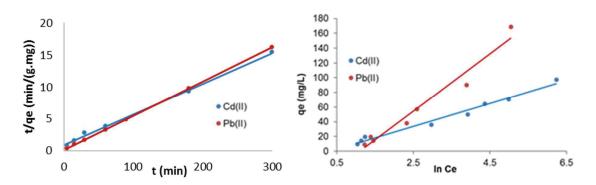


Figure 13 (a) Cinétique d'adsorption du pseudo-second-ordre (b) Isotherme de Temkin

Les études thermodynamiques montrent quant à elles que notre système suit un modèle d'adsorption appelé isotherme de Temkin (Figure 13b).

Les différents résultats présentés précédemment ont été obtenus en immergeant notre papier modifié dans les différentes solutions aqueuses. Il est à noter qu'il est possible d'utiliser ce papier comme membrane de filtration afin de dépolluer l'eau. Par exemple pour le cadmium nous avons obtenu des résultats similaires en termes de dépollution que l'on utilise notre dispositif comme adsorbant ou comme membrane (à concentrations et temps de contact équivalents).

En conclusion, nous avons développé un outil universel pour la décontamination des eaux contenant des métaux lourds. La préparation de cette membrane est rapide et peu couteuse et permet d'éliminer de nombreux métaux comme par exemple le plomb, le cadmium, l'argent, le nickel ou encore le zinc.

Conclusion

Les objectifs de cette thèse étaient de développer de nouveaux matériaux à base de papier grâce à des méthodes de fonctionnalisations covalentes de ce dernier.

En utilisant principalement des réactions d'estérifications, nous avons fonctionnalisé en peu d'étapes la cellulose avec divers composés permettant ainsi la préparation de matériaux aux propriétés nouvelles.

Ces matériaux ont été utilisés pour différentes applications allant de la photoimpression à la décontamination des eaux en passant par la détection de polluants.

Ces différents travaux ouvrent de nombreuses perspectives pour le développement de nouveaux matériaux à base de cellulose fonctionnalisés de manière covalentes. La preuve de concept que nous avons apportée au sujet de la photoimpression peut certainement être améliorée en utilisant d'autres types de molécules et pourquoi pas un mélange de plusieurs molécules. La préparation de sondes moléculaires greffées à la surface du papier offre des outils de détection des polluants pratiques et simples d'utilisation. Afin de pouvoir analyser la présence d'autres polluants dans l'eau (métaux ou polluants organiques) il est nécessaire de développer de nouvelles sondes. Enfin, la préparation d'une membrane pour la dépollution de l'eau a montrée de bons résultats pour les métaux lourds, il est possible d'envisager la préparation de membranes capables d'éliminer d'autres types de polluants, notamment des composés organiques.





Thèse de Doctorat

Martin d'HALLUIN

Fonctionnalisation covalente de la cellulose : Préparation de dispositifs à base de papier Covalent Functionalisation of cellulose: Preparation of paper based devices

Résumé

Depuis des siècles la cellulose est utilisée par l'Homme comme source d'énergie, support pour l'écriture ou matériau de base pour la fabrication du textile. Ce biomatériau renouvelable et durable continue de susciter un vif intérêt dans de nombreux domaines d'application. La modification chimique de la cellulose permet d'obtenir des matériaux dotés de nouvelles propriétés. Si la modification par des procédés de physisorption a été massivement étudiée et permet d'apporter de nouvelles fonctionnalités à ce matériau, ces procédés présentent l'inconvénient d'être sensible à la désorption. C'est pourquoi le développement de matériaux cellulosiques plus robustes reste un enjeu considérable. C'est dans ce contexte que ce travail de thèse s'inscrit, via la fonctionnalisation covalente de la cellulose, afin de préparer de nouveaux dispositifs à base de papier.

Dans un premier temps, une nouvelle approche permettant le stockage d'informations à la surface du papier a été développée. Le concept d'écriture covalente sur un papier devenu photosensible par le greffage de coumarines a été possible en utilisant la photodimérisation spatialement contrôlée des coumarines et permettant ainsi l'encodage d'informations. Dans un second temps, une étude concernant la modification de la surface de la cellulose en greffant de manière covalente des sondes sélectives des ions HSO4- et Cu2+ a été réalisée. Ce dernier dispositif s'est révélé aussi être un très bon réducteur du Cu(II) en Cu(I) et a été mis à profit dans la réaction de Huisgen. Enfin, le greffage covalent d'EDTA sur du papier a permis d'obtenir une membrane efficace pour la décontamination d'eau polluée par des métaux lourds.

Mots clés

Cellulose, Papier, Fonctionnalisation covalente, Sondes, Stockage d'informations, Chimie click, Réaction de Huisgen, Décontamination.

Abstract

For centuries, cellulose has been used by humans as energy crop, media for writing and material for textile. Nowadays, this renewable and sustainable biomaterial continues to generate a huge interest in many domains of applications. The chemical modification of cellulose gives rise to materials with new properties. The cellulose modification by physisorption processes has been extensively studied and brings new functionalities to this material. However, these strategies suffer from a low stability with molecules having a low affinity for cellulose. Thus, the development of more robust cellulosic materials remains a major concern. It is in this context that the present thesis has been drawn up, via the covalent functionalization of cellulose in order to prepare new paper-based devices.

First, a new strategy enabling data storage on the surface of paper has been developed. The covalent writing onto a photosensitive paper thanks to the grafting of coumarins has been made possible through the spatially resolved photodimerization of coumarins enabling data encoding. In a second time, a study concerning the covalent immobilization of selective sensors for HSO4- and Cu2+ ions has been conducted. The latter device also presents the ability of reducing Cu(II) to Cu(I) and has found application in the Huisgen reaction. Finally, the covalent grafting of EDTA onto paper has enabled the preparation of a powerful membrane for the decontamination of heavy metals containing water.

Key Words

Cellulose, Paper, Covalent functionalisation, Sensors, Data storage, Click chemistry, Huisgen reaction, Decontamination.